FLORIDA INTERNATIONAL UNIVERSITY

Miami, Florida

MECHANISMS OF CHLOROPEROXIDASES-CATALYZED ENANTIOSELECTIVE TRANSFORMATIONS FROM SPECTROSCOPIC AND X-RAY CRYSTALLOGRAPHIC STUDIES OF ENZYME-SUBSTRATE COMPLEXES

A dissertation submitted in partial fulfillment of

the requirement of the degree of

DOCTOR OF PHILOSPHY

in

BIOCHEMISTRY

by

Xiaoqing Tang

2021

To: Dean Michael R. Heithaus
College of Arts, Sciences, and Education

This dissertation, written by Xiaoqing Tang, and entitled Mechanisms of Chloroperoxidases-Catalyzed Enantioselective Transformations from Spectroscopic and X-ray Crystallographic Studies of Enzyme-substrate Complexes, having been approved in respect to style and intellectual content, is referred to you for judgment.

We have read this dissertation and recommend that it be approved.

_____

Yuan Liu

_____

Barry Philip Rosen

_____

Manuel Alejandro Barbieri

_____

Xiaotang Wang, Major Professor

Date of Defense: October 27, 2021

The dissertation of Xiaoqing Tang is approved.

_____

Dean Michael R. Heithaus
College of Arts, Sciences and Education

_____

Andrés G. Gil
Vice President for Research and Economic Development
and Dean of the University Graduate School

Florida International University, 2021

DEDICATION

I dedicate this dissertation to my mother, Chuanmei Wang and my father, Xianwen Tang. Without their support, understanding, patience and most of all love, it would not have been possible for me to complete this work.

ACKNOWLEDGMENTS

I joined the Biochemistry Ph.D. Program of Florida International University in 2016. Actually it was my first time to live in a strange place abroad. Although Miami is an intriguing city with magnificent scenery, I felt lost and lonely once the novelty had worn off. As an international student, language had been the greatest challenge, which had bothered me in both communication and learning. Fortunately, I met many very friendly and helpful people here and all of them have impressed me deeply. This is sure to be a memorable experience.

First, I sincerely appreciate my major professor, Dr. Xiaotang Wang. He is my great mentor who has raised me up to a new level of my research and also my life. He is my first teacher when I entered science and his support, patience, encouragement as well as guidance has shaped who I am today. Having him as my supervisor is my greatest happiness. Then my thanks go to other committee members, Dr. Barry Philp Rosen, Dr. Yuan Liu and Dr. Manuel Alejandro Barbieri, for their helpful advice and continuous support. I would also like to thank my teammates Dr. Elwood Kwong Lam, Dr. Yongjian Guo and Jieying Zhou, for all the inspiring discussions, kind help and pleasant research environment. Especially I want to express my sincere thanks to Dr. Venkadesh Sarkarai Nadar in Dr. Rosen's group for his professional assistance on all aspects of crystallography. Finally, I would like to thank all my family and friends for their endless love and supports which are my spiritual pillar in times of sorrow and depression.

ABSTRACT OF THE DISSERTATION

MECHANISMS OF CHLOROPEROXIDASES-CATALYZED ENANTIOSELECTIVE TRANSFORMATIONS FROM SPECTROSCOPIC AND X-RAY CRYSTALLOGRAPHIC STUDIES OF ENZYME-SUBSTRATE COMPLEXES

by

Xiaoqing Tang

Florida International University, 2021

Miami, Florida

Professor Xiaotang Wang, Major Professor

The chloroperoxidase secreted from *Caldariomyces fumago* catalyzes broad spectrum of reactions. The crystallography combined with X-ray diffraction analysis was conducted to reveal recombinant CPO expressed in a modified *Aspergillus niger* system. Our results indicated that despite functional similarities with wild type CPO, recombinant CPO is over glycosylated with more mannose. Besides, ten iodide ion binding sites were identified in rCPO and six of them were found to be well superimposed on previously reported structure of the wild type CPO. Therefore, recombinant CPO shares almost the same structure with wild type CPO, and the *Aspergillus niger* is a potential system for heterologous heme peroxidase expression.

The most striking feature of *C. fumago* chloroperoxidase is its ability to efficiently catalyze asymmetric epoxidations of alkenes with excellent enantioselectivity. To elucidate the structural basis for the mechanism of CPO-catalyzed enantioselective epoxidation of

selected olefins, the structures of the CPO and its olefin complex were studied by both crystallographic and computational techniques. The crystal structure demonstrated that ethyl 3-methylbut-3-enoate forms a complex with CPO at the entrance of a wide channel. This substrate is between Phe-103 and Phe-186 and stabilized by hydrophobic interations of these two amino acids, ensuring its enantioselective transformation. CPO mutants of C29H, F186A and F103A/186A were expressed in *A. niger* and results of catalytic assays dwarfed the effects of thiolate-ligand, while confirming the roles of Phe103 and Phe186 in enzyme-substrate interactions and catalytic activities. The prokaryotic system was applied to express mutant CPO-C29H. Our work demonstrated that the heme binding of C29H is improved with the assistance of *ChuA* gene, but C29H expressed in *E. coli* cells is inactive in either chlorination or peroxidation, indicating the requirement of post-translational modifications for mutant CPO.

TABLE OF CONTENTS

CHAPTER PAGE

LIST OF TABLES

TABLE PAGE

LIST OF FIGURES

ABBREVIATIONS AND ACRONYMS

aa	Amino acid
ABTS	2,2’ -azino-bis(3-ethylbenzothiazoline-6- sulfonic acid)
Ala/A	Alanine
AmdS	Acetamidase gene
A. nidulans	Aspergillus nidulans
A. niger	Aspergillus niger
ATCC	American type culture collection
C. fumago	Caldariomyces fumago
CPO	Chloroperoxidase
Cys/C	Cysteine
DCD	Dichlorodimedone
DEAE	Diethylaminoethanol
DNA	Deoxyribonucleic acid
dNTP	Deoxyribonucleotide
ee	Enantiomeric excess
GLA	Glucoamylase
Glu/E	Glutamic acid

His/H	Histidine
HPLC	High performance liquid chromatography
IPTG	Isopropyl β-D-1-thiogalactopyranoside
LiP	Lignin peroxidase
MCD	Monochlorodimedone
MM	Minimal medium
MPO	Myeloperoxidase
NAD(P)H	Nicotinamide adenine dinucleotide (phosphate)
NMR	Nuclear magnetic resonance
P450	Cytochrome P450 monooxygenase
PCR	Polymerase chain reaction
PDB	Protein data base
PglaA	glucoamylase promoter
Phe/F	Phenylalanine
RZ value	Reinheitzahl value
SDS-PAGE	Sodium dodecyl sulfate polyacrylamide gel electrophoresis
TBHP	tert-butyl hydroperoxide
trpC	anthranilate synthase terminator

Tyr/Y	Tyrosine
UV-Vis	Ultraviolet-Visible
WT	Wild-type

CHAPTER I. GENERAL INTRODUCTION

1.1 Heme Proteins and Heme Peroxidase

Heme proteins are proteins containing the heme cofactor which acts as the prosthetic group. These proteins are ubiquitous in either eukaryotic or prokaryotic organisms and participate in various reactions [1]. There are many different forms of heme, including heme *a*, heme *b*, heme *c* and heme *d*. Among them, heme *b* and heme *c* most generally exist in heme proteins [2]. Regardless of the forms, the heme, or iron-protoporphyrin IX contains a central ferrous iron connected to four nitrogen atoms of pyrrole and is used for either electron transfer or oxygen transport. Heme proteins have been identified to function as catalysts, be responsible for oxygen transportation and storage, ligand binding, signal transduction and gene expression control [3]. These versatile activities derive from not only the diversity of heme molecules but also different protein environments like iron ligands, amino acid groups and characteristics of solvents [1]. In the past decades, hemoglobin and myoglobin , typically regarded as oxygen transport and storage proteins, have been the focus of numerous structure characterizations [4], [5]. Structural investigations are the basis for estimating the interactions in the heme center, which provides insights into the structure-function relationships and catalytic mechanisms of heme-proteins.

Heme-proteins with peroxidase activity that catalyze one-electron and two electron oxidation reactions with the stimulation of oxidants, usually hydrogen peroxide, are termed as heme peroxidases. In the heme pocket of typical heme peroxidases, the central iron is coordinated with four nitrogens in pyrrole and with the fifth nitrogen in imidazole of

proximal histidine residue. Generally, heme peroxidase-catalyzed oxidations could be classified into four categories, in which H_2O_2 is reduced to water while substrates are oxidized to corresponding products. In one-electron transfer reactions (Reaction 1), substrates (AH2) are oxidized to the corresponding radicals (.AH). Two-electron reactions include halogenation (Reaction 2) and catalytic reaction (Reaction 3). Besides, organic substrates are able to undergo per-oxygenation reaction or oxygen-insertion reaction with the catalysis of some heme peroxidase (Reaction 4).

$$H_2O_2 + 2AH_2 \rightarrow H2O + 2^{\cdot}AH \quad (1)$$

$$H_2O_2 + X^- + H+ \rightarrow H_2O + HOX \quad (2)$$

$$H_2O_2 + H_2O_2 \rightarrow 2H_2O + O_2 \quad (3)$$

$$H2O2 + RH \rightarrow H2O + ROH \quad (4)$$

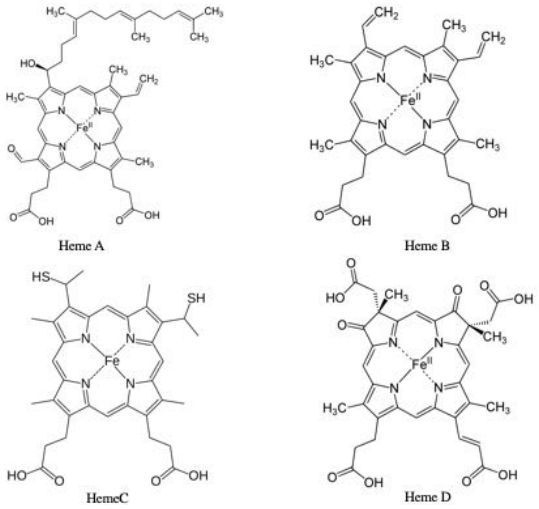

Figure 1.1 Four general types of heme groups in hemoproteins.

1.2 Cytochromes P450

Over half of heme proteins are cytochromes participating in electron transfer and redox catalysis of cell metabolism. Among them, cytochromes P450 have been developed considerably as mono-oxygenases, since understanding the metabolism and toxicity of drugs or other chemicals has long been an important task [6], [7], [8], [9]. Cytochromes P450 have been recognized as the control of development and homeostasis in the biosynthesis of crucial signaling molecules, and as the major enzymes involved in the metabolism of xenobiotics [10]. Unlike most classical heme peroxidases in which the proximal heme ligand is an imidazolate, cytochromes P450 are thiolate-ligated heme proteins in which the heme iron is coordinated to a sulfur atom of the proximal cysteine. These metabolic functions together with the unique structural properties of cytochromes P450 are of great interest to the scientific community.

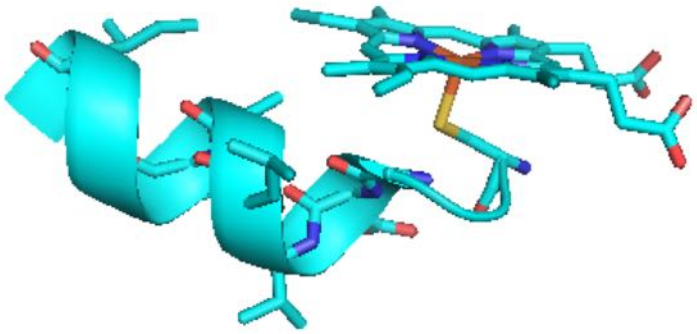

Figure 1.2 The active site of cytochrome P450 3A5 (PDB file 5VEU). The heme iron (brick red) is coordinated to the sulfur atom (yellow) of the proximal cysteine.

The catalytic cycle of cytochromes P450 has been proved to consist of seven steps with utilization of NAD(P)H. The first step is initiated by the binding of a substrate to the active site of P450, which induces a conformational change in the enzyme, resulting in the

conversion of the heme iron from low-spin to high-spin state (2). The change in the electronic state of the active site favors the transfer of an electron from NAD(P)H via an electron transfer chain, reducing the ferric heme iron to the ferrous state (3). Then a molecular oxygen binds covalently to the ferrous ion to form [Fe^{3+}—O_2], which is rapidly reduced by a second electron transfer to produce a negatively charged per-oxo group [Fe^{3+}—O_2^-] (4). The O_2^{2-} then reacts with two protons from its surrounding amino acid side chains, releasing water and leaving an oxo-ferryl porphyrin cation radical complex [(Fe^{4+}=O^+)], Compound I (6). Compound I is proposed to be protonated by the substrate to form transient Fe^{IV}—hydroxide complex (Compound II) (7), which further reacts to the radical to generate the oxygenated product [11]. Moreover, in the absence of reducing cofactors NAD(P)H, a ferric P450 would react with hydrogen peroxide or organic peroxides through a "peroxide shunt" pathway to undergo several specific reactions [12], [13].

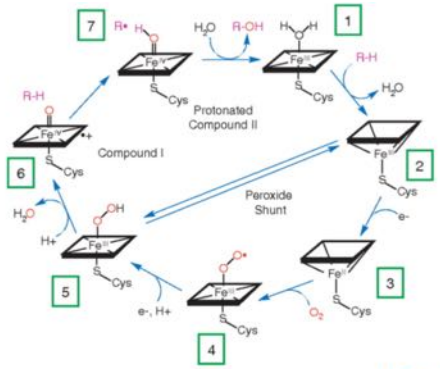

Figure 1.3 The catalytic cycle of cytochrome P450-BM3 (CYP102A1) and peroxide shunt pathway [11].

1.3 Introduction to Chloroperoxidase

1.3.1 Structural Properties of Chloroperoxidase

Chloroperoxidase (CPO), a thiolate-ligated heme protein, was first isolated from filamentous fungus *C. fumago* by Morris and Hager in 1966 [14]. The primary industrial application of this enzyme is to catalyze the chlorination in the biosynthesis of the antibiotic caldariomycin [15, 16]. Spectroscopic investigations combined with crystallographic studies have demonstrated that chloroperoxidase is a hybrid of peroxidase and cytochrome P450 [17]. As a member of heme peroxidase, CPO contains a heme b (iron protoporphyrin IX), a prosthetic group as found in most typical peroxidases. However, similar to P450, the heme-iron in CPO is coordinated to a sulfur atom of the proximal cysteine, which enables CPO to differ significantly from classical peroxidases in which the heme iron is penta-coordinated to the nitrogen atom of the imidazole group of the proximal histidine. In addition, the proximal helix situated in the C-terminal is parallel to the porphyrin ring for both P450 and other peroxidases, while the corresponding helix in CPO is located in the N-terminal and is perpendicular to the heme plane [18].

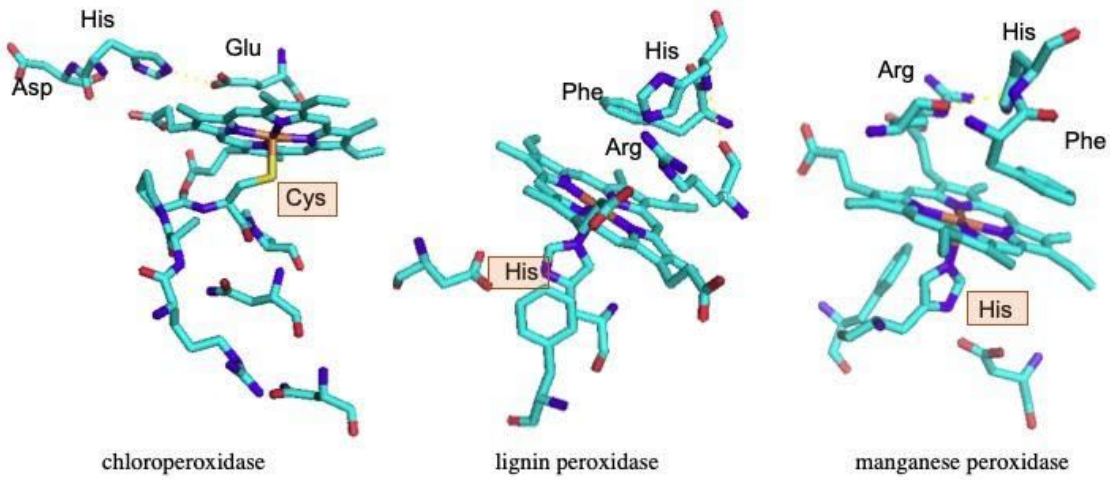

Figure 1.4 Active sites of chloroperoxidase from Calderiomyces fumago (PDB file 2CPO), lignin peroxidase (Lip) from Phanerodontia chrysosporium (PDB file 1LLP) and manganese peroxidase (MnP) from Phanerodontia chrysosporium (PDB file 1YZP).

The heme center together with its surrounding amino acids are critical to catalytic activities of heme proteins. In most peroxidases, substrates interact with the heme edge, so the access to heme center is constrained [19]. Conversely, crystallographic studies have indicated that the substrate-binding pocket of CPO is above the heme center and allows for direct access to the heme, which is analogous to P450 [20]. Although CPO shares a similar polar distal pocket with other peroxidases, unlike that in P450 who possesses non-polar residues, the two conserved distal residues critical to the proper function of most classical peroxidases, a histidine and an arginine, do not exist in CPO. Instead, a glutamic acid (Glu183) which contributes to the peroxide bond cleavage to generate the active intermediate Compound I in the process of CPO-catalyzed reactions, is observed in the distal pocket [21].

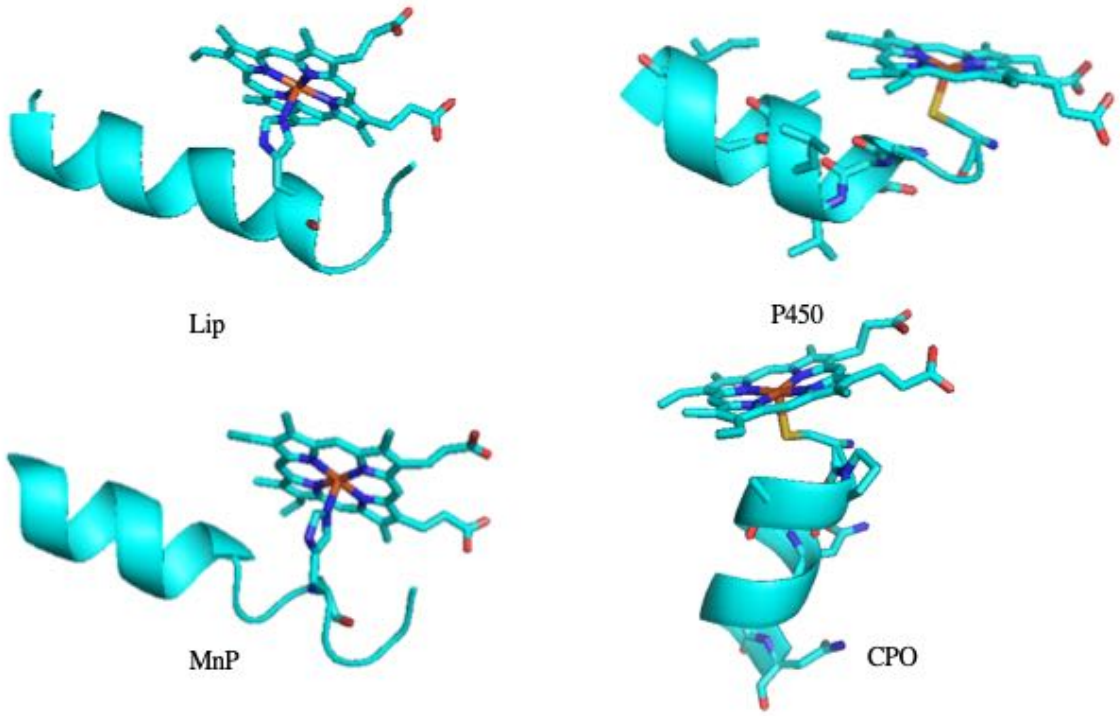

Figure 1.5 Proximal helix of chloroperoxidase cytochrome P450 3A5 (PDB file 5VEU), CPO from Calderiomyces fumago (PDB file 2CPO), lignin peroxidase (Lip) (PDB file 1LLP) and manganese peroxidase (MnP) (PDB file 1YZP). For P450, Lip and MnP, the proximal helix is parallel to porphyrin ring while in CPO the proximal helix is perpendicular to the heme plane.

1.3.2 Chloroperoxidase-catalyzed Reactions

In addition to its unique structure, CPO is notable among heme-containing enzymes given that it catalyzes a broad spectrum of reactions, including peroxidase reactions, catalase reactions and P450-like oxidation reactions [22]. In terms of CPO, the catalytic cycle starts with the binding of a hydrogen peroxide molecule, followed by oxidation of the heme iron in the high-spin ferric state or resting state, leading to the formation of Compound I, an oxo-ferryl porphyrin cation-radical ($[Fe^{4+}=O]^{\cdot+}$). The proximal hydrogen of the peroxide is then deprotonated by the distal amino acid side chain, Glu183, forming

the transient intermediate [Fe(III)-OOH] Compound 0. Then the Glu183 forms a hydrogen bond with the distal oxygen of the peroxide and donates a proton to the departing OH radical to break the O-O bond, releasing H_2O and thus leaving an oxo-ferryl porphyrin cation radical complex [Fe(IV)=$O^{\cdot+}$] Compound I [21], [23]. Unlike P450 which requires NADP or NADPH as a cofactor and involves molecular oxygen (i.e. O_2), CPO utilizes H_2O_2 as the oxygen source, via the 'peroxide shunt' pathway, in which the activation of oxygen or participation of cofactor is not required. Once Compound I forms, CPO is able to follow different pathways to undergo various reactions, including peroxidation, halogenation, oxygen insertion and dismutation pathways [24-27]. Thus, reactions catalyzed by CPO are highly efficient and versatile.

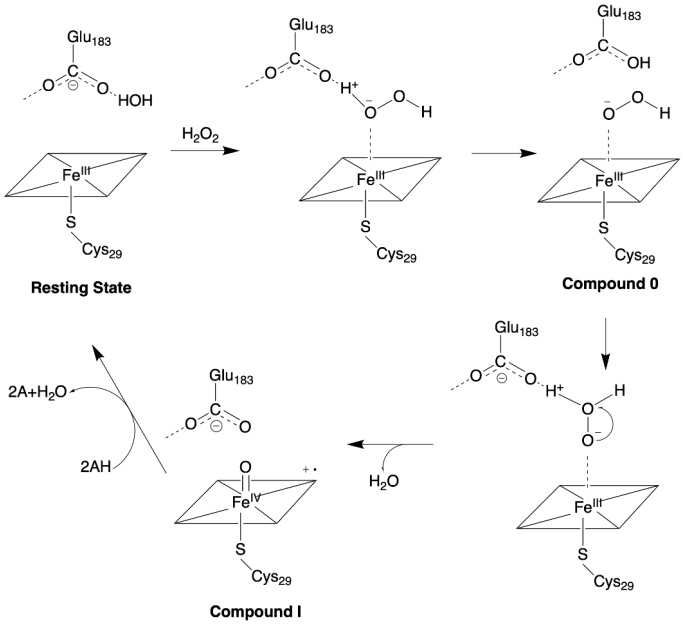

Figure 1.6 Schematic representation of the consensus formation of CPO-Compound 0 and CPO-Compound I.

Reaction Type	
Halogenation	$RH + H_2O_2 + X^- + H+ \rightarrow R—X + 2H_2O$
Dehydrogenation	$2RH + H_2O_2 \rightarrow R—R + 2H_2O$
H_2O_2 Decomposition	$2H_2O_2 \rightarrow O_2 + 2H_2O$
Oxygen Insertion	$RH + H_2O_2 \rightarrow R—OH + H_2O$

Table 1.1 Reactions catalyzed by chloroperoxidase.

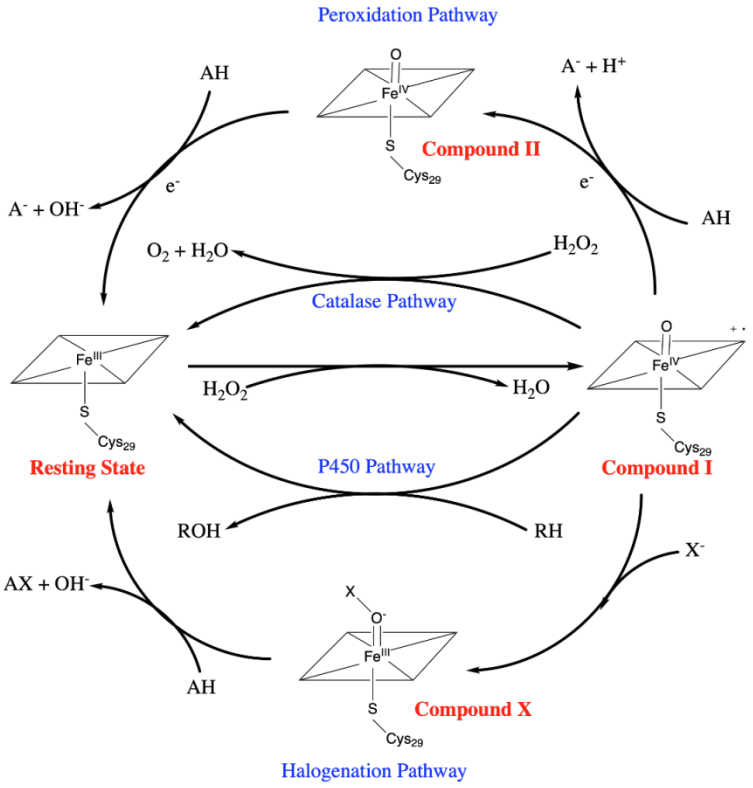

Figure 1.7 Overall catalytic cycle of chloroperoxidase. First, hydrogen peroxide removes one electron from the iron atom and the other electron from the porphyrin of native CPO to form a oxyferryl (Fe4+=O) porphyrin π cation radical. Then the Compound I is reduced to the resting state through peroxidation, catalase, P450 (RH represents organic substrate) or halogenation (X- represents halide ion) pathway.

1.3.3 Chloroperoxidase Catalyzed Enantioselective Transformations

1.3.3.1 Asymmetric Epoxidations

Chloroperoxidase has been developed to catalyze enantioselective epoxidation of olefins because reactions occur cofactor-independently and produce enantiopure products with excellent enantiomeric excesses [28]. Substrates like simple alkenes and some derivatives have been proved to yield corresponding enantio-products with over 90% ee. Among them, cis-alkenes, typically unsaturated carboxylic esters, terminal bromine substituted alkenes and unsaturated acetic esters have been investigated [29-31]. Although most of these epoxidation reactions show high conversion rates and yields, several substrates with longer carbon chains present low reactivity or productivity, even they have exhibited excellent enantioselectivities [30].

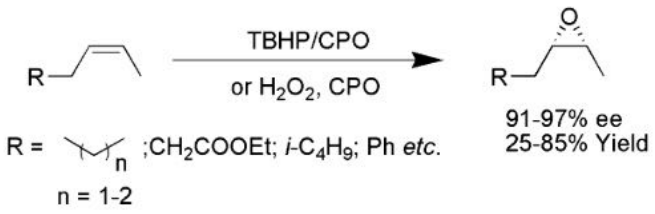

Figure 1.8 Schematic representation of CPO-catalyzed enantioselective epoxidation of simple alkenes and their derivatives.

substrate	product	conversion, ee
	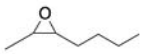	100%, ee 95%
		40%, ee 95%
	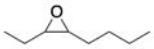	20%, ee 95%
		20%, ee 94%

Table 1.2 CPO-catalyzed epoxidation of some simple olefins with excellent enantioselectivity.

However, in cases of trans-olefins, epoxidations hardly occur. Aleksey Zaks and David R. Dodds's work indicated that CPO-catalyzed oxidation of trans-2-heptene preferred to form aldehyde (35% yield) rather than epoxide. Similarly, in oxidations of trans-3-heptene and trans-β-methylstyrene, no epoxidation products were observed [32]. Interestingly, the epoxidation of trans-[^{2}H]-styrene catalyzed by chloroperoxidase was proved to occur without significant decrease of enantioselectivity [33], which indicated that styrene and its derivatives might be reactive substrates. Previous studies showed that styrene was oxidized to a mixture of 40% styrene epoxide (ee 49%), 24% phenylacetaldehyde and 4% phenylacetic acid; while α-methylstyrene was able to form epoxide (ee 89%) with high efficiency (90% conversion). The corresponding aldehyde and acetic acid were also observed [32, 34]. The epoxidation of cis-β-methylstyrene proceeds efficiently with excellent stereoselectivity (ee 96%), which is consist with the above-mentioned statement: cis-alkenes could function as good substrates for CPO-catalyzed epoxidations.

substrate	epoxide	byproduct
	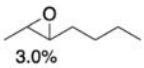 3.0%	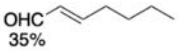 35%
	no epoxide is formed	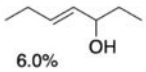 6.0%
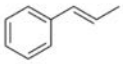	no epoxide is formed	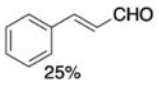 25% 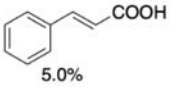 5.0%
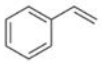	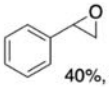 40%, ee 49%	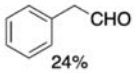 24% 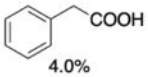 4.0%

Table 1.3 CPO-catalyzed asymmetric epoxidation of trans-alkenes.1.3.3.2 Factors Related to Stereoselectivity of Epoxidation

1.3.3.2 Factors Related to Stereoselectivity of Epoxidation

1.3.3.2.1 Reaction Conditions

Oxidants are required for classic asymmetric epoxidation of alkenes and their derivatives, as the same is true for CPO-catalyzed reactions. Typical oxidants including hydrogen peroxide (H_2O_2) and tert-butyl hydroperoxide (TBHP) were both investigated and little influence on the enantioselectivity was observed, even TBHP could speed up the epoxidation of 3-chloropropene [35]. It is worth noting that CPO is able to decompose H_2O_2 into oxygen and water [36], so there is one possible problem that the catalase activity of CPO might far exceed its epoxidation rate [37]. Thus, TBHP has been widely applied in most studies of CPO catalyzed epoxidation reactions. Chloroperoxidase was usually dissolved in 0.1 M phosphate buffer, pH 5.9, with relatively high stability. Once in alkaline or strong acidic conditions, CPO would become extremely unstable [35, 38], so

epoxidation reactions catalyzed by CPO are usually conducted in citrate or phosphate buffer at pH 5.0 or pH 5.5.

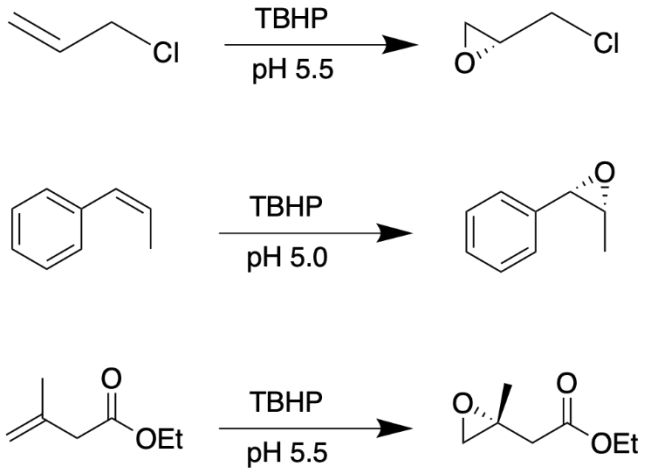

Figure 1.9 Conditions of CPO-catalyzed epoxidations of 3-chloropropene [35], cis-β-methylstyrene [28], and 3-methyl-3-buten-ol [39].

It should be noted that alkenes exhibit higher reactivity and enantioselectivity once acetone is used as a co-solvent, except for cis-β-methylstyrene [28]. However, the presence of organic solvents like DMSO, DMF, CH_3OH, CH_3CN and CH_3OCH_3 was observed to inhibit epoxidation of CPO-catalyzed 3-chloropropene, because the conformation and the local environment around the active site had been changed [35]. In most cases, epoxidations catalyzed by CPO are carried out in aqueous media. The study of non-aqueous system was first reported by Manoj, which demonstrated the epoxidation of indene in glycerol in order to eliminate the hydrolyzation of epoxide products in the presence of water [40]. Interestingly, CPO was observed to remain highly active even in 99% (v/v) tert-butanol, which shed light on the study of CPO-catalyzed reactions in non-aqueous media [37]. Moreover, CPO was found to conjugate with polystyrene to form a surfactant-like structure that self-assembled at oil-water interfaces and catalyze styrene epoxidations,

resulting in a relatively enhanced catalytic efficiency, as compared to that in reactions under the bulk aqueous phase. This improvement could be explained by theories including the simultaneous access to the reactants dissolved in both aqueous and non-aqueous phases, the suppression of unwanted side reactions by the interface-bound CPO, the stabilization of CPO by restricting its exposure to harmful reactants, and the allowance for continuous feeding of reactants [41]. Recently, ionic liquids were reported to enhance the activity, stability and enantioselectivity of epoxidations due to the increase of substrate solubility in the reaction medium and the improvement in affinity and selectivity of CPO to substrate [42].

1.3.3.2.2 Steric Effects of Substrates

Although chloroperoxidase is able to catalyze a broad spectrum of reactions, the number of substrates presenting excellent stereoselectivity for epoxidations are limited. As reported from previous studies, the configuration of substrate *does* affect the reactivity and enantioselectivity of epoxidations. Some cis-alkenes have been found to be good candidates, among which cis-disubstituted alkenes bearing alkyl substituents are outstanding [31]. Alkyl substituents with branches were also acceptable, and the branch position has been found to be related to enantioselectivities [28]. On the other hand, trans alkenes, even disubstituted ones exhibit poor reactivity for epoxidations, which could be attributed to the conformational mobility of the cis-olefin's transition state [43].

As for 1, 1-disubstitued terminal alkenes, 2-methyl-1-alkenes were observed to be oxidized to form (R)-epoxides displaying high enantioselectivities, with less than one equiv of CPO [31, 34, 44]. Noticeably, the carbon chain length of aliphatic terminal alkenes was

proved to affect the stereoselectivity. In the case of CPO-catalyzed epoxidation of ω-bromo-2-methyl-1-alkenes, the conversion rate declines when enantioselectivity increases as the chain lengthens to an optimum and then starts to decrease. Substrates with short carbon length (methallyl bromide and 4-bromo-2-methyl-1-butene) displayed modest stereoselectivity, which could be elucidated by the little asymmetry effect derived from slight difference between bromide atom and methyl group substitutions. The decrease of enantioselectivity observed in 2-methylalkenes with, especially, long chains resulted from higher energy required by the substrate to overcome the steric restrictions in the enzyme's active site [29]. Although some monosubstituted olefins, such as allylbenzene and allyacetate, are poor substrates for CPO and also inhibit the enzyme activity, high ee values and product yields could still be observed once the ethenyl is attached directly to a bulk group [34, 44].

substrate	epoxide	ee %	yield %
	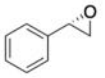	49	89
	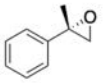	89	55
	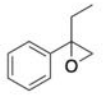	81	1
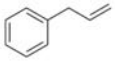	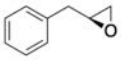	37	7
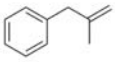	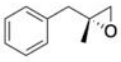	70	41
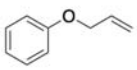	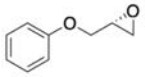	46	1
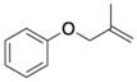	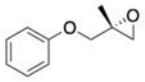	89	22
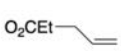	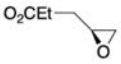	24	12
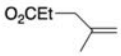	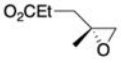	94	34
		10	2
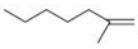	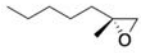	95	23

Table 1.4 Epoxidations of various substrates by CPO. Cis-disubstituted alkenes bearing alkyl substituents are excellent candidates for enantioselective epoxidations, while trans-alkenes are poor substrates.

1.3.3.3 Effects of Distal and Proximal Pockets on CPO-catalyzed Epoxidation of Olefins

The catalytic cycle of CPO starts with the addition of oxidant (eg. H_2O_2 or TBHP) and the basicity of the deprotonated Glu183 in the distal pocket, leading to the formation

of the transient intermediate [Fe(III)-OOH] Compound 0. This iron hydroperoxide species undergoes a heterolytic O—O bond cleavage to form Compound-I (CPO-I), an oxo-ferryl π-cation radical intermediate which has been recognized as a critical intermediate [21]. CPO possesses a peroxidase-like distal pocket, but a glutamic acid (Glu183), instead of a histidine which is commonly employed to form the Compound I in traditional heme peroxidases, plays the role [45]. Also, His105 was proposed to participate in CPO-I formation via hydrogen bonding with Glu183 and, at the same time, helps to position Glu183 in the most favorable orientation to facilitate heterolytic cleavage of the peroxide bond, ensuring the formation of CPO-I [46, 47].

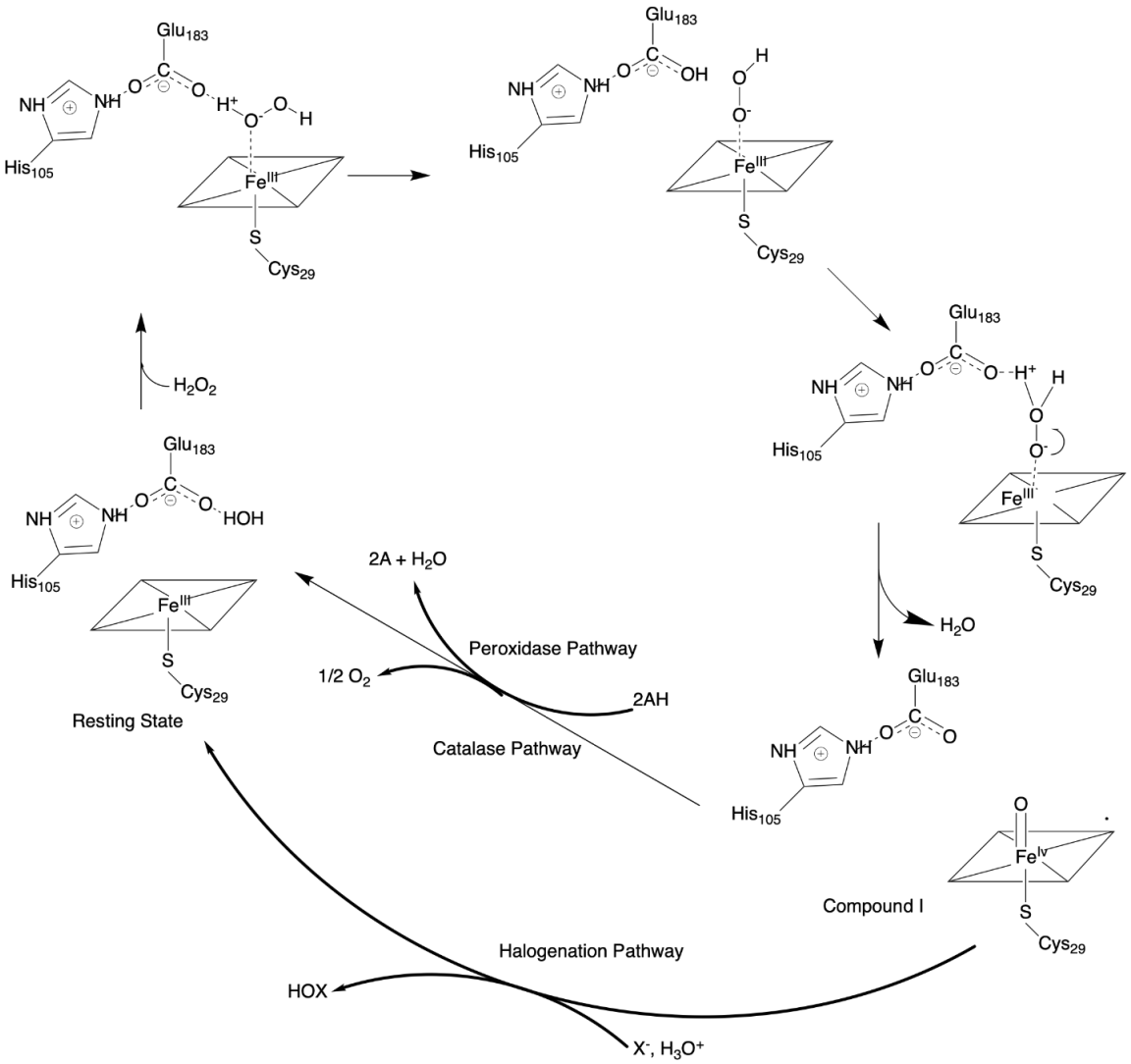

Figure 1.10 Schematic representation of proposed hydrogen bonding effects of His105 on the formation of CPO-Compound I.

A site-directed mutagenesis of Glu183 to histidine was found to result in approximately 2.5-fold increase in activity compared to that in wild type CPO epoxidation reaction, possibly due to a closer approach of olefins to the enzyme's active site [48]. Meanwhile, the alkylation of His105 was reported to inhibit epoxidations which are two-electron oxidations, rather than one-electron peroxidations [24]. This disparity indicated that epoxidations proceed via a specific mechanism mainly occurring at the distal pocket, which is quite different from that of one-electron, peroxidase-like oxidations [24, 49].

So far, investigations on the roles of the distal pocket in CPO-catalyzed epoxidation of cis-β-methylstyrene (CBMS) have been focused on density functional theory (DFT) and molecular mechanics (MM) methods [45, 49, 50]. It was found that the distal pocket environment reduces the reaction barrier for epoxidation of CBMS through a flexible method, in which the pocket size is adjusted spontaneously to fit in the binding stage and the transition state. In addition, the Glu183 was observed to interact within the distal pocket to move away from the ferryl oxygen group, rendering access to the heme center for substrates, and consequently transferred the distal pocket from a polar peroxidase-resembling form to a hydrophobic P450-like moiety [49, 50].

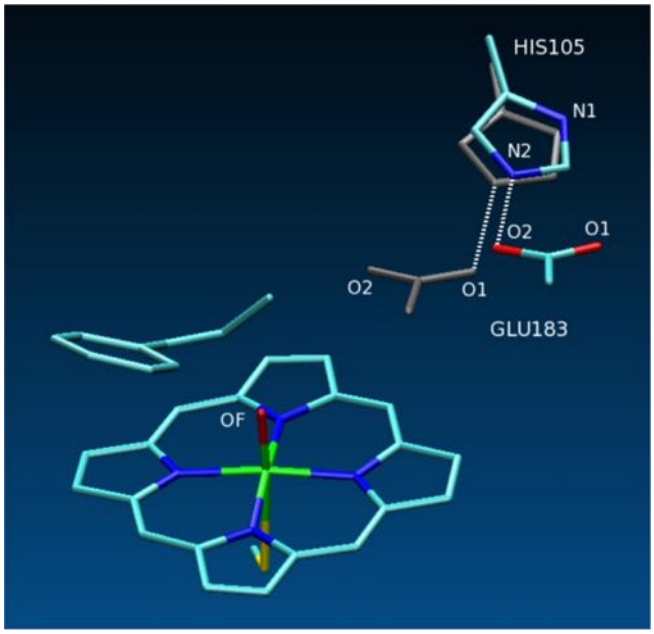

Figure 1.11 The rearrangement of Glu183 in the transition state of CPO (indicated in cyan). CPO's resting state is indicated in grey [50].

Unlike typical heme peroxidases, CPO contains a P450-type proximal pocket, in which the heme iron is coordinated to a sulfur atom of the proximal cysteine. This thiolate ligand is analogous to that found in P450 and has been proposed to act as a strong

electron donor to iron, leading to a trade-off between heme redox potential and the basicity of the distal axial ligand, and consequent cleavage of inert C—H bond in substrates [16, 51]. As for CPO, the sulfur atom in the proximal pocket was found to form hydrogen bonds with surrounding amino acid side chains including Cys29, Leu32 and Ala 31 [17], reducing the barrier to the formation of Compound 0 and thus increasing its stability. Also, these NH−S hydrogen bonds were proposed to reduce the stability of protonated Compound 0 and result in the cleavage of O—O bond [52].

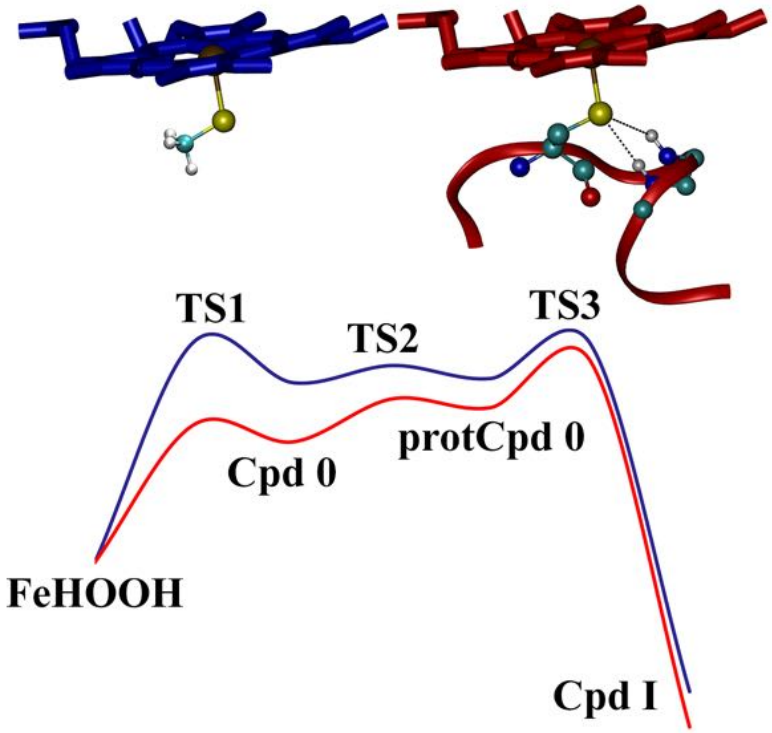

Figure 1.12 Density function theory (DFT) results of the effect of NH—S hydrogen bonds on CPO-Compound I formation. NH—S hydrogen bonds were found to reduce the barrier for the formation of Compound 0 [52].

The thiolate ligand is positioned at the proximal α helix which is perpendicular to the heme plane and has been reported to affect the negative charge on the thiolate ligand [53]. Studies on CPO-catalyzed epoxidation of olefins indicated that the proximal pocket

improved the reaction activity by lowering the rate-limiting barrier through the combination of the NH−S hydrogen bonds with the dipole moment of the proximal helix [34, 54]. Significantly, the replacement of Cys29 with a histidine was observed to catalyze epoxidations with equivalent activity compared to native CPO, which dwarfs the influence of thiolate-ligand [55]. However, the proximal pocket was recently proved to play an essential role on the enantioselectivity of epoxidation reactions, and in this case, it could be termed as much important as the distal pocket. The reason for this comparable effect was that the electron transfer mechanism preference was dependent on the proximal pocket, and inclination to the π* orbitals enabled an interaction of the substrate orientation in the distal pocket with the asymmetry of π-donation by the proximal thiolate [56].

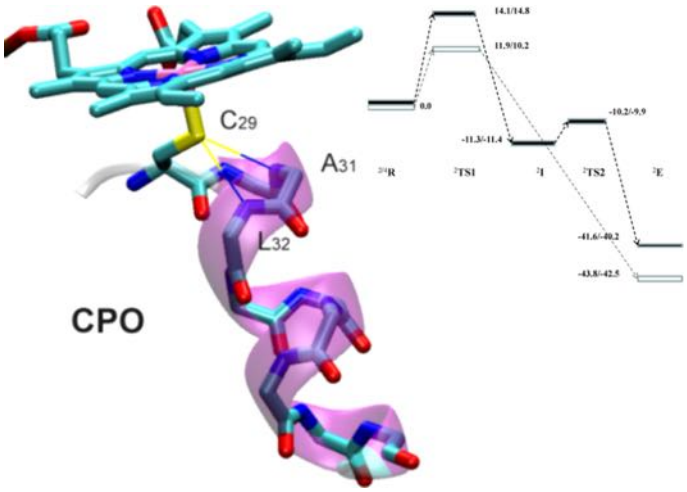

Figure 1.13 The effect of NH—S bonds is amplified by the dipole moment of the proximal helix, which reduces the reaction barrier of CPO-catalyzed epoxidation of cis-β-methylstyrene [54].

1.3.4 Potential Applications in Pharmaceutical and Biochemical Synthesis

(R)-mevalonolactone is an essential intermediate for the synthesis of terpenes, steroids, carotenoids, isoprenoids and vitamins [57-60], thus development of cost-efficient

synthetic routes for this chemical is highly important. The Sharpless asymmetric epoxidation has been widely employed in most chemical methods [61-64], although large scale of application is unavailable due to expensive costs and environmental-unfriendly procedures [58]. Moreover, traditional chemical routes yield relatively low enantioselectivity, while CPO-catalyzed epoxidation of 3-methylbut-3-enoate and derivatives was reported to overcome this challenge [39]. The reactions were performed under a moderate condition with TBHP as oxidant, and substrates like 3-methylbut-3-enoate and 2-methylallyl propionate generally gave excellent enantioselectivity.

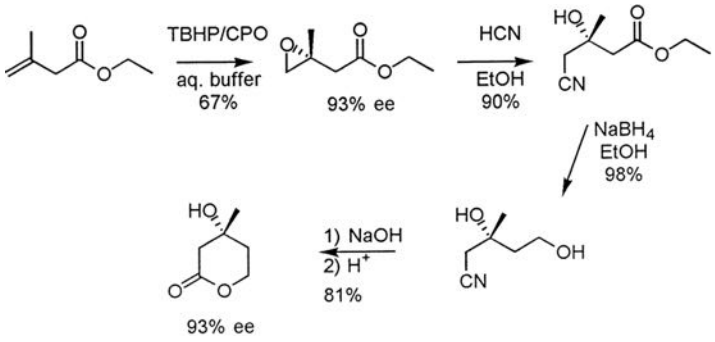

Figure 1.14 The synthesis of (R)-(-)-mevalonolactone [34].

α-methylamino acids were reported to stabilize preferred conformations of peptide backbones due to the restrictions on bond rotations [65], therefore they were recognized as essential building blocks for the synthesis of either medicinal or biochemical products [66-68]. Specifically, α-methyltryptophan, α-methylhistidine, and α-methyldopa have been applied in pharmaceutical field [69], while α-methylcysteines were found to have biological potential for natural product synthesis [70]. Studies have indicated that aziridine carboxylate esters are common precursors to optically active α-methylamino acids, which undergo high regio- and stereo-selective ring-opening reactions with either heteroatom

nucleophiles or carbon nucleophiles [32, 65, 71, 72]. Although various chemical methods for the synthesis of aziridine carboxylates have been well-established, most of them require tedious works with relatively modest yields and enantioselectivities [72-74]. Particularly, chloroperoxidase was found to epoxidize methylamine to produce (R)-enantiomer with excellent stereoselectivity (ee 92%). This reaction undertakes 4 simple steps and is not specifically strict on the purity of choloperoxidase, because supernatant of *C. fumugo* culture medium is observed to show similar results with purified enzyme [66].

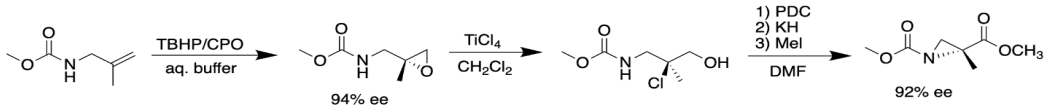

Figure 1.15 The synthesis of R.-dimethyl 2-methylaziridine-1,2-dicarboxylate [66].

As mentioned above, cis-β-methylstyrene has been recognized as an excellent substrate for CPO, and the epoxidation product cis-β-methylstyrene oxide could be easily converted to the decongestant pseudoephedrine by oxirane- opening reaction with methyl amine [34, 75, 76]. Phenylethanolamines and their derivatives could serve as precursors of many drugs, indicating potential applications of CPO-catalyzed asymmetric epoxidations in pharmaceutical synthesis.

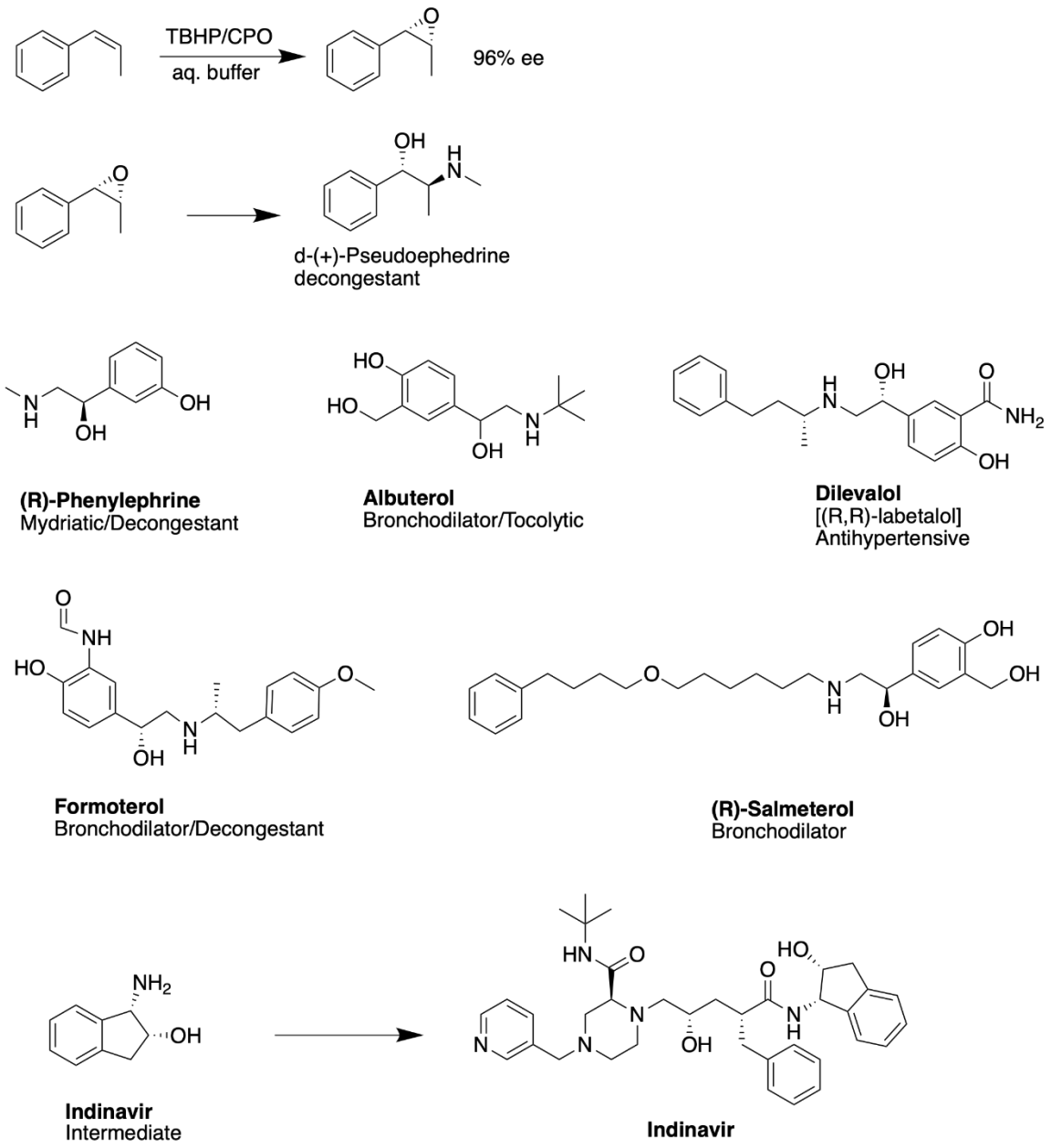

Figure 1.16 Possible phenethylamine-type target drugs from substituted styrene.

1.4 Asymmetric Sulfoxidations

Besides epoxidations, chloroperoxidase is able to catalyze another enantioselective oxidation reaction, the sulfoxidation of various alkyl, aryl, dialkyl and heterocyclic sulfides [77], generating (R)-sulfoxides as the main product [78], [79], [80], [81]. Specifically, β-carbonyl sulfides have been recognized as excellent substrates for CPO-catalyzed sulfoxidations once H_2O_2 is used as oxidant. However, substrates methylphenyl sulfide and 2-(ethylthio)cyclohexane-1-one were not observed to be oxidized [82]. The reason for this poor reactivity is the presence of organic solvents like ethanol, acetonitrile and acetone, since methanol is a substrate for CPO and either acetonitrile or acetone was indicated to decrease the enantioselectivity of CPO-catalyzed sulfoxidations [83], [84].

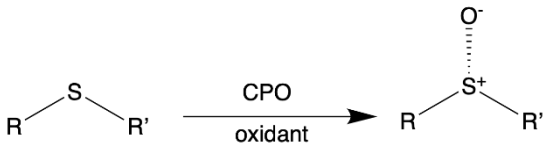

Figure 1.17 Chloroperoxidase-catalyzed sulfoxidations of β-carbonyl sulfides.

Similar with epoxidations, substrates with long carbon chains are poorly reactive because there is not enough space in the active site of CPO for large substrate. This was demonstrated in the study of CPO-catalyzed propyl phenyl sulfide oxidation, in which the product yield is only 3% [85]. Steric effects like the sulfur atom bonded alkyl groups, are critical to sulfoxides productions. Compared with methyl p-tolyl sulfide, the substrate ethyl p-tolyl sulfide and isopropyl p-tolyl sulfide were observed to produce sulfoxides with significantly lower yields and enantioselectivities (Table I.5) [80]. Also, electronic effects

influence both chemical and optical yield of the reaction. That is, para substitution was reported to present higher enantioselectivity compared to ortho substitution (Table I.6) [80]. The aromatic ring was observed as an important group for substrates since activating or poorly deactivating substituents on aromatic rings can produce sulfoxides with high ee values [80].

substrate	product	yield (%)	ee (%)
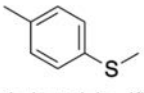 methyl p-tolyl sulfide	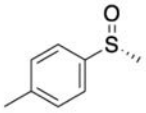 (R)-methyl p-tolyl sulfoxide	60	86
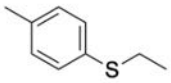 ethyl p-tolyl sulfide	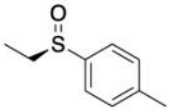 (R)-ethyl p-tolyl sulfoxide	40	30
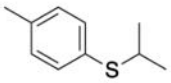 isopropyl p-tolyl sulfide	N/A	24	0
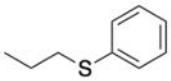 propyl phenyl sulfide	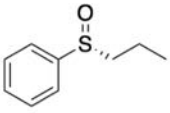 (R)-propyl phenyl sulfoxide	3	n.d.

Table 1.5 Steric effects of substrates on CPO-catalyzed sulfoxidations. n.d.-not determined.

Other conditions like the pH of buffer and the reaction temperature are critical to the stereoselectivity of sulfoxidations. Investigations on CPO-catalyzed oxidations of methyl p-tolyl sulfide, p-methoxyphenyl methyl sulfide and ethyl p-tolyl sulfide indicated

that the enantioselectivity is about 20% higher at pH 5.0 than at pH 7.0 [80]. Besides, increased temperature was observed to lower the enantioselectivity. Studies of CPO-catalyzed sulfoxidation of methyl p-tolyl sulfide showed that the use of H_2O_2 decreased the optical yield significantly, while CPO would not be denatured in the reaction system with the use of TBHP, one of the best oxidants [80]. In addition, the concentration of the oxidant H_2O_2 was reported to affect the yield of CPO-catalyzed sulfoxidations, because large amount of H_2O_2 leads to inactivation of CPO [85]. Thus, in sulfoxidation reaction system, the concentration of H_2O_2 should be controlled as low as possible.

substrate	product	yield (%)	ee (%)
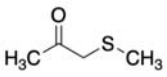	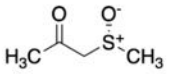	100	> 99
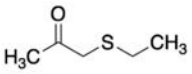	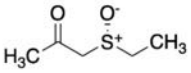	100	> 99
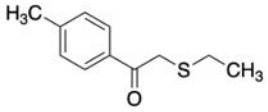	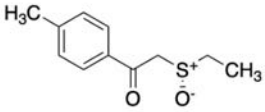	31	92
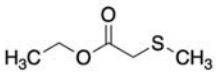	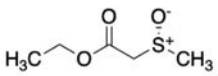	97	94
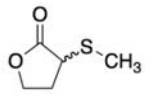	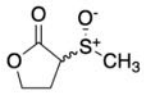	45	> 95

Table 1.6 Electronic effects of substrates on CPO-catalyzed sulfoxidations.

CPO-catalyzed stereoselective sulfoxidations carry huge potential significance since the enantiopure sulfoxides are essential building blocks in asymmetric synthesis of pharmaceuticals. One typical example is the synthesis of (R)-modafinil, an effective drug in treating excessive drowsiness related to sleep disorders, narcolepsy, and obstructive sleep [86]. CPO was reported to catalyze sulfoxidation of 2-(diphenylmethylthio) acetamide, with (R)-modafinil yield of 40.8% and excellent enantioselectivity [87]. Significantly, the organosulfur compounds in straight-run diesel fuel could be oxidized enzymatically by CPO to produce respective sulfoxides or sulfones, and these oxidation products could be removed through distillation, indicating potential applications of of CPO-catalyzed sulfoxidations in environmental protection [88], [89].

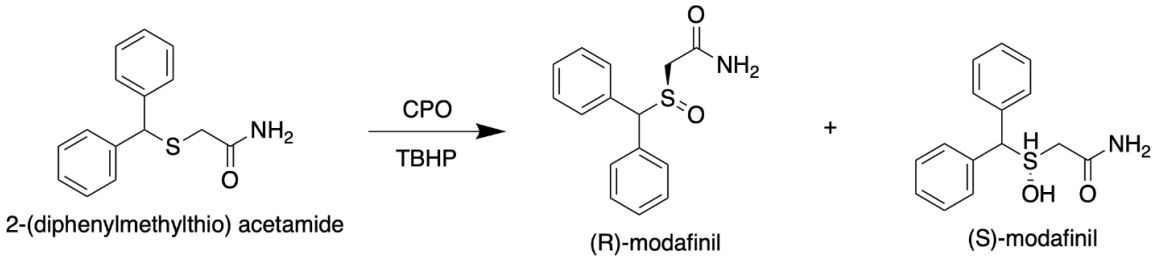

Figure 1.18 Scheme Sulfoxidation of CPO-catalyzed 2-(diphenylmethylthio) acetamide.

The work presented in this dissertation addressed the effects of the thiolate ligand as well as the distal pocket on CPO-catalyzed enantioselective epoxidations. In this work, the structure of recombinant CPO expressed in *A. niger* system was obtained by crystallography to confirm the feasibility of this heterologous expression system. Since Cys 29, Phe 103 and Phe 186 were reported to be related to the high stereoselectivity of CPO-catalyzed epoxidations, three CPO mutants including C29H, F186A and F103A/F186A were introduced via site-directed mutagenesis and expressed successfully

in *A. niger*. In order to explore roles of these specific amino acid side chains, crystallography was applied to obtain structures of mutant CPO. Furthermore, three typical substrates were used to co-crystallize with CPO to investigate the structural basis for CPO-catalyzed enantioselective epoxidations by resolving the three-dimensional structure of protein-substrate complexes. Finally, the possibility of expressing CPO in *E. Coli* was explored with the assistance of an outer-membrane heme receptor gene. Our results showed that although CPO can be expressed in the system we created, the protein is essentially inactive, possibly due to lack of glycosylation that is critical to proper folding of CPO.

CHAPTER II. THE CRYSTAL STRUCTURE AND MOLECULAR MODELING OF CHLORPEROXIDASE-SUBSTRATE COMPLEX

2.1 Background and Theory

Enantiopure epoxides are extremely essential precursors for fine chemical industry, especially for the pharmaceutical, agrochemical and biochemical industries [1]. However, harsh reaction conditions, low yield of target products, and large amounts of undesirable side products always hinder the synthesis [2, 3]. Due to the increasing demand for optically pure chiral compounds and wide applications of epoxides in medicinal and industrial synthesis, development of efficient approaches to the synthesis of enantiopure epoxides has been highly important. Traditionally, chemical methods including the Sharpless epoxidation [4], the Katsuki-Jacobsen epoxidation, [5] and the Shi's epoxidation [6] are employed for enantioselective reactions, while biocatalysts are more promising since they are capable of catalyzing alkene epoxidations under mild conditions, and more significantly, with excellent enantiomeric excesses. Among all available enzymes, cytochromes P450 were reported to catalyze epoxidations with high yield and stereoselectivity. Unfortunately, the dependence on cofactors like NAD(P)H results in high expenses, restricting large-scale applications of P450-catalyzed epoxidations [7].

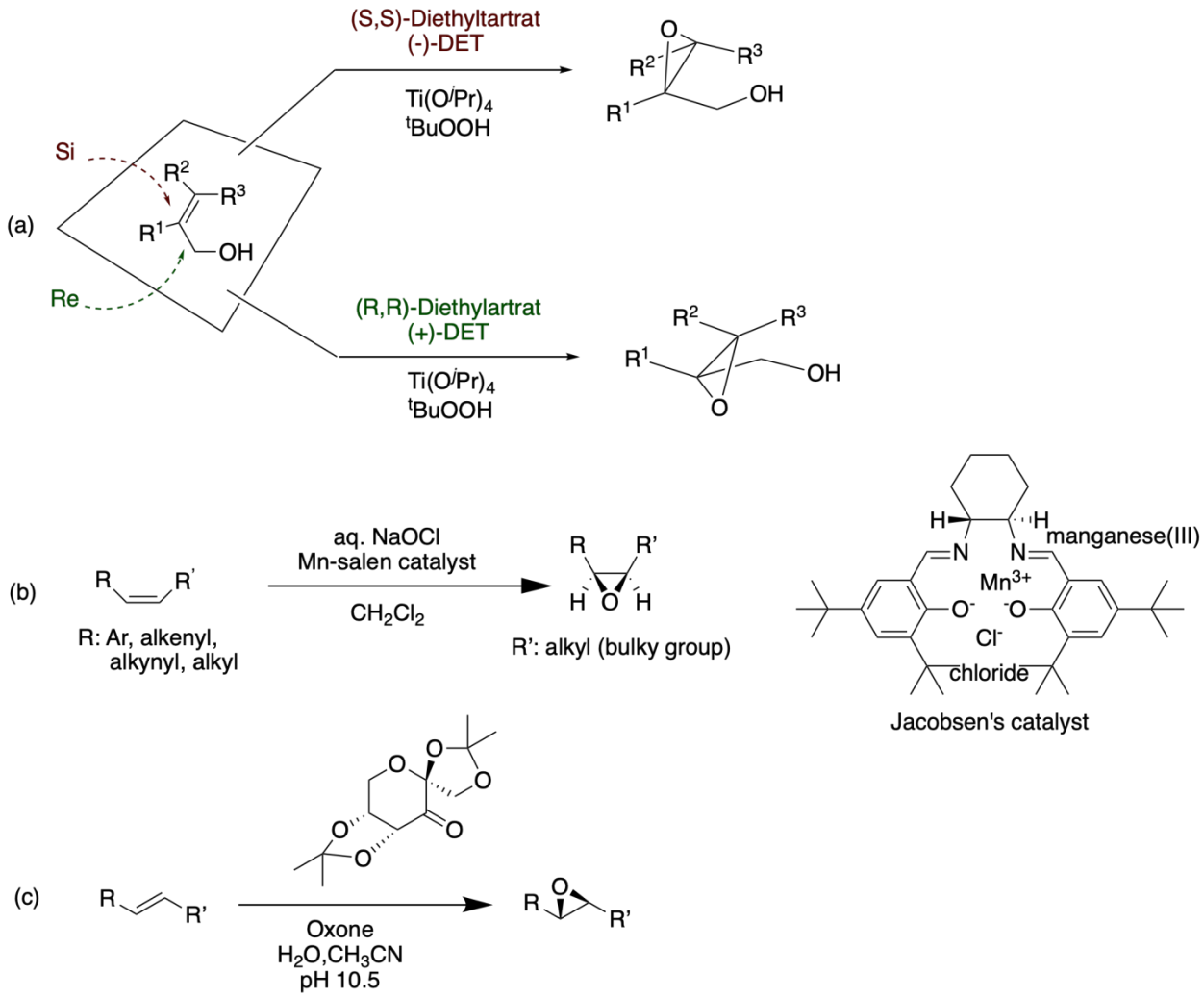

Figure 2.1 Schemes of Sharpless epoxidation (a), Katsuki-Jacobsen epoxidation (b) and Shi's epoxidation (c).

Significantly, another specific enzyme, chloroperoxidase (CPO) has emerged as a promising enzyme for numerous synthetic applications. CPO-catalyzed epoxidations have a biotechnological potential because they are highly effective in terms of enantioselectivity. Many enantiopure epoxides derived from CPO-catalyzed reactions have been considered to serve as chiral synthons for drug and natural product synthesis [8]. For example, the epoxide generated from *cis-β*-methylstyrene is a crucial intermediate for the synthesis of the decongestant D-(+)-pseudoephedrine [8]. CPO-catalyzed epoxidation of 3-methylbut-

3-enoate and their derivatives, was reported to afford critical intermediates for the synthesis of (R)-mevalonolactone [9]. Methylamine was found to be epoxidized with the catalysis of CPO to yield (R)-enantiomer with high stereoselectivity (ee 92%) [10].

So far, large number of investigations via either experimental approaches [1, 11-15] or computational simulations [16-23] have been undertaken. Although several factors like the nature of oxidant, the chain length and electric properties as well as steric effects of substituents on the aromatic rings of the substrates, have been proposed to influence asymmetric oxidations, the specific mechanism of CPO-catalyzed enantioselective transformations remain to be elucidated. Many studies have indicated that the unique P450-like polar proximal pocket contributes to epoxidations: hydrogen bonding to the sulfur atom of the proximal cysteine and the dipole moment of the proximal helix increase the electron density transfer to the proximal pocket residues, and subsequently decrease the epoxidation barrier [20]. In addition, CPO's crystal structure demonstrates the side chains at the bottom of a small channel above the heme are able to react with substrates, indicating conformational adjustments of these side chains to facilitate substrate binding [24].

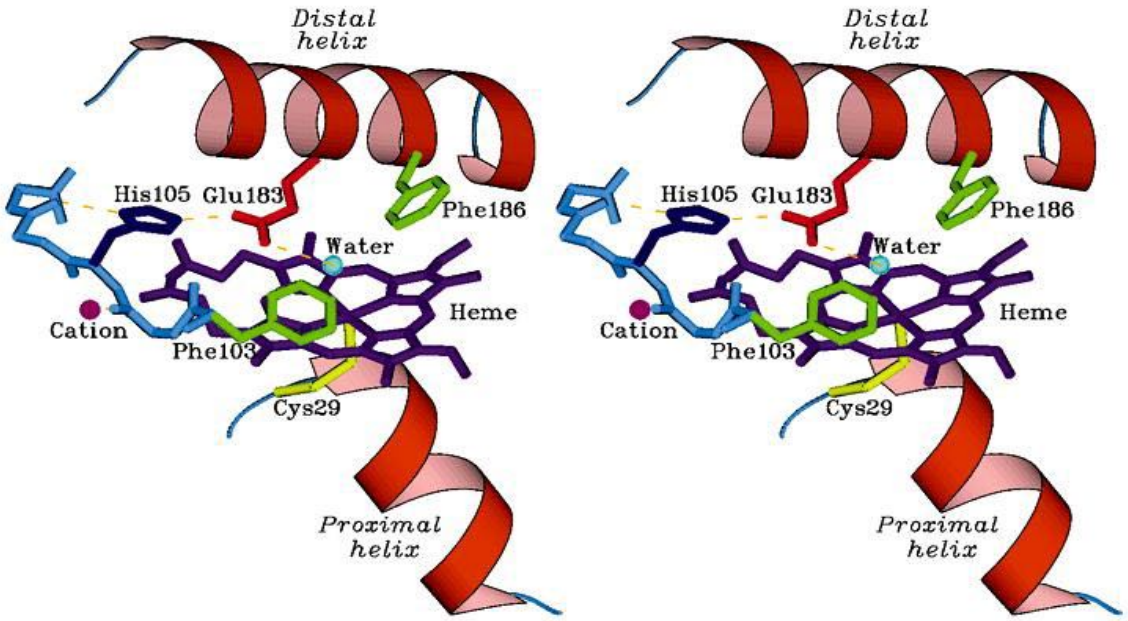

Figure 2.2 Stereoview of the CPO active site. Substrates are proposed to be sandwiched between Phe103 and Phe186 [17].

Chloroperoxidase was reported to catalyze the peroxidative chlorination of cyclopentanedione (CPD) to produce late intermediates in the biosynthesis of caldariomycin [25]. Particularly, the crystal structure of CPO-CPD complex was determined successfully and showed that CPD binds above the heme and is sandwiched between Phe103 and Phe186, which leads to a minor conformational change in the substrate binding site [26]. This study indicated the side chain of Phe103 moved 0.5 Å away from the active site to provide space for substrate binding. Therefore, co-crystallization of CPO-substrate complex is critical to the investigation of specific mechanisms of CPO-catalyzed reactions, especially for the interaction between substrate and the active site of CPO.

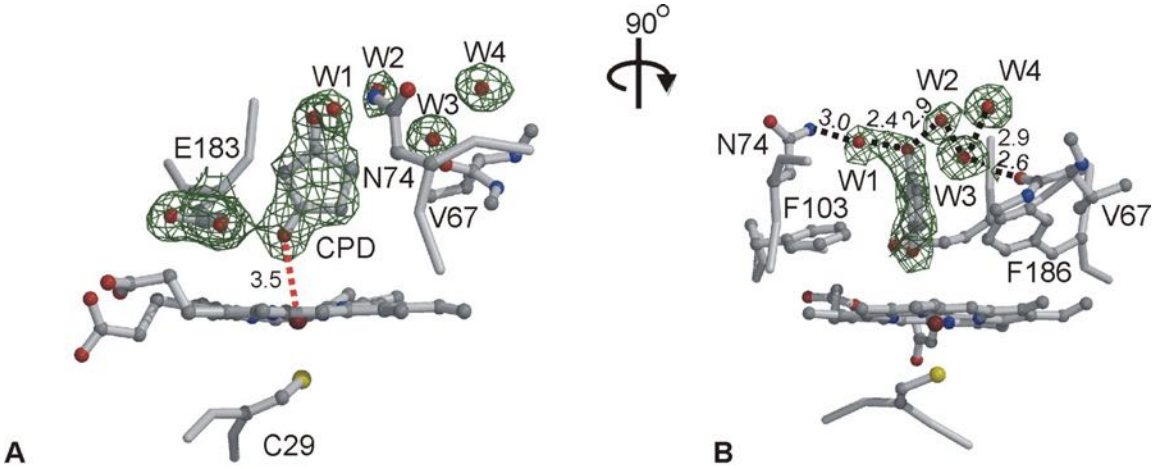

Figure 2.3 Stereoview of CPO-CPD complex at the active site in two orientations. CPD is positioned above the heme and sandwiched between Phe103 and Phe186 [26].

Significantly, CPO was reported to catalyze the epoxidation of 3-methylbut-3-enoate and its derivatives with excellent enantioselectivity [9], so three typical substrates, ethyl 3-methyl-3-butanoate [9], 2-methylallyl propionate [27] and 3-methylbut-3-en-1-yl [9], were used to co-crystallized with the wild type chloroperoxidase. Additionally, molecular modeling and dynamics simulations of CPO with ethyl 3-methyl-3-butanoate was also performed to provide structural and energetic insights into CPO-catalyzed epoxidation of olefins.

substrate	epoxide	ee %
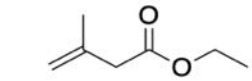 ethyl 3-methyl-3-butanoate	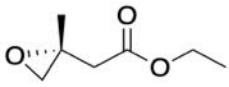	93
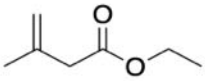 2-methylallyl propionate	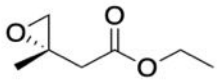	94
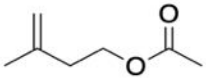 3-methylbut-3-en-1-yl	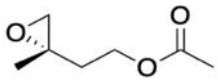	43

Table 2.1 CPO-catalyze epoxidation of 3-methylbut-3-enoate and its derivatives.

2.2 Experimental Methods

2.2.1 Materials and Reagents

Caldariomyces fumago (ATCC catalog #16373) was purchased from America Type Culture Collection (ATCC) (Manassas, VA). All buffers and media were freshly prepared using water purified through Milli-Q Biocel (Millipore, Billerica, MA). All other chemicals and materials were purchased from Fisher Scientific (Waltham, MA) unless otherwise specified.

2.2.2 Expression and Purification of Chloroperoxidase

2.2.2.1 Caldariomyces fumago Culture

In order to express wild type CPO, frozen stocked *C. fumago* was spread on PDA (potato dextrose agar) plate and grew at room temperature for about one week. Then the colony on PDA plate was cut and transferred into six 125 mL flasks with 50 mL of liquid

culture medium containing fructose. The fructose rather than glucose was applied as the carbon source since *C. fumago* was reported to express CPO at a higher level in fructose media [28]. Then the cut colony was disrupted into small pieces by a blender to grow under the condition of 20 ℃， 200 rpm. After about 2 days, the MCD (monochlorodimedone) kinetic assay [29] was performed to confirm the secretion of CPO. Once a negative slope had been observed, cultures were transferred from the six 125 mL flasks to six 2 L flasks containing 1 L of medium, respectively, under the same growing conditions. The MCD assay was performed frequently during this growth period, until the peak (negative) slope appeared, which means the slope started to increase (less negative) or decrease with negligible changes.

2.2.2.2 Acetone Precipitation and Dialysis

When the peak slope of MCD assay was observed, the *C. fumago* cultures in the six 2 L flasks was combined and filtered with more than four layers of Miracloth and precipitates were discarded. Acetone precipitation was accomplished based on the siphon effect, which means the 3 L (33%) acetone was placed on a higher altitude than the filtered medium collected from the previous step, and the acetone was transferred to medium at a lower level with a long clear tube. This procedure was undertaken in a -20 ℃ fridge to avoid protein degradation, and on a stirring plate to ensure the formation of a thorough mixture of acetone and filtrate. In addition, the tube was placed with one end centered above the filtrate while the other end on the bottom of the container with 3 L acetone at a higher level. The parafilm was applied to wrap the open end of the tube above the filtrate in order to control the flow speed of acetone at 1-2 drops per second.

When the acetone ran out, the 9 L mixture (6 L medium and 3 L acetone) was removed from the -20°C fridge and filtered with Miracloth to remain the filtrate, whereas the black precipitate was disposed of. The approximate 9 L filtrates was again precipitated with 6 L (60% final v/v) acetone, referring to the previous procedure. Then the brown precipitate was collected and air-dried to obtain a semi-solid caramel-like product. After that, a minimal volume (less than 150 mL) of Buffer A (50 mM Potassium Phosphate KH_2PO_4, pH= 5.9; filtered through 0.22 μm filter and degassed for 15 minutes) was applied to re-dissolve the air-died product. Then Buffer A-dissolved brown solution was transferred into a molecular porous membrane tubing, leaving some spaces to avoid popping, and placed in 5 L Buffer A for dialysis. This step was repeated till minimal color change of Buffer A was observed.

2.2.2.3 Amicon Ultrafiltration

The dialysis product was further filtered by ultrafiltration membrane (10,000 Dalton), with constant stirring in an ice bath and a pressure of 30 psi, till the final volume was less than 50 mL. The filtrate was scanned by UV-Vis to ensure no CPO leaking, and the remaining brown solution was filtered through a 0.45 μm filter to be used for the following purification steps.

2.2.2.4 Ion-Exchange Chromatography

First, about 25 g of DEAE-Sephadex A-50 was completely soaked in more than 1 L Buffer A and then the equilibrated resin was packed in a column, keeping the column standing for one day to enable the Sephadex to be condensed. The upper layer in the column was removed and then additional resin was packed to reach the desired level. The solution

containing crude CPO passed through the 0.45μm filter was pumped to the column, and the gradient elution with the utilization of gradually increasing concentrations (5%-30%, diluted by Buffer A) of Buffer B (50 mM KH_2PO_4, 0.5 M NaCl, pH= 5.9; filtered through 0.22 μm filter and degassed for 15 minutes) was undertaken. An auto-collector was employed to collect all fractions, among which the CPO fraction was recognized by its red to brown color. All colored fractions were kept and then scanned by UV-Vis to determine the Reinheitzahl (Rz) value (Abs 398 nm/Abs 280nm), and fractions with Rz value greater than 0.8 was pooled and further concentrated to less than 2 mL for the next step, with a centricon centrifugal filter tube (10,000 Dalton) at a speed of 1200x g.

2.2.2.5 Gel-Filtration Chromatography

The Gel-Filtration chromatography was carried out using an Sephadex G-75 (Amersham) column (2.6 × 100 cm). Similarly, the beads were soaked in Buffer A and approximately 24 grams of G75 bead was packed to the column. Then the concentrated sample from ion-exchange chromatography was injected into the column and the same auto-collector was used to collect colored fractions. After that, the UV-Vis scan was applied to guide the collection of fractions with Rz value greater than 0.8, and these fractions was concentrated for further analysis.

2.2.3 Synthesis of Substrates

2.2.3.1 Synthesis of 2-methylallyl Propionate

Propanoic anhydride (108.0 g, 0.832 mol) was added to a solution of 2-methylallyl alcohol (50.0 g, 0.693 mol) in 1000 mL of dichloromethane (DCM), and pyridine (109.0 g, 1.38 mol) was dropped into the mixture at 0 ℃ for about 30 min. Then the reaction was

proceeded for 8 to 9 hours at 40 ℃under the monitor of Thin-Layer Chromatography (TLC) with petroleum ether/ethyl acetate (1:3). The reaction mixture was extracted with HCl (4 mol/L), and the separation layer was washed with 400 mL of saturated aqueous $NaHCO_3$ for 7 times, followed with 400 mL of water for 2 times and finally with 400 mL of saturated aqueous NaCl for 2 times. The mixture of organic layers was dried over Na_2SO_4, and concentrated on an evaporator under atmospheric pressure to remove dichloromethane, then concentrated under reduced pressure to remove pyridine and 2-methylallyl alcohol to obtain the product as a colorless oil: 1H NMR (300 MHz, DMSO-*d6*) δ 4.90~4.86 (2H, d, J=12.0 Hz,-C=CH_2), 4.43 (2H, s, -O-CH_2), 2.37~2.26 (2H, q, J1=7.5 Hz, CH3-CH2-CO-), 1.67 (3H, s, CH3-C=CH_2), 1.02 (3H, t, J=7.5 Hz, CH_3-CH_2-CO) ppm.

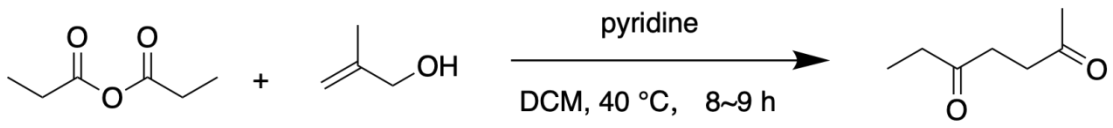

Figure 2.4 The synthesis of ethyl 3-methylbut-3-enoate (substrate 1).

2.2.3.2 Synthesis of Ethyl 3-methylbut-3-enoate

Isobutenylcarbinol (10 mL, 0.099 mol) solution was added into 500 mL of acetone, and the Jones reagent (52 mL, 0.138 mol) was dropped into the mixture at 0 ℃. Then the reaction was stirred for 1h hours at 0 ℃ under the monitor of Thin-Layer Chromatography (TLC) with petroleum ether/ethyl acetate (1:3). The reaction mixture was added by 2N of NaOH (water 92.33%, NaOH 7.67%) and stirred for 30 minutes. Then HCl (4 mol/L) was added to adjust the pH to 3.0-4.0, and 300 mL of diethyl ether was used to extract for 7

times. The separation layer was washed with 300 mL of saturated aqueous NaCl for 2 times and dried over anhydrous Na_2SO_4, then concentrated by evaporation and distillation to obtain the intermediate 3-methylbut-3-enoic acid. This intermediate (5g, 0.05 mol) was added to 1 mL of methane sulfonic acid (MSA) in 30 mL of ethanol and the mixture was stirred for 2h at 70 ℃under the monitor of TLC. Then the reaction mixture was extracted by 50 mL of n-pentane for 5 times, washed with 50 mL of water for 5 times followed with 50 mL of saturated aqueous NaCl for 5 times and dried over anhydrous Na2SO4. 1H NMR spectra was applied to conform this compound. After evaporation and distillation, the compound was obtained as a colorless oil: 1 H NMR (300 MHz, DMSO-*d6*) δ 4.86~4.82 (2H, d, J=10.0 Hz, -C=CH_2), 4.11~4.04 (2H, q, J_1=7.11 Hz, J_2=14.2 Hz, CH_3-CH_2-O-), 3.04 (2H, s, -CO-CH_2-), 1.74 (3H, s, CH_3-C=CH_2), 1.19 (3H, t, J=7.11 Hz, CH_3-CH_2-O-) ppm.

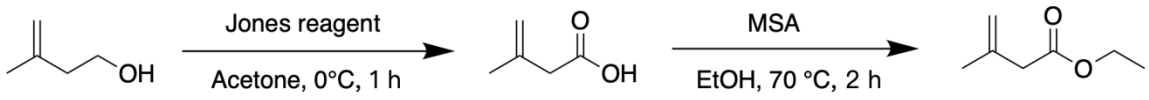

Figure 2.5 The synthesis of 2-methylallyl propionate (substrate 2).

2.2.3.3 Synthesis of 3-methylbut-3-en-1-yl

3-methylbut-3-en-1-ol (25.0g, 0.290 mol) was added to a solution of acetic anhydride (37.6g, 0.348 mol) in 300 of dichloromethane (DCM), and pyridine (45.8 g, 0.580 mol) was dropped into the mixture at 0 ℃. Then the reaction was proceeded for 8 to 9 hours at 40 ℃under the monitor of Thin-Layer Chromatography (TLC) with petroleum ether/ethyl acetate (1:3). The reaction mixture was extracted with HCl (4 mol/L), and the separation layer was washed with 200 mL of saturated aqueous NaHCO3 for 7 times,

followed with 200 mL of water for 2 times and finally with 200 mL of saturated aqueous NaCl for 2 times. The mixture of organic layers was dried over anhydrous Na2SO4, and concentrated by evaporation as well as distillation to obtain the product as a colorless oil: 1H NMR (300 MHz, DMSO-d_6) δ 4.78~4.72 (2H, d, J=17.1Hz, -C=CH_2), 4.11 (2H, t, J=6.7 Hz, -O-CH_2-CH_2-), 2.31 (2H, t, J=6.7 Hz, -O-CH_2-CH_2-), 1.98 (3H, s, CH_3-CO-), 1.71 (3H, s, CH_3-C=CH_2) ppm.

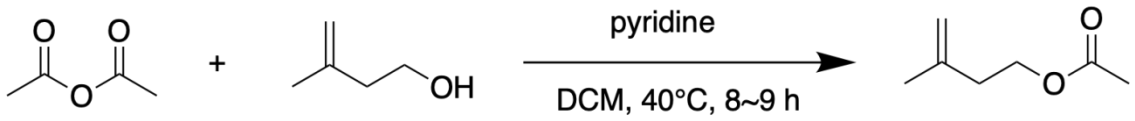

Figure 2.6 The synthesis of 3-methylbut-3-en-1-yl (substrate 3).

2.2.4 The Crystal Structure of Chloroperoxidase-substrate Complexes

0.4 mM of CPO was mixed with 0.3 M of substrates, respectively, to form CPO-substrate complexes. The complex of CPO-substrate 1 was crystallized under the condition of 0.2 M ammonium sulfate, 0.1 M sodium cacodylate pH 6.5 and 30% PEG 8000. As for the complex of CPO-substrate 2, the crystal was grown under the condition of 0.1 M sodium citrate pH 5.6, 0.2 M ammonium acetate and 30% PEG 3000. The complex of CPO-substrate 3 was obtained in 0.1 M magnisium acetate tetrahydrate, 0.1 M sodium cacodylate pH 6.5 and 20% PEG 8000. All crystallizations were performed by the hanging drop method at 20 ℃.

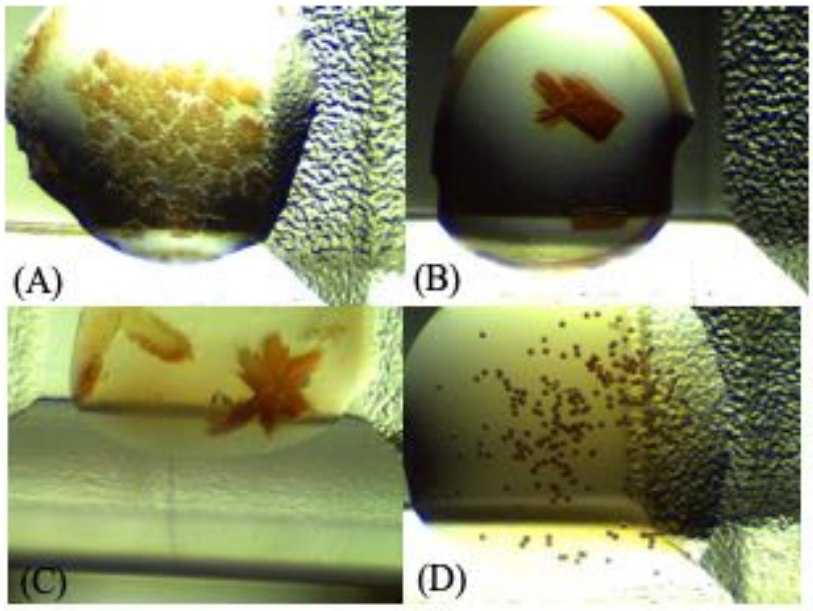

Figure 2.7 (A) Crystals of CPO-substrate 1; (B), (C) Crystals of CPO-substrate 2; (D) Crystals of CPO-substrate 3.

The XRD results of CPO-substrate 2 were available for structure refinement and the structure has been refined in space group P_1 with unit cell dimensions a=57.31, b= 86.33, c=88.00, at 2.10 Å.

Table 2.2 X-ray Data Collection Statistics	
Space group	P_1
Cell dimensions	
a, b, c (Å)	57.31, 86.33, 88.00
α, β, ϒ (°)	60.8, 86.0, 77.2
Resolution range (Å)	50.0 – 2.10 (2.14 – 2.10)
Rmerge (%)	18.7 (38.7)
Completeness	85.3 (85.9)
Multiplicity	6.9 (7.1)
I/σI	2.8 (2.4)
Number of Unique reflections	70438 (3537)

(Values in parenthesis are highest resolution shell)

Table 2.3 Current Refinement Statistics	
R/Rfree (%)	18.5/25.7
Number of atoms	
Protein (4 molecures)	9264
Mn	1
Heme (4 molecule)	176
N-acetylglucosamine (22 molecules)	1254
Mannose (13 molecules)	352
Water	798
R.m.s. deviations	
Bond length (Å)	0.007
Bond angle (°)	1.6

The crystallographic asymmetric unit contains 4 molecules (Figure 2.8).

Despite no substrate being observed in molecule A or molecule D, both molecule B and C were found to bond the substrate. The binding site of this substrate is at the entrance of a wide channel and likely serves as a docking site for the substrate ethyl 3-methylbut-3-enoate and its derivatives (Figure 2.9). This substrate binds at the active site of CPO and is surrounded by hydrophobic residues like Phe 186, Val 182, Leu 70,Ile 179 and Ala 71. The shortest distance between the Fe atom of Heme and ethyl 3-methylbut-3-enoate is 3.8 Å (Figure 2.12). Ethyl 3-methylbut-3-enoate binds above the heme and is stabilized by hydrophobic interactions of Phe 103 and Phe 186, with a distance of 3.4 Å and 3.1 Å to the aromatic side chains of Phe 103 and Phe 186 respectively (Figure 2.12).

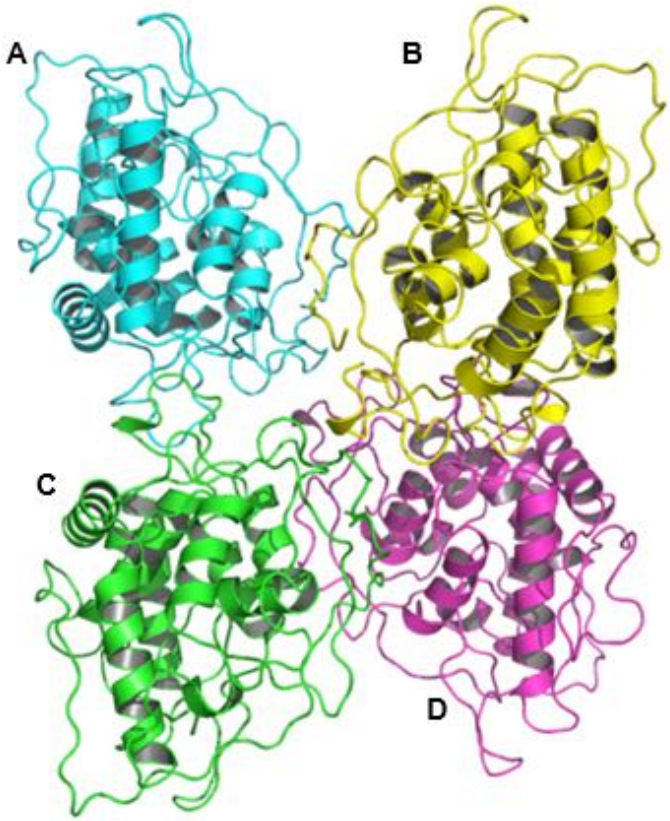

Figure 2.8 The crystallographic asymmetric unit of CPO-substrate 2 complex.

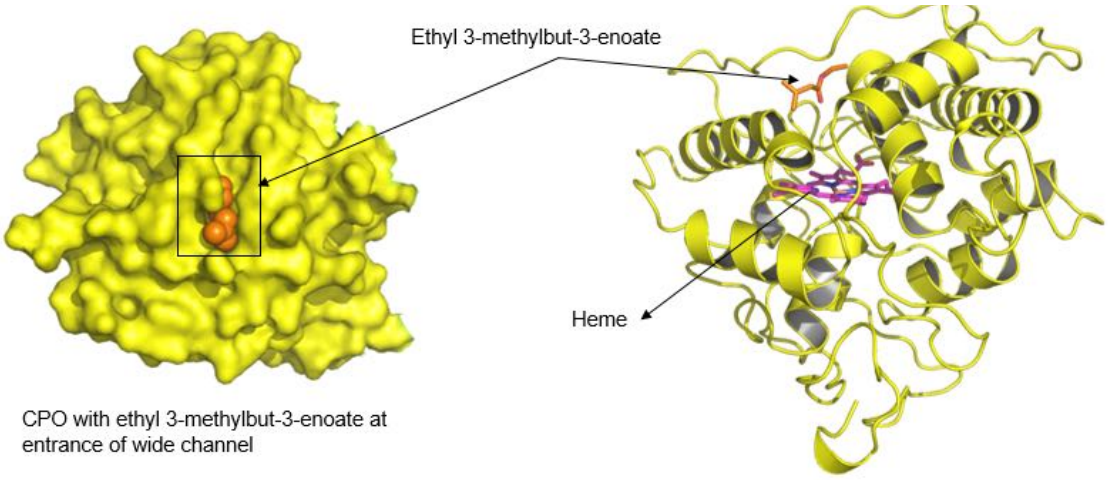

Figure 2.9 CPO with ethyl 3-methylbut-3-enoate at the entrance of a wide channel.

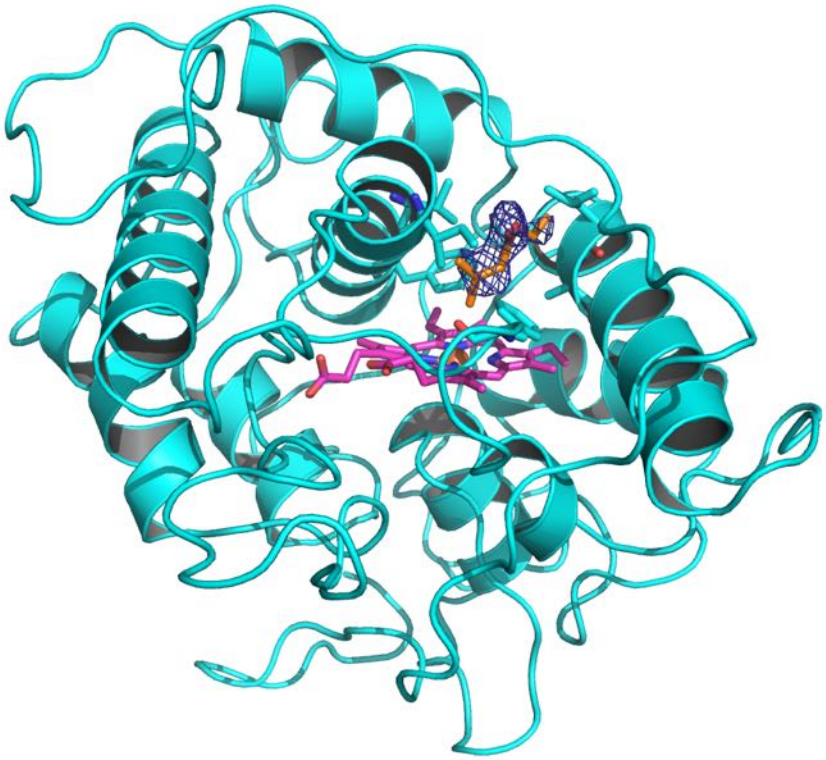

Figure 2.10 CPO binds with ethyl 3-methylbut-3-enoate at the active site. 2Fo-FC map (contoured at 1.0 σ level) is shown in blue mesh surrounded by ethyl 3-methylbut-3-enoate.

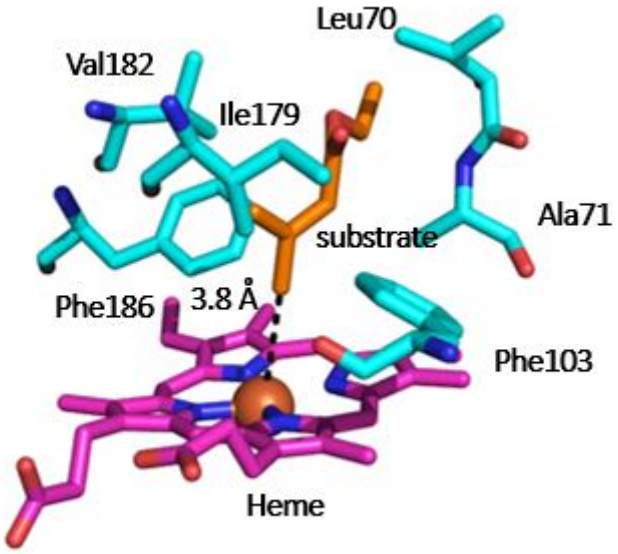

Figure 2.11 The interaction of ethyl 3-methylbut-3-enoate with CPO.

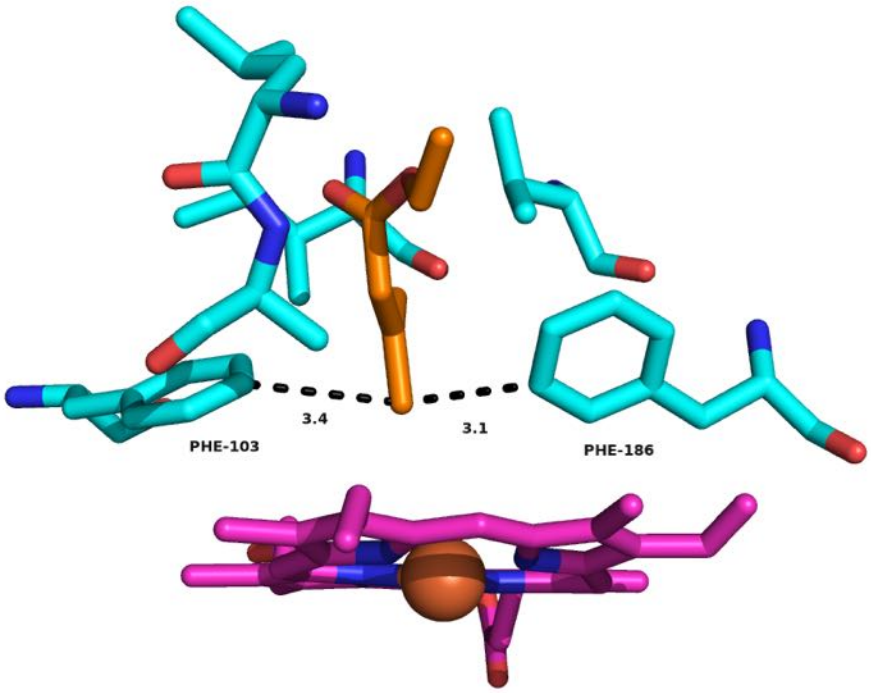

Figure 2.12 The interaction of ethyl 3-methylbut-3-enoate with Phe 186 and Phe 103.

2.2.5 Molecular Modeling of Chloroperoxidase-substrate Complex

The molecular dynamic and energy minimization simulation were performed by using NAMD with CHARMM36m force field. The system was minimized for 100 ns equilibration at 310 K, 1 atm with 2-fs time step. The Van Der Waals (VDW) force was set to zero at a cutoff distance of 12.0 Å. Docking of CPO-substrate complex was performed by AutoDock Vina 1.1.2. The published pdb files of CPO structure (pdb code: 2cpo) and the substrate ethyl 3-methylbut-3-enoate were both converted to pdbqt files and the resulting docking poses were generated on the energetic basis.

2.3 Molecular Modeling Results of CPO-substrate Complex

Enzyme's function is intimately linked to internal dynamics, thus computer simulations were employed to numerically simulate protein dynamics. Here the Root Mean Square Deviation (rmsd) was a measurement for equilibration and protein flexibility. (During the equilibrium or minimization, the distance between the carbon-carbon double bond and the heme center was not constrained.) From 100 nanosecond, the RMSD was observed to be constant (Figure 2.13), which means the protein is equilibrated.

After complete energy equilibrium and minimization, the resulting minimized structures close to the active site were obtained. Among them, one possible substrate binding site was identified close to the heme, in which the carbon-carbon double bound is oriented to the heme center. The location of the binding pocket is shown in Figure 2.14. This pocket was positioned just above the heme, and three alpha helix of the backbone could be observed (Figure 2.15), which might contribute to the stabilization of the binding structures.

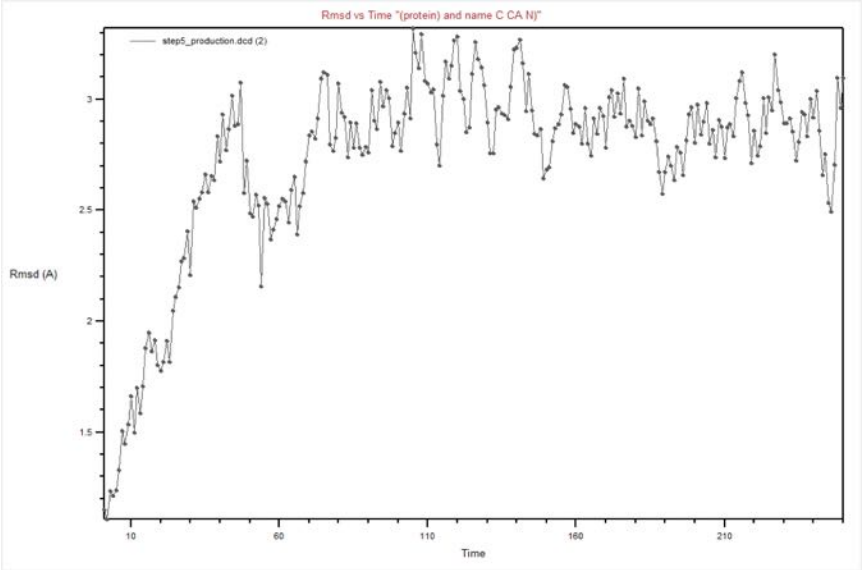

Figure 2.13 Energy equilibrium indicated as Rmsd versus time.

Figure 2.14 Stereo view of the energy-minimized complexes formed between ethyl 3-methylbut-3-enoate and CPO. The -C=C- in substrate is oriented to the heme center.

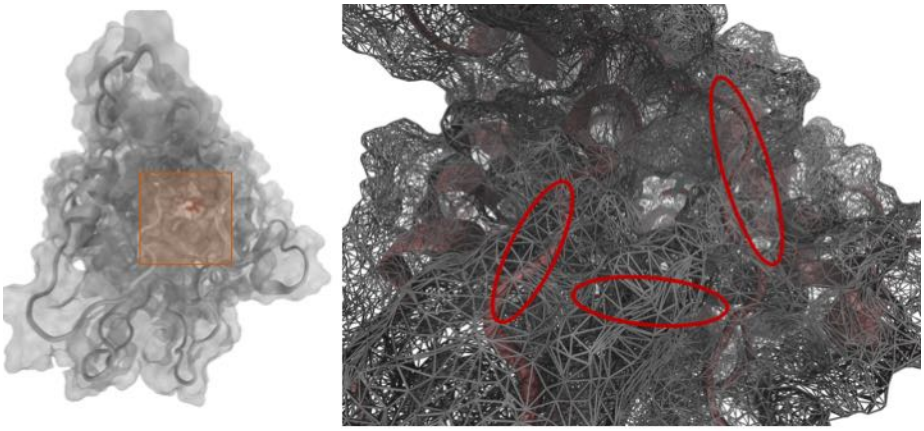

Figure 2.15 Three alpha helixes in the binding pocket (indicated with red oval).

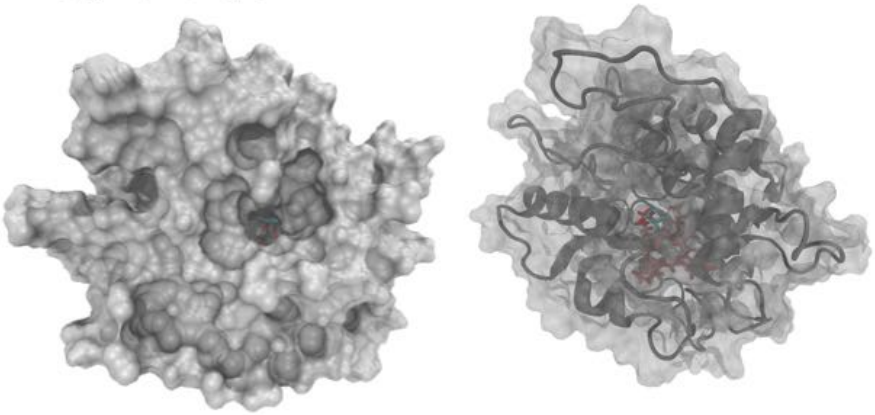

Figure 2.16 Stereoscopic views of the substrate binding channel in CPO. This is a semi-transparent molecular surface diagram showing the docked ethyl 3-methylbut-3-enoate (blue) in the substrate binding pocket which is just above the heme (red).

The docked poses of CPO catalytic site with the substrate, interacting residues and interaction types are shown in Figure 2.17. In docking, a hydrophobic substrate was assumed to displace the solvent molecules in favor of substrate-protein nonbonded interactions. The modeling results showed that the substrate ethyl 3-methyl-3-butanoate formed pi-alkyl interactions within active sites of Phe186, His396 and Val182. The Pi-alkyl interaction involves charge transfer which helps in intercalating the substrate in the

binding site of CPO. This work indicated that the distance between substrate carbon-carbon double bond and the heme center as well as the orientation of the carbon-carbon double bond were both in favor of the experimentally observed high enantioselective conversions; and the Pi-interactions with Phe186, Val 182, His 396 as well as the Van Der Waals (VDW) force with Ile 68 are involved in the substrate binding, thereby stabilizing the formation of CPO-substrate complex.

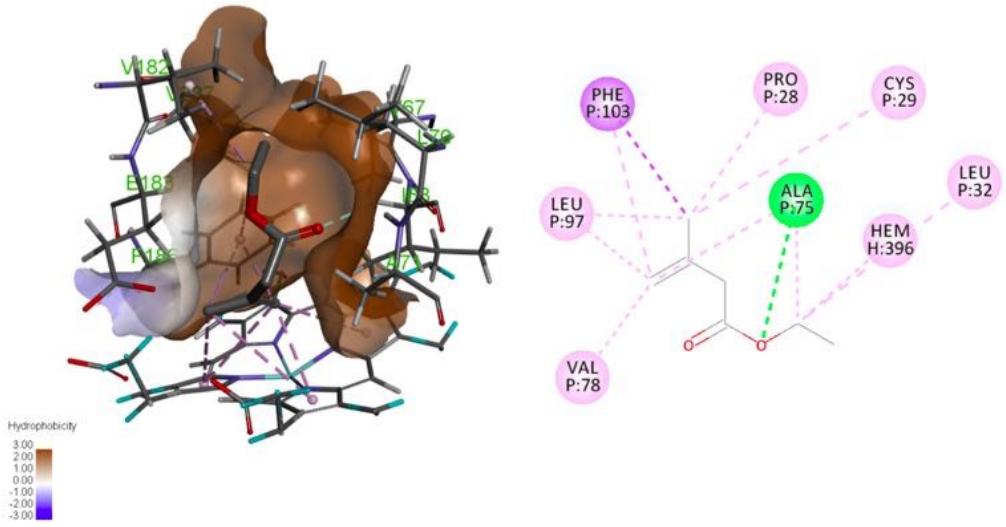

Figure 2.17 3D view of interaction residues (left); 2D view of interaction types (right). Here the pink dotted line represents Pi-alkyl interactions and green dotted line is VDW force.

Additionally, the second substrate binding site away from the heme center was identified from this work (Figure 2.18). This channel is consisted of random coils which are less stable than alpha helixes, making it more flexible than the first substrate binding site described above. Interestingly, there is a hydrogen bond between ethyl 3-methyl-3-butanoate and Ala75, indicating a strong interaction between CPO and this substrate. Other noticeable pi interactions are with Phe103, Val78, Leu97, Cys29, Leu32 and H396 shown in Figure 2.18. Therefore, the hydrogen bonding interaction with Ala75 and Pi-interactions

with specific amino acids create a strong cohesive environment to form the CPO-substrate complex, and the enhanced combinatory affinity was mostly attributed to hydrogen bond interactions formed between substrate and Ala75.

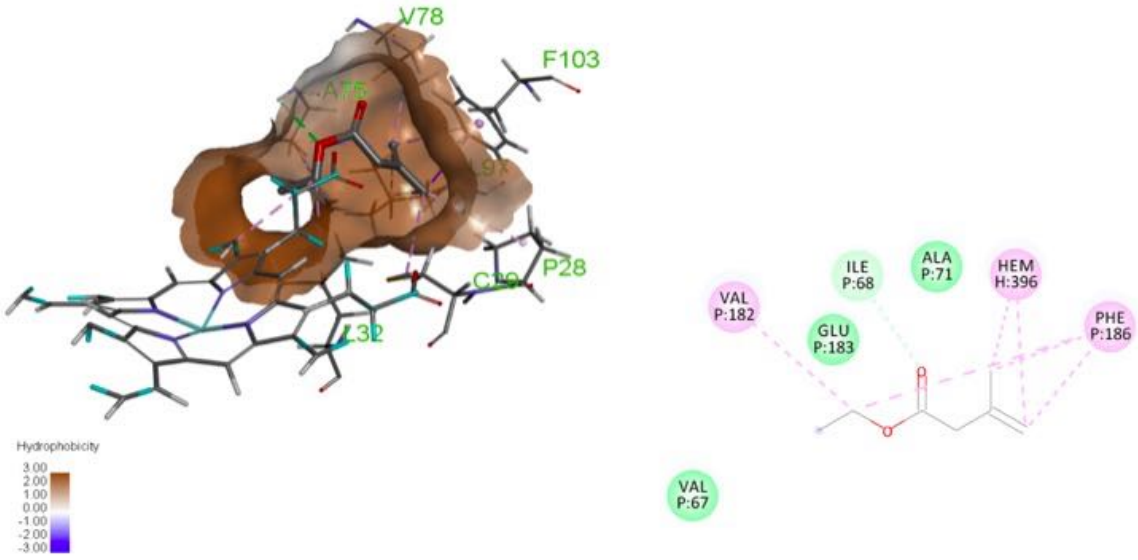

Figure 2.18 3D view of interaction residues (left); 2D view of interaction types (right). Here the pink dotted line represents Pi-alkyl interactions and green dotted line is VDW force.

2.4 Conclusion and Discussion

CPO has been proposed to catalyze epoxidations of alkenes and their derivatives. Compared to epoxidations catalyzed by P450, CPO catalyzed epoxidations have much higher enantioselectivity, and the reactions are catalyzed by a single protein which does not require cofactors, making the system much easier to manipulate [30]. This finding has stimulated us to investigate CPO-catalyzed enantioselective transformations in depth, since enantiopure epoxides serve as excellent intermediates for the synthesis of optically active fine chemicals [1]. The three-dimensional structure of chloroperoxidase on its own and in complex with the substrate CPD were previously determined [31], [24]. We had tried to

crystallize the complexes of CPO with three typical substrates to define the catalytic mechanism of enantioselective epoxidations. The substrate ethyl 3-methylbut-3-enoate was observed to form a complex with CPO above the active site and between Phe-103 and Phe-186 and at the entrance of a wide channel. The crystal structure of CPO-substrate 2 complex demonstrated the hydrophobic interactions between ethyl 3-methylbut-3-enoate and aromatic side chains of Phe 103 and Phe 186. To our knowledge, this is the first report of crystal structure of CPO-substrate complex in epoxidation investigations. This finding suggests roles of Phe-103 and Phe-186 in CPO catalyzed enantioselective epoxidations.

Despite crystals of all three complexes were observed, only the crystal structure of CPO-substrate 2 complex was obtained, and structures of other two complexes with high resolutions have not been obtained. The preparation of good diffracting crystals and skillful handling are essential to X-ray analysis [32]. Some amino acid side chains of CPO were reported to interact with substrates at the active site. The approach we applied here was co-crystallization with substrates, which could induce configurational changes in CPO, thus the crystal quality as well as the resolution of three-dimensional structure are affected. The other approach to obtaining the crystal of CPO-substrate complex is soaking the crystal of CPO into substrate solution, which could be an alternative way. This method might eliminate unnecessary interactions between CPO and substrate since CPO had been crystallized first. For future work, we will further investigate suitable conditions for CPO-substrate complex crystallization to obtain high quality crystals with excellent resolution.

In this part, investigations on molecular dynamics of CPO-substrate complex have been performed to establish specific structural and energetic basis of CPO-catalyzed enantioselective epoxidations. The simulations indicated two possible substrate binding

sites: one is stable, close to the heme center with weak CPO-substrate binding interactions, while the other site is relatively flexible, away from the heme but with strong CPO-substrate binding interactions. This led us to think about which site is more rational.

For the stable site, the Pi-alkyl interaction between Phe186 and the carbon-carbon double bond could be rationalized as an inducing effect to adjust the orientation of the substrate, leading to the formation of main product, which contributes to enantioselective transformations. Besides, this site is wrapped by three alpha helixes, which not only functions as stabilization effects but also serves as a restriction on the access of the substrate to the heme. In this way, only substrates with appropriate chain lengths and configurations could approach the reaction center of CPO. This offers a possible explanation for CPO's preference to epoxidate cis-alkenes and derivatives with high enantioselectivity.

As for the flexible substrate binding site consisted of random coils, restrictions of substrate binding to heme center could be considered relatively less due to its wider space or instability. However, the hydrogen bond interaction formed between the substrate ethyl 3-methyl-3-butanoate and Ala75 provides a strong effect on the formation of the CPO-substrate complex.

In the previous study of the crystal structure of CPO-CPD complex, the Phe103 was observed to move 0.5 Å away from the active site [26], indicating possible effects of Phe103 on interactions between CPO and organic substrates. Also, spectroscopic studies of UV-vis and NMR indicated the formation of CPO-substrate complex [33, 34]. Thus, from all discussions presented above, the molecular docking results demonstrated that

Phe103 and Phe186 play indispensable roles in CPO catalyzed epoxidations, providing theoretical support for the experimentally observed enantioselective epoxidation of ethyl 3-methylbut-3-enoate; and the substrate ethyl 3-methylbut-3-enoate trends to form a complex with CPO at a relatively flexible substrate binding site containing hydrogen bonding interaction with Ala75 and other Pi-interactions.

CHAPTER III. THE CRYSTAL STRUCTURE OF RECOMBINANT CHLOROPEROXIDASE EXPRESSED IN ASPERGILLUS NIGER

3.1 Background and Theory

The unique structure of CPO, especially certain amino acid residues like Cys29 involved in NH—S hydrogen bonds, Phe103 and Phe186 which have been indicated to facilitate substrate binding [24], is a key to revealing the mechanism of enantioselective oxidations as well as the versatility of CPO-catalyzed reactions. In the past decade, site-directed mutagenesis has been identified as an effective way to investigate structure-function relationships in P450 and peroxidases, which has not only defined the roles of active site residues but also revealed substrate binding sites [35-37]. Although the replacement of CPO cysteine 29 with histidine was feasible in *C. fumago* cultures, expression of another CPO mutant E183H in this system was failed [38, 39]. Therefore, an alternative expression system for *cpo* gene is crucial to further understanding the structure-activity relationship of this structurally unique but functionally diverse heme peroxidase.

As a heme protein with various post-translational modifications like glycosylation, proteolytic processing and prosthetic group incorporation [40], [41], CPO was considered inappropriate to be expressed in *Escherichia coli* (*E. coli*), a prokaryotic host that lacks the ability to perform post-translational modifications. Additionally, studies have indicated that CPO shows few sequence similarity to traditional heme proxidases [42], [43], [44], [45], [46], but particularly analogous to the *Aspergillus nidulans StcC* [47], [48]. Fortunately, the *Aspergillus niger* (*A. niger*) system had been claimed to express wild type CPO gene

successfully, and structural properties of the recombinant CPO (rCPO) were determined to be comparable to native CPO. Even though some spectroscopic methods, molecular biology analysis and catalytic activity assays of rCPO expressed in *A. niger* have been undertaken [47], its tertiary structure is an unsolved problem. Generally, crystallography combined with X-ray diffraction technique (XRD) determines the arrangements of atoms in crystalline proteins, so it has been considered as one of the most powerful tool to establish the structure and function relationship of heme proteins [49-51]. Therefore, I purified and crystallized rCPO to further compare its structural characteristics with those of wtCPO.

3.2 Experimental Methods

3.2.1 Materials and Reagents

The *A. niger* MGG029 strain was purchased from America Type Culture Collection (ATCC) (Manassas, VA). The CPO expression vector pCPO3.1-Amds [47] and the assistant plasmid pAB4.1 [52], were obtained from Dr. Punt (TNO Nutrition and Food Research Institute, The Netherlands). All buffers and media were freshly prepared by water purified through Milli-Q Biocel (Millipore, Billerica, MA). Reagents were purchased from Fisher Scientific (Waltham, MA) unless otherwise stated.

3.2.2 Expression of Recombinant CPO

The rCPO was expressed in *A. niger* system as described by Ana Conesa et al. [47], with necessary modifications. The *A. niger* MGG029 strain was inoculated in a 125 mL flask with 50 mL of minimal medium (MM) containing 0.5% yeast extract, 0.5% Casamino acids, 5% fructose, 70 mM $NaNO_3$, 7 mM KCl, 6 mM KH_2PO_4, 6 mM K_2HPO_4, 2 mM

$MgSO_4$, 10 mM uridine, 25 μL of carbenicillin (100 mg/mL stock), 50 uL of the Hutner trace elements solution [53]. Fungus was first grown at 37°C, 250 rpm for about 1 day, and then at 30°C for about 5 additional days until yellow mycelium was observed. The mycelium was disrupted by homogenizer and transferred to a 2 L flask with 1 L of MM. The culture was next incubated for 16~20 h at 30℃ with 250 rpm shaking, and then mycelium was collected by filtration through 4 layers of Miracloth and resuspended in 1.7 osmolarity solution. Then protoplasts of *A. niger* MGG029 was obtained by incubation with lysing enzyme for 4 or 4.5 hr at 37℃ with 150 rpm shaking, filtration extraction, centrifugation (3500 rpm, 15 min, 0℃) and resuspension in 100 to 150 μL of STC1700 solution. Then the CPO expression vector of pCPO3.1-Amds which is under the control of *A. niger* glucoamylase promoter and *Aspergillus nidulans* TrpC terminator, together with the assistant plasmid pAB4.1 containing *A. nidulans* AmdS selection marker, were co-transformed into protoplasts of *A. niger* MGG029 and incubated at 25℃ for 25 min [47]. The transformants were plated on 1.2 M sorbitol selective (acrylamide) agar medium which is devoid of uridine and incubated for 2-4 days at 30°C for both antibiotic and nutritional selection. The survival fungi colony, or successful co-transformed strain was then cultured in 2-L flasks with 1 L of MM containing 50 μM hemin and 100 μM δ-aminolevulinic acid, without the supplement of uridine. Fungus was originally incubated in a rotary shaker at 225 rpm for 48 h at 25 ℃, and then the temperature was lowered to 22 ℃ for 5 additional days. The MCD assay was undertaken periodically to determinate the expression of rCPO, until the catalytic activity reaches a plateau.

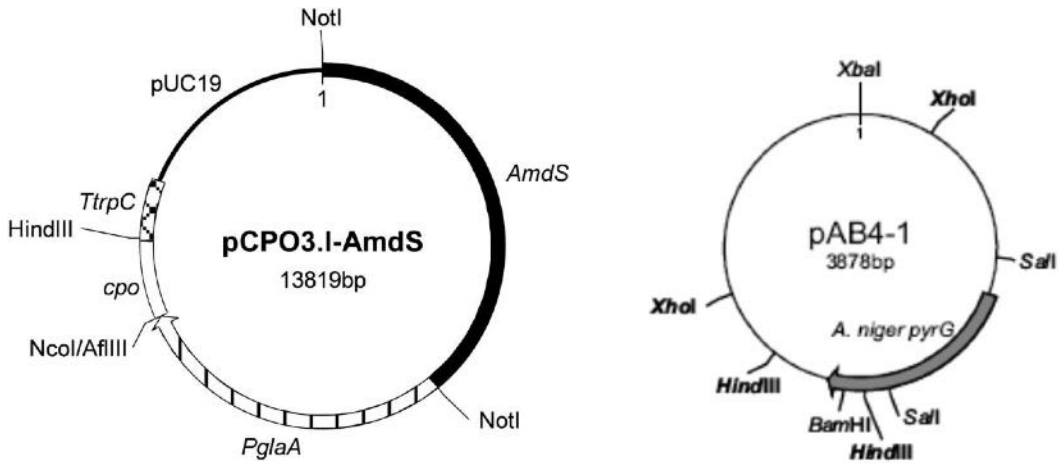

Figure 3.1 The CPO expression vector pCPO3.I-AmdS and the assistant plasmid pAB4-1 conntaining A. niger PyrG gene. The sequence of CPO is under the control of the A. niger glucoamylse promotor and A nidulans trpC terminator. The A. nidulans AmdS selection marker is introduced at NotI site.

3.2.3 Purification of Recombinant CPO

The fungal cultures were filtered through a Miracloth and then centrifuged at 9500 rpm for 1 h combined with a further filtration through 0.8 μm filters to obtain crude medium samples. The filtrate was concentrated to about 20 mL through an ultrafiltration membrane (Millipore, 10 kDa cut off) with an Amicon high-pressure cell. The concentrated medium was dialyzed, at least, twice against 25 mM potassium phosphate buffer (4 L) at pH 5.9 for about 12 h. The sample was then applied to a DEAE Sepharose ion exchange chromatography column (2.6 × 20 cm). The gradient elution by potassium phosphate buffer (25 mM, pH 5.9) containing increasing concentrations of sodium chloride (0-0.5 M) was applied. The flow rate was set at no more than 1 mL/min and the temperature was 4 ℃. Fractions with Rz values (Abs400 nm/Abs280 nm) over 0.9 were combined and further concentrated by centriprep centrifugal filter (Millipore, 30 kDa cut off). The gel filtration

chromatography on a Sephadex G-75 column (2.6 × 100 cm) was performed in further purification. The protein was eluted by potassium phosphate buffer (25 mM, pH 5.9) with a flow rate of 0.5 mL/min. Similarly, fractions with Rz values greater than 0.8 were collected and concentrated for sodium dodecyl sulfate polyacrylamide gel electrophoresis (SDS-PAGE).

3.2.4 UV-Visible Spectroscopic Characterization of Recombinant Chloroperoxidase

Both wtCPO and rCPO were diluted by 50 mM phosphate buffer at pH 5.9 and the diluted samples were transferred into quartz cuvettes. The UV-Vis spectroscopic analysis of CPO was performed by a VARIAN Cary 300 spectrophotometer from 200 to 600 nm with 1 cm quartz cuvettes. The concentration of rCPO was calculated with the theoretical extinction coefficient of 46995 $M^{-1}cm^{-1}$ at 280 nm. Then wtCPO and rCPO with the same concentration were scanned by UV-Vis spectrometer.

3.2.5 Enzyme Activity Assays

3.2.5.1 MCD Assay

MCD assay, based on the chlorination of monochlorodimedone (MCD) to dichlorodimedone, was used to determine the catalytic activity of CPO. Studies have shown chlorination activities of both wtCPO and rCPO are optimum at pH 2.75 [47]. The reaction mixture is composed of 100 mM potassium phosphate buffer with 20 mM KCl at pH 2.75, 0.17 mM monochlorodimedone and CPO. The reaction was initiated by the addition of 2.0 mM H_2O_2 and the loss of absorbance at 278 nm was monitored (VARIAN

Cary 300 spectrophotometer, 1 cm path length quartz cuvette) [39]. One unit of chlorination activity corresponds to the conversion of 1 μmol of MCD per minute.

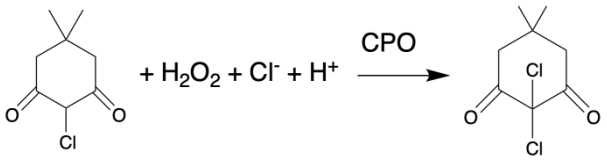

Figure 3.2 Chloroperoxidase-catalyzed chlorination of monochlorodimedone.

3.2.5.2 ABTS Assay

The 2,2'-Azino-bis(3-Ethylbenzthiazoline-6-Sulfonic Acid) (ABTS) is a typical substrate for peroxidases. This assay is based on the oxidation of ABTS with the catalysis of peroxidase and the initiation of the oxidant H_2O_2. The reaction system contains 100 mM sodium phosphate-citric buffer (pH 4.0), 38.9 μM ABTS, 3.6 mM H_2O_2 and CPO. First, all reagents except H_2O_2 were mixed in room temperature and the absorbance at 405 nm was monitored by UV-Vis spectrometer until a constant reading is reached, then H_2O_2 was added into the mixture immediately to initiate the reaction. The increase in the absorbance at 405 nm was monitored for approximately 2 minutes. The enzyme activity was calculated by the following equation:

Units/ml enzyme =(ΔA_{405nm}/min Test - ΔA_{405nm}/min Blank)(3.05)(df)/(36.8) (0.05)

Where, 3.05 = Total volume (in milliliters) of assay

df = Dilution factor

36.8 = Millimolar extinction coefficient of oxidized ABTS at 405nm

0.05 = Volume (in milliliter) of enzyme used

Units/mg solid = units/ml enzyme / mg solid/ml enzyme

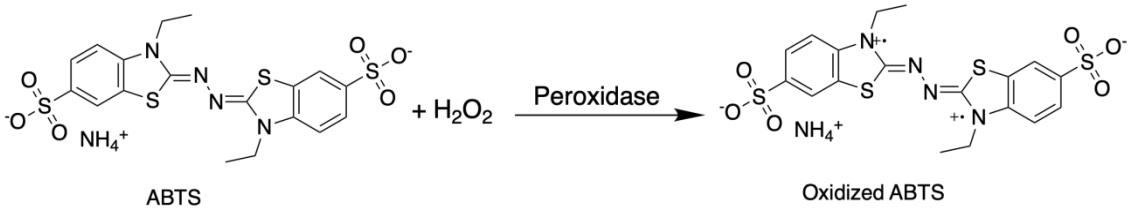

Figure 3.3 Chloroperoxidase-catalyzed oxidantion of 2,2'-Azino-bis(3-Ethylbenzthiazoline-6-Sulfonic Acid).

3.2.5.3 Epoxidation Assay

The epoxidation activity was determined by CPO-catalyzed styrene oxidation. This reaction system contained 0.01 M sodium citrate buffer (pH 5.5), 25 μL of substrate mixture (40% styrene and 60% tert-butyl-hydroperoxide) and 1.6 mg CPO. The epoxidation was initiated by tert-butyl-hydroperoxide and quenched by 10 μL of 1 M $Na_2S_2O_3$ in a saturated solution of $NaHCO_3$. Epoxidized enantiomers were extracted by isooctane and separated with HPLC (Waters 1525 Binary HPLC Pump, Waters 2996 Photo Diode Array Detector) on (S,S)-Whelk-O 1 column. The mobile phase was pure hexane and the flow rate was 1 mL/min. The absorbance at 254 nm was monitored at room temperature. One unit of enantioselectivity referred to the formation of 1 μmol (R)-styrene oxide.

3.2.6 Crystallization and XRD Analysis of rCPO

Both chunk and needle forms of rCPO crystals were obtained under the condition of 0.2M NaI, 20% polyethylene glycol (PEG) 3350 by the sitting drop method at 20℃. The chunk form was used in XRD analysis considering its shape was much more appropriate. The single molecule in the asymmetric unit was used in the structure determination: $C222_1$ (a=58.05 Å, b=150.92 Å, c=100.85 Å) which diffracts to a resolution of about 1.69 Å.

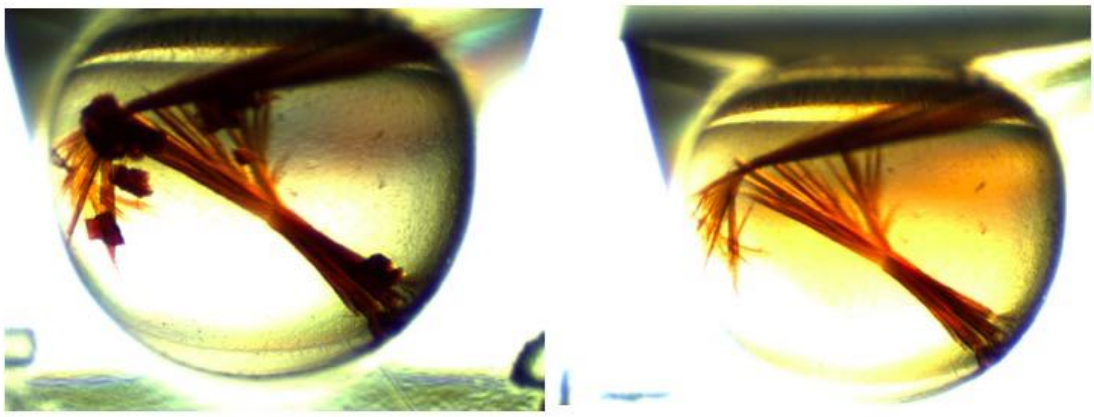

Figure 3.4 Red chunky crystal and red needle-like crystal of recombinant chloroperoxidase.

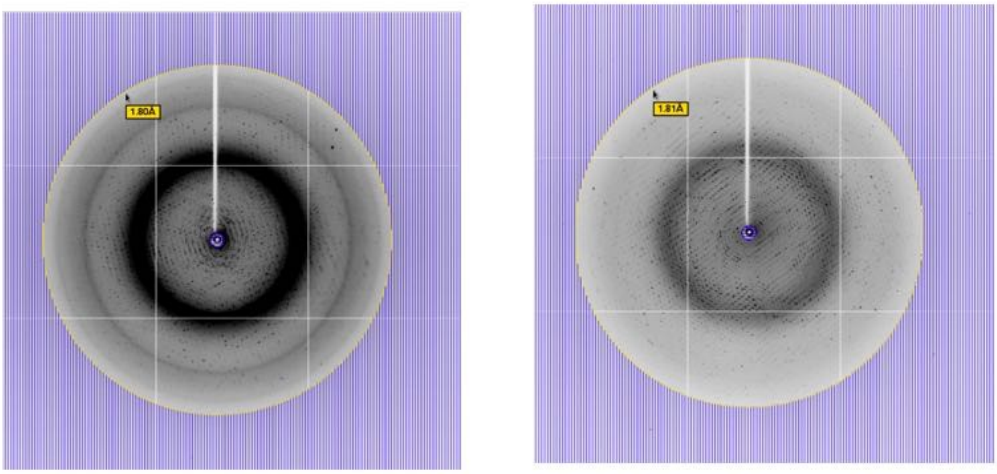

Figure 3.5 X-ray diffraction result of chloroperoxidase crystals.

The structure was solved by molecular replacement method using PDB ID: 2cj0 (Chloroperoxidase from *Leptoxyphium fumago*) as an initial model with software Phaser in CCP4 suite.

3.3 Results

3.3.1 UV-Visible Spectroscopic Properties of Wild-type and Recombinant Chloroperoxidase

The UV-vis spectra of rCPO and wild type CPO were compared to assess their optical characteristics. The spectrum of rCPO was observed to be essentially identical to that of the wild type CPO, except for a slight decrease of the Soret band absorbance at 400 nm.

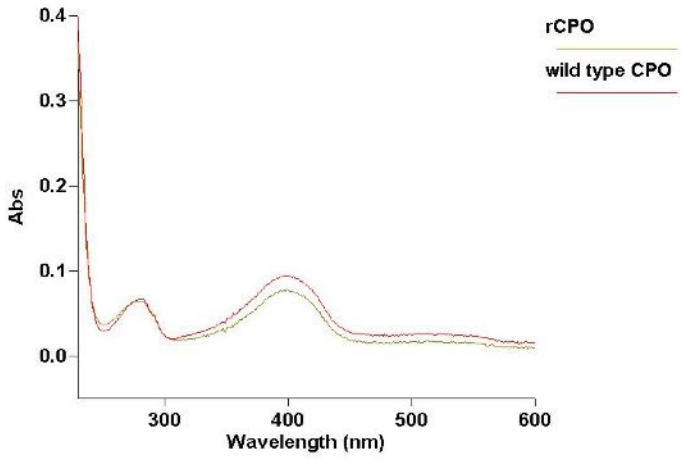

Figure 3.6 The Soret band of wtCPO and rCPO were both observed at 400 nm.

3.3.2 Chlorination of Monochlorodimedone, Peroxidation of ABTS, and Epoxidation of Styrene

The chlorination activity of rCPO was measured by MCD assay at pH 2.75, and results showed rCPO expressed in *A. niger* system was active in both chlorination and peroxidation reactions. For the MCD assay, the catalytic activity of rCPO is approximately 25% more active than that of the wtCPO, while for ABTS assay, rCPO showed about a two-fold improvement in catalytic activity compared to that of the wtCPO.

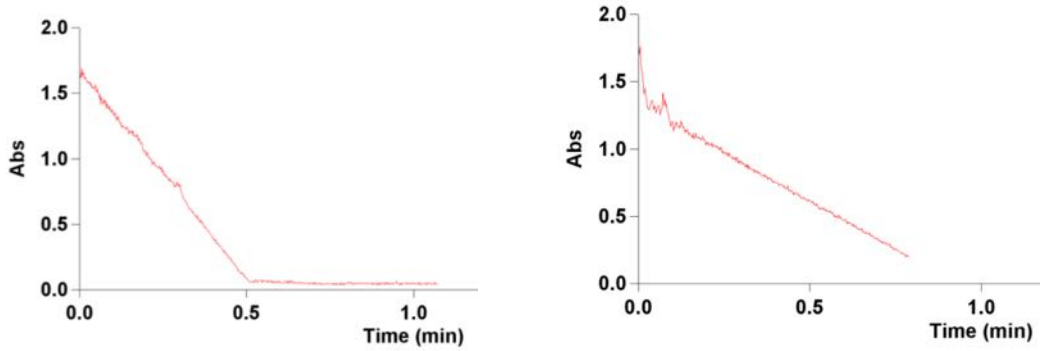

Figure 3.7 Chlorination reaction of MCD catalyzed by 0.1 μM of the rCPO (left) and 0.065 μM of the wt CPO (right) monitored at 278 nm.

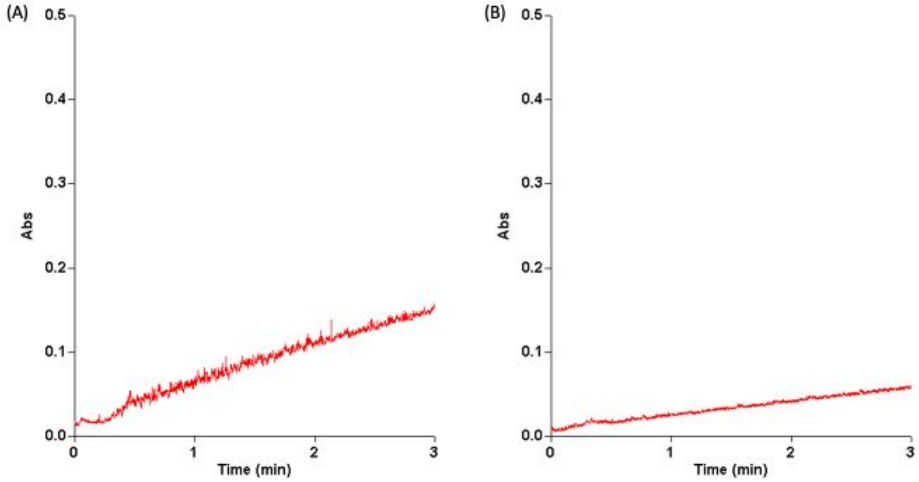

Figure 3.8 Peroxidation reaction of ABTS catalyzed by 0.1 μM rCPO (A) and 0.065 μM of wt CPO (B) monitored at 405 nm.

The epoxidation of styrene was employed to determine the enantioselectivity of rCPO. The peak of standard (R)-styrene oxide was observed at 4.049 min and the ee % was 68.7%. HPLC results indicated that rCPO catalyzed styrene epoxidation with ~40% higher enantioselectivity compared with wtCPO.

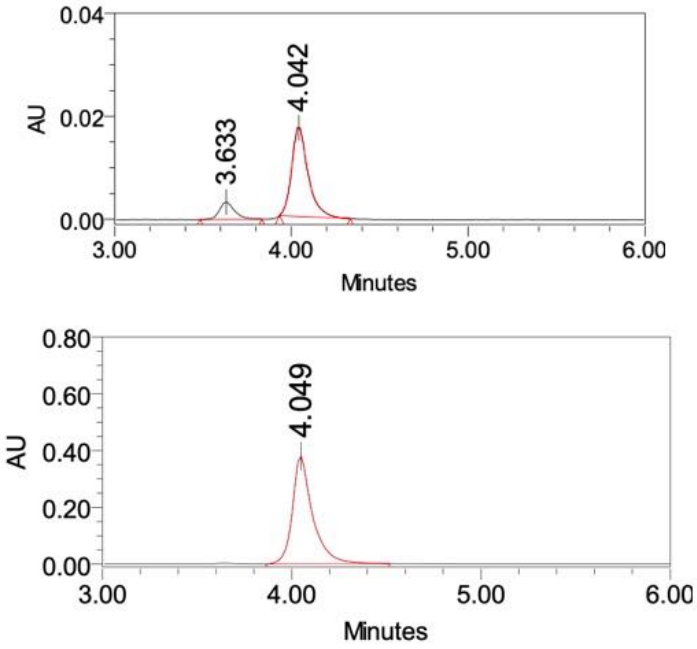

Figure 3.9 Chiral separation of styrene epoxide from styrene epoxidation catalyzed by rCPO.

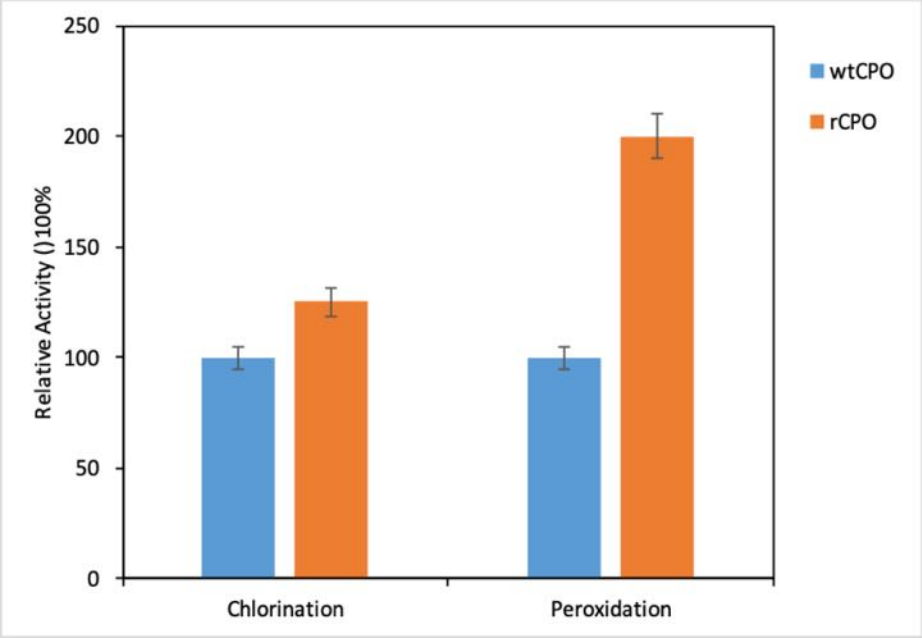

Figure 3.10 Relative activities of wtCPO and rCPO in MCD and ABTS assays.

3.3.3 Overall Structure of Recombinant Chlroperoxidase

The structure has been refined in space group $C222_1$, an orthorhombic crystal system with unit cell dimensions a=58.05, b= 150.92, c=100.85, at 1.69 Å.

Table 3.1 X-ray Data Collection Statistics	
Space group	$C222_1$
Cell dimensions	
a, b, c (Å)	58.05, 150.92, 100.85
α, β, ϒ (°)	90.0, 90.0, 90.0
Resolution range (Å)	37.3 – 1.69 (1.78 -1.69)
Rmerge (%)	10.9 (59.7)
Completeness	90.5 (100.0)
Multiplicity	6.9 (7.1)
I/σI	9.4 (2.4)
Number of Unique reflections	45316 (7220)

(Values in parenthesis are highest resolution shell)

Table 3.2 Current Refinement Statistics	
R/Rfree (%)	17.0/20.9
Number of atoms	
Protein	2345
Mn	1
Heme (1 molecule)	44
N-acetylglucosamine (5 molecules)	70
Mannose (13 molecules)	143
Water	468
Iodide	10
R.m.s. deviations	
Bond length (Å)	0.008
Bond angle (°)	1.241

Recombinant CPO folds into N-terminal and C-terminal domains with the heme sandwiched between the two domains (Figure 3.11). Compared with wtCPO, rCPO also contains the heme prosthetic group in which a central iron is coordinated to four nitrogen atoms of four pyrroles (Figure 3.11(b)). For the proximal helix of rCPO, the cysteine ligand (Cys29) is directly coordinated with iron atom (Figure 3.12 (a)), and this unique iron-sulfur bond which presents in P450, observed in both rCPO and wtCPO, distinguishes them from other peroxidases. However, P450's proximal helix is parallel to the porphyrin plane while rCPO's is perpendicular to the heme, similar to that in wtCPO. Like wtCPO, the Mn^{2+} binding site was also modeled in rCPO. Mn^{2+} forms octahedral geometry with six

coordination ligands, including a propionate group from the heme molecule, three amino acids, and two water molecules, which shares cation arrangement with a traditional peroxidase—manganese peroxidase (Figure 3.12 (b)) [24].

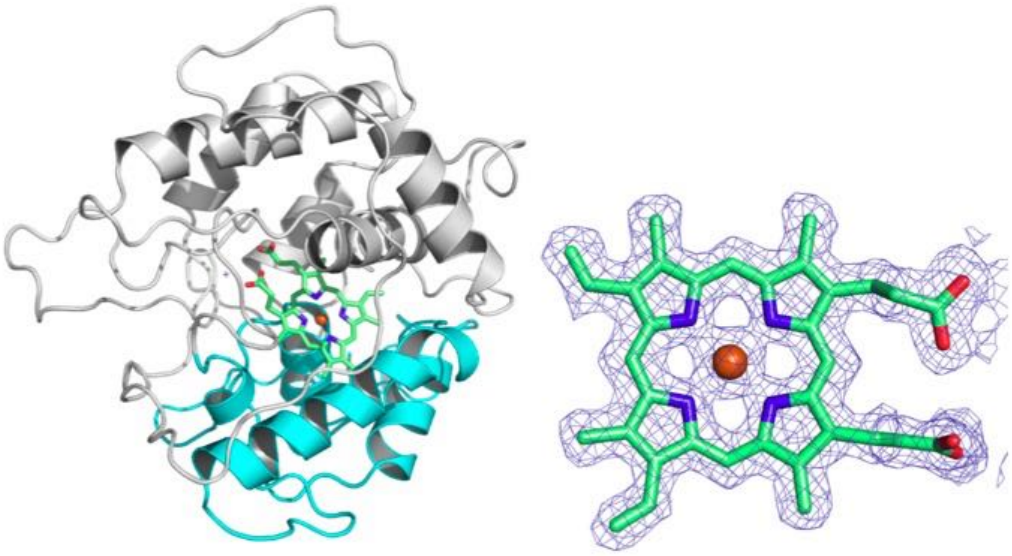

(a) (b)

Figure 3.11 (a) Overall structure of rCPO. The heme center (green) is sandwiched between C-terminal (gray) and N-terminal domains (cyan). (b) 2Fo-Fc electron density map of heme contoured at 1.5σ cutoff. (Figure made with Pymol)

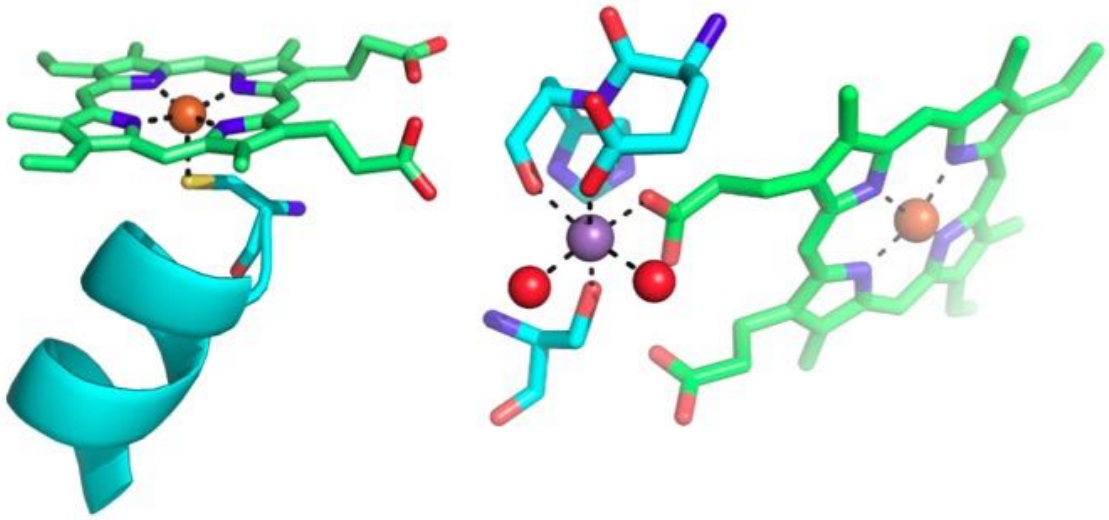

(a) (b)

Figure 3.12 (a) Proximal helix of rCPO with heme molecule. (b) Cation-binding site of CPO. Ligand interactions with the cation are indicated by dashed lines. Mn makes octahedral geometry with six coordination with ligands (three amino acids (cyan), one heme molecule (green) and two water molecules (red sphere)). (Figure made with Pymol)

3.3.4 Glycosylation of Recombinant Chloroperoxidase

Glycosylation, a common type of post-translational modifications, was also shown in the crystal structure of rCPO. Interestingly, rCPO is over-glycosylated relative to wtCPO since there are three more glycosylation sites in rCPO: Asn74 interacted with N-acetyl-D-glucosamine, Ser254 with mannose and Ser271 with mannose as well. In addition, the carbohydrate at Ser248 in rCPO is mannose while in wtCPO is xylose (Table 3). In eukaryotic systems, glycosylation is prerequisite for correct protein folding which is essential for enzyme activity [54]. However, it has been reported that carbohydrate binding interactions in CPO are not required for its catalytic properties [55], and over-glycosylation

effects on its catalytic activity is negligible [56]. Here this subtle influence was also confirmed by comparable activity of rCPO in both MCD and epoxidation assays.

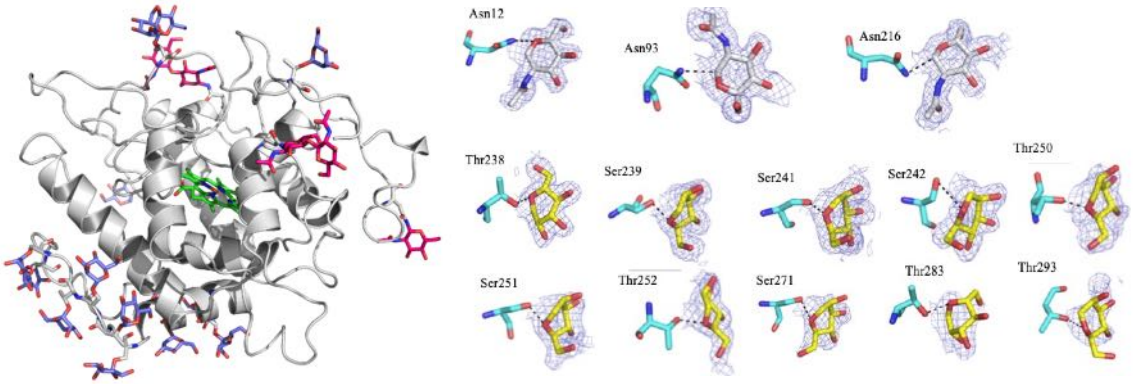

(a) (b)

Figure 3.13 (a) Carbohydrate attachment sites in rCPO (Mannose: purple stick; N-acetyl-D-glucosamine: magenta stick). (b) Interaction with Carbohydrates: protein residues are in cyan, N-acetylglucosamine in gray and mannose in yellow[better to use the same color for the same carbohydrate.]. The electron density map (2Fo-Fc) at 1σ confirm the presence of carbohydrates. (Figure made with Pymol)

Table 3.3 Carbohydrate Binding Interactions in rCPO and wtCPO

Glycosylation site	Recombinant CPO	Wild-type CPO
Asn12	N-acetyl-D-glucosamine	N-acetyl-D-glucosamine
Asn74	N-acetyl-D-glucosamine	No carbohydrate
Asn93	N-acetyl-D-glucosamine	N-acetyl-D-glucosamine
Asn216	N-acetyl-D-glucosamine	N-acetyl-D-glucosamine
Thr238	Mannose	Mannose
Ser239	Mannose	Mannose
Ser241	Mannose	Mannose
Ser242	Mannose	Mannose
Ser248	Mannose	Xylose
Thr250	Mannose	Mannose
Ser251	Mannose	Mannose
Thr252	Mannose	Mannose
Ser254	Mannose	No carbohydrate
Ser271	Mannose	No carbohydrate
Thr283	Mannose	Mannose
Thr293	Mannose	Mannose

3.3.5 The Iodide-bound Structure of Recombinant Chloroperoxidase

Once Compound I forms, CPO is able to form an oxo-ferric Compound X by reacting with halide ion through the halogenation pathway. Then Compound X is reduced to the resting state of CPO as it interacts with a substrate to release halogenation product. The rCPO was crystallized in 0.2 M NaI, and significantly, ten iodide ions were identified using anomalous difference electron density maps (Figure 3.14).

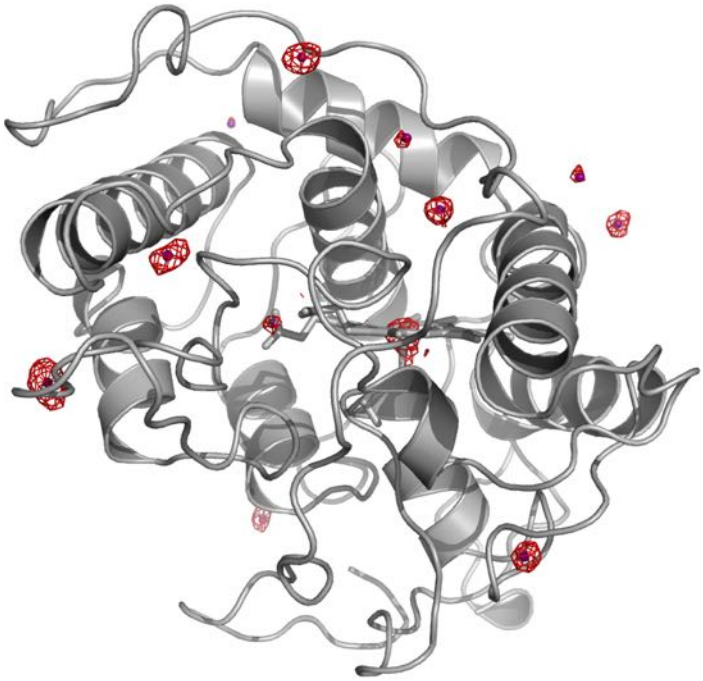

Figure 3.14 Biding of iodide to rCPO. There are ten iodide ions (shown in red mesh) identified and the positions were confirmed using anomalous difference map (Fo-Fc) (contoured at 4.0 σ level).

This iodide binding site could be recognized as a docking site for halide anions and iodide ions placed near the heme are stabilized by hydrophobic interactions with surrounding amino acids such as Leu70, Phe103, Val182 and Ile179. Iodide ions were identified in previously reported structure of wtCPO (PDB ID: 2CIW), in which only six

iodides were observed. Here it was superimposed over the current structure of rCPO, and the positions of the six iodides were well superimposed (Figure 3.15), further confirming that rCPO shares almost the same overall structure with that of wtCPO.

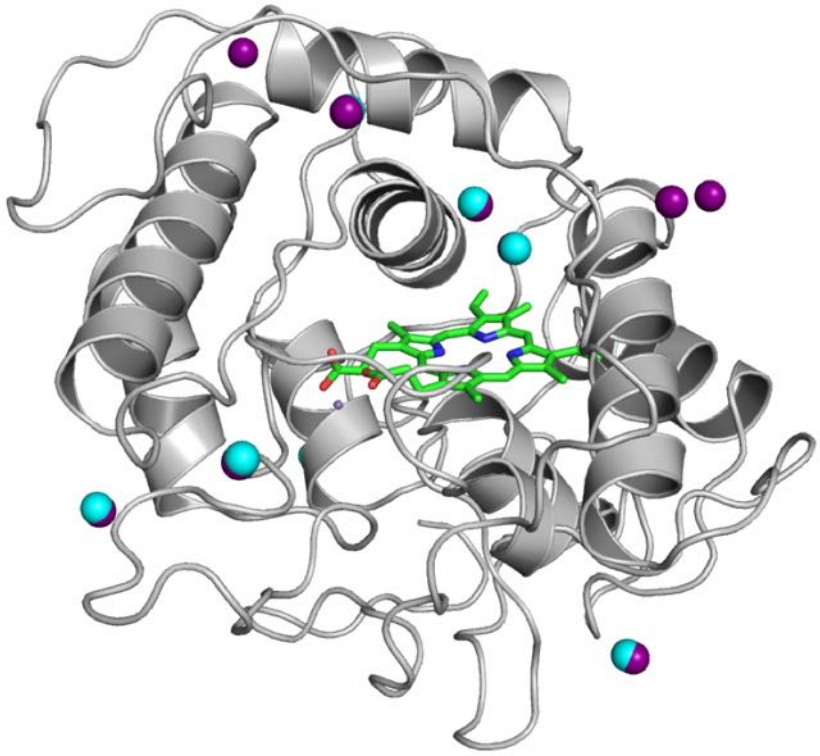

Figure 3.15 Superimpose of CPOs current structure with previously reported structure (PDB id: 2ciw). The current structure has ten iodide ions (magenta) and previously reported structure has only six iodide (cyan) and the positions of the six iodide are well superimposed.

In addition, a narrow channel and a wide channel were identified, and both channels lead to the active site (Figure 3.16 (A)). There were three iodide ions inside the narrow channel whereas no iodide was observed within the wide channel. Instead, one iodide ion was identified near the entrance of the wide channel. Despite no binding sites for iodide

was recognized, it is not reasonable to exclude the possibility of halide ions diffusion through the wide channel to the active site of rCPO.

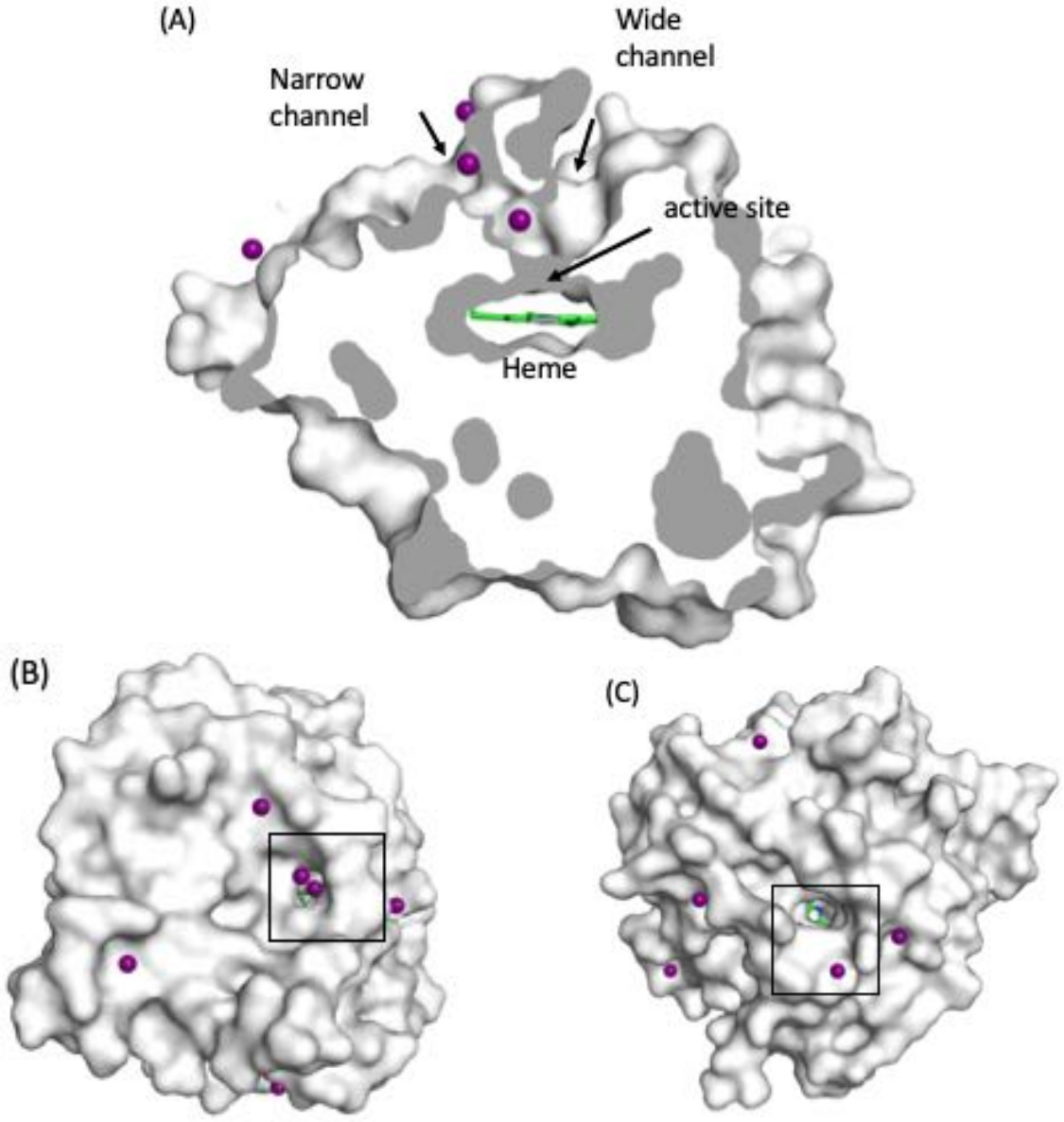

Figure 3.16 Slice through surface representation of the recombinant CPO, without sugars. (A) The narrow channel and the wide channel both leading towards active site. (B) Top view of the narrow channel. Three iodide ions inside the narrow channel were observed.

(C) Top view of the wide channel. One iodide ion was identified close to the entrance of the wide channel.

3.4 Conclusion and Discussion

Chloroperoxidase from *Caldariomyces fumago* is a versatile enzyme among heme proteins considering the fact that it catalyzes various reactions including halogenation, peroxidation, dismutation and P450-like reactions. It shares both catalytic characteristics and structural properties with not only heme peroxidases but also cytochromes P450. Compared with P450 and traditional peroxidases, CPO is more efficient and offers high potentials in pharmaceutical, environmental, and chemical industries, which stimulates researchers to investigate its structure-function relationship to reveal the catalytic mechanism. Therefore, a heterologous expression system for CPO is highly desired.

Although Conesa et al. expressed cpo gene successfully in *A. niger* system, the Rz value of rCPO is less than half of that of CPO expressed in *C. fumago* system, which indicated rCPO is only partially incorporated with heme. Here we added both heme and heme precursor (δ-aminolevulinic acid) according to a reported culture condition for a mutant CPO expressed in *A. niger* [39]. In addition, fungus culture was performed initially at 25 ℃ for exponential growth and then the temperature was lowered to 22 ℃ to provide a moderate environment for protein secretion, instead of a 48 h incubation at 30 ℃. The gel filtration chromatography was also adjusted to a lower flow rate to optimize the purification process, and the final purified rCPO was determined with Rz value of 1.4 and concentration of 1.5 mM, suitable for crystallization.

Results of both MCD assay and epoxidation assay indicate that the catalytic activity of rCPO is comparable to that of wtCPO, in agreement with the commonly accepted

proposal that overglycosylation has little or no effects on either chlorination or enantioselective oxidation activity of CPO. The three-dimensional structure of rCPO indicates that rCPO expressed in *A. niger* has almost the same tertiary structure with CPO expressed in *C. fumago*. The crystal structure also further confirms overglycosylation of rCPO expressed in *A. niger*. My results are in harmony with previous studies demonstrating that extra carbohydrate binding interactions have little influence on either structural or catalytic characteristics of rCPO [55, 56]. Although a bromide/iodide binding site at the surface of CPO had been reported previously, only one halide ion (binding site 2) was identified within the narrow channel, and this binding site combined with the other two halide sites (halide binding site 1 and iodide site 3) implicate a rational pathway of halide ions to access the active site of CPO (Figure 3.17) [26]. However, our work indicated three iodide ions inside the narrow channel, which provides new insights into a pathway of the halide access to the heme.

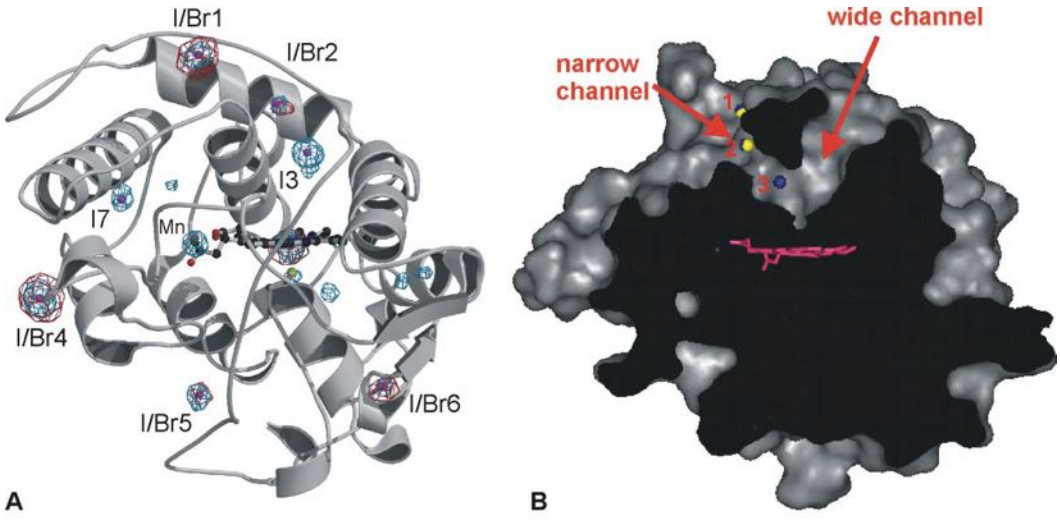

Figure 3.17 Binding of halides to CPO from previous work. The halide binding site 2 (yellow sphere, bromide; blue, iodide) is located within the narrow channel. The iodide

binding site 3 is at the end of the channel and the halide binding site 1 is at the surface of this channel [26].

As far as we are aware of, this is the first study on the crystal structure of rCPO expressed heterologously and we also update the iodide binding sites of chloroperoxidase. Our work indicated the potential application of *A. niger* system on other peroxidases and the availability of this system in structure-function relationship investigation of chloroperoxidase.

CHAPTER IV. CRYSTALLIZATION OF MUTANT CHLOROPEROXIDASE C29H, F186A AND F103A/186A

4.1 Background and Theory

CPO-catalyzed epoxidations have shown a promising potential in the biochemical field because they display high enantioselectivity, and thus generate prochiral or chiral products [57]. Unlike other heme peroxidases, the heme iron in CPO is coordinated to a sulfur atom of the proximal cysteine, resembling a P450-like proximal pocket. In the past decades, numerous investigations on the enantioselective transformations, especially on CPO's thiolate ligand and proximal helix have been carried out. The sulfur atom in the proximal pocket was observed to form hydrogen bonds with surrounding amino acids, and consequently increase the reactivity of the heme. Besides, the dipole moment of the proximal helix as well as NH—S bonds were reported to decrease the reaction barrier of CPO-catalyzed epoxidation of olefins, attributable to the increased electron density transfer to the proximal pocket residues [20]. Further researches indicated that NH—S bonds combined with the dipole moment of the proximal helix decrease the electron-donating effect of the proximal thiolate-ligand, leading to the increase of the heme redox potential and decrease of the basicity of the ferryl oxygen [58].

As for the distal site, crystallographic studies proposed that CPO's substrate-binding pocket is bracketed by Phe103 and Phe186 [24]. Particularly, there are indications that the bottom of the pocket can adjust to substrate binding, since Phe103, one of the residues at the bottom of the channel, is expected to contact substrates, appears to be flexible [24]. In addition, CPO was reported to form complexes with organic substrate CPD

and acetate. The crystal structures of both CPO-CPD and CPO-acetate complexes indicated that the substrate CPD as well as acetate are sandwiched between Phe103 and Phe186, and the aromatic side chain of Phe103 is observed to move 0.5 Å away from the active site [26].

Although many studies have demonstrated the influence of the proximal and distal regions of CPO on its stereoselectivity, the specific mechanism of CPO catalyzed enantioselective transformation is still unknown. So far, site-directed mutagenesis has been considered as an effective way to investigate structure-function relationships in both P450 and peroxidases [35-37]. The *A. niger* system was reported to express mutant CPO successfully [39], so here three CPO mutants including C29H, F186A and F103A/186A were expressed in this heterologous system and purified for crystallography to establish three dimensional structures.

C29H is a mutant whose cysteine 29 is replaced by a histidine, in order to remove the thiolate ligand which differs CPO from traditional peroxidases and is proposed to influence the reactivity of heme. Similarly, F186A is a mutant with an alanine replacement of phenylalanine 186, while in F103A/186A, both phenylalanine 103 and 186 are replaced by alanine. Either F186A or F103A/186A is designed to remove the effects of surrounding phenylalanine on organic substrates at CPO's active site so that the distal region's effects on enantioselective oxidations would be explored.

4.2 Experimental Methods

4.2.1 Materials and Reagents

The QuickChange II XL site-directed mutagenesis kit was purchased from Stratagene (La Jolla, CA). Restriction Enzymes were purchased from New England Biolabs (Ipswich,

MA). Purified oligonucleotide primers were purchased from Eurofins Genomics (Louisville, KY). The Mini-prep Kit used for plasmid extraction was purchased from QIAGEN. All buffers and media were freshly prepared by water purified through Milli-Q Biocel (Millipore, Billerica, MA). All other strains and chemicals applied are the same as described in 3.2.1 unless otherwise stated.

4.2.2 Expression and Purification of CPO Mutants

4.2.2.1 Construction of C29H, F186A and F103/186A CPO Genes

The genes of three CPO mutants, C29H, F186A and F103A/186A, were introduced into the pCPO3.1-AmdS vector, respectively, via polymerase chain reaction (PCR) amplification with the QuickChange II XL site-directed mutagenesis kit. The corresponding primers are listed below.

C29H forward primer

5’- CTACCGACTCTCGTGCTCCTCACCCAGCTCTGAACGCTCTTG - 3’

C29H reverse primer

5’- CAAGAGCGTTCAGAGCTGGGTGAGGAGCACGAGAGTCGGTAG - 3’

F186A forward primer

5’- CGTCGAGTCTGGCGCCATCTTCGCCCTTG - 3’

F186A reverse primer

5’- GCGAAGATGGCGCCAGACTCGACGTTCTG - 3’

F103A/186A forward primer

5’-CACGCTGCCGAGCACGACCACTC - 3’

F103A/F186A reverse primer

5’-TGCTCGGCAGCGTGGGGCTCG - 3’

The PCR was performed for 20 cycles of 98 ℃ for 50 seconds, 60 ℃ for 50 seconds and 72℃ for 14 minutes, followed by a 7-min final extension cycle at 72 ℃. The amplified product was digested with Dpn I restriction endonuclease to remove the template DNA (pCPO3.I-AmdS containing wild type cpo gene) and then transformed into *Escherichia coli* (DH5α strain) for antibiotic selection. The plasmids pCPO3.I-AmdS containing mutant CPO genes were purified by Mini-prep Kit and the extracted products were confirmed by agarose gel electrophoresis and DNA sequencing (Figure 4.1).

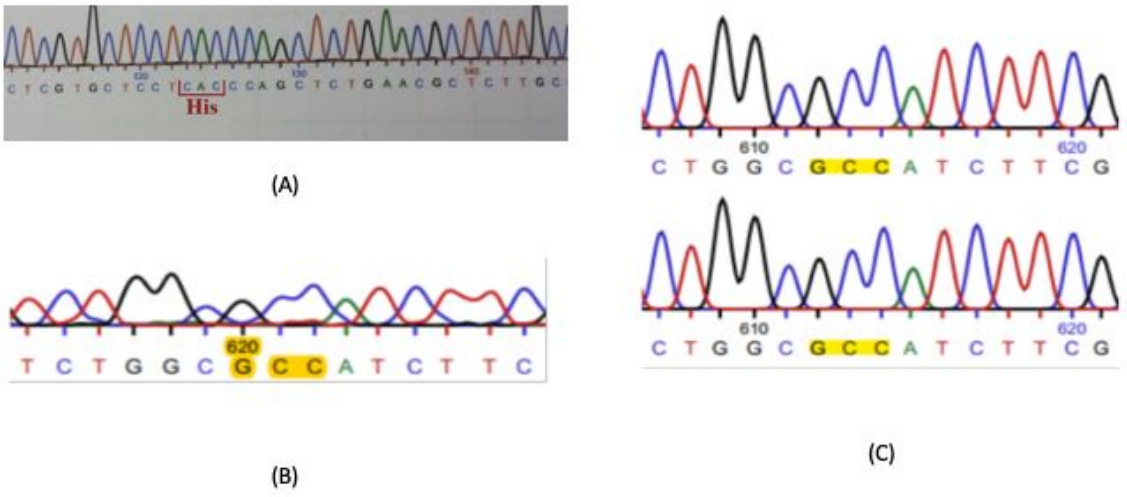

Figure 4.1 DNA Sequencing results of C29H (A), F186A (B) and F103/186A (C).

4.2.2.2 Transformation, Expression and Purification of Mutant CPO

The plasmids pCPO3.I-AmdS containing C29H, F186A and F103A/F186 A were respectively transformed together with the assistant plasmid pAB4-1 into the protoplast of *A niger* through the procedures described in 3.2.2. Then the transformants were cultured as methods described in 3.3.2, but the enzyme activity was monitored by ABTS assay instead of MCD assay applied for wtCPO and rCPO. The mutant CPO was purified through the same procedures described in 3.2.3.

4.2.3 Enzymatic Activity of Mutant CPO

4.2.3.1 MCD Assay

This assay was performed with the similar procedures described in section 3.2.5.1, except a slight modification of pH for the reaction buffer of C29H. In this part, C29H was added into the 100 mM potassium phosphate buffer with 20 mM KCl at pH 3.25 which is the optimum pH of MCD assay for mutant C29H [38].

4.2.3.2 ABTS Assay

The ABTS assay was carried out with the same procedures as described in section 3.2.5.2 to determine the peroxidation activities of CPO mutants.

4.2.3.3 Enantioselective Activity Assay of CPO Mutants

The enantioselective activity was determined by CPO-catalyzed epoxidations of styrene. This reaction system contained 100 μL of 0.01 M sodium citrate buffer (pH 5.5), 10 μL of substrate styrene, 15 μL of tert-butyl-hydroperoxide and 0.4 μM of mutant CPO.

The epoxidation was initiated by the oxidant tert-butyl-hydroperoxide and quenched by 10 μL of 1 M $Na_2S_2O_3$ in a saturated solution of $NaHCO_3$. The enantiomers were extracted by isooctane and separated with the application of HPLC (Waters 1525 Binary HPLC Pump, Waters 2996 Photo Diode Array Detector) on (S,S)-Whelk-O 1 column. The mobile phase was pure hexane and the flow rate was 1 mL/min. The absorbance at 212-220 nm was monitored at room temperature. One unit of enantioselectivity referred to the formation of 1 μmol (R)-styrene oxide.

4.2.4 Crystallization and XRD Analysis of CPO Mutants

The purified mutant CPO of C29H, F103A and F103/186A were applied for crystallization using the MembFacTM Crystal Screen Kit by sitting drop at 20℃. The mutant CPO C29H was observed to form red needle-like crystal under the condition of 50% 2-methyl-2,4-pentaediol, 0.01 M $ZnCl_2$ and 0.1 M sodium acetate at pH 5.0. As for the other two mutants F186A and F103A/F186A, no crystals were observed even though several hundred of conditions were tried.

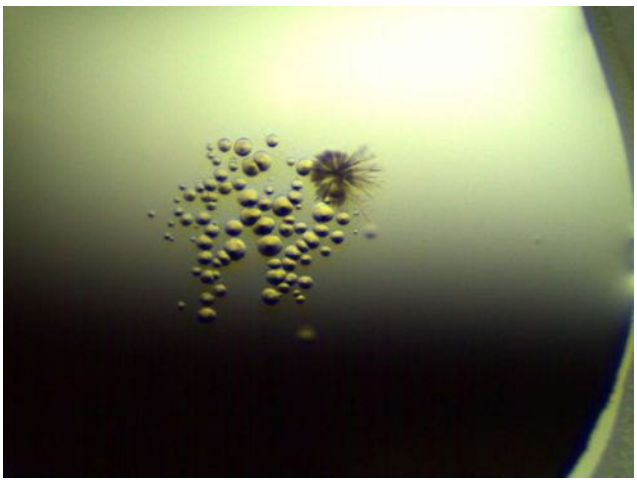

Figure 4.2 Needle-like crystal of the mutant CPO-C29H.

4.3 Results

4.3.1 Chlorination Activity of C29H, F186A and F103/F186A

For the mutant CPO C29H, the chlorination activity was determined to be about only 0.48% of the wild type CPO (Figure 4.3), which might be derived from the heterogeneous expression system. As for F186A and F103A/F186A, there was no chlorination activity observed. The crystal structure of rCPO described in Chapter III indicated that the halogenation binding sites were stabilized by hydrophobic interactions with Phe103 and some other surrounding amino acids, so the inability of F186A and F103/186A to catalyze the halogenation of monochlorodimedone could be attributed to the configuration changes in the halide binding sites and the consequent restrictions on the access of halide ions to the heme.

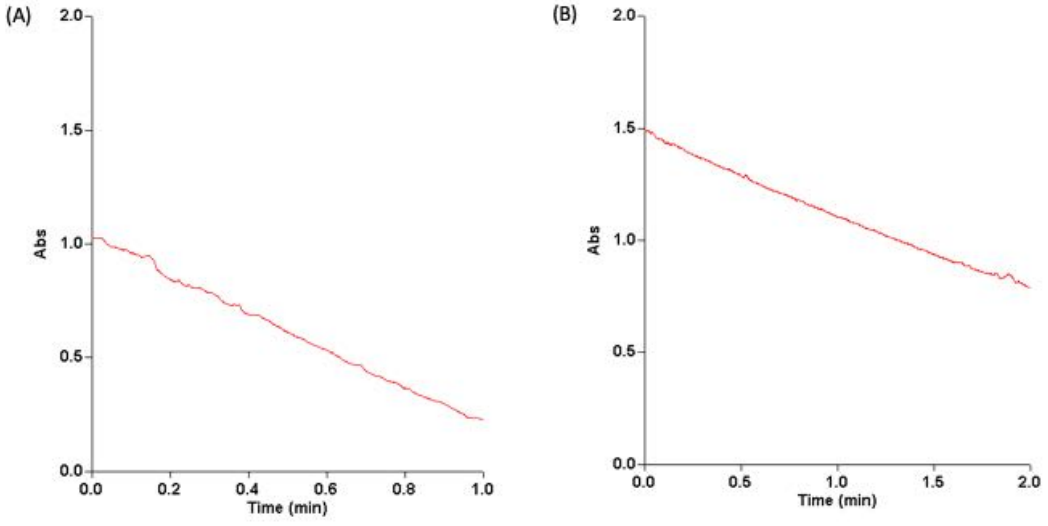

Figure 4.3 Chlorination reaction of MCD catalyzed by 0.025 μM of the wild type CPO at pH 2.75 (A) and 2.5 μM of the mutant CPO C29H at pH 3.25 (B) monitored at 278 nm.

4.3.2 Peroxidation Activities of C29H, F186A and F103A/F186A

CPO possesses the peroxidase-like activity, which catalyzes the peroxidation of ABTS via two one-eletctron transfer steps to produce $ABTS^{2+}$ and this reaction could be determined by monitoring the increase in absorbance at 405 nm. Our results indicated that all three mutants present significant improvements in peroxidation activities. Among them, C29H showed about 40-fold higher peroxidation activity than that of wtCPO. This outstanding increase could be explained as the result of the change in the basicity of the distal ligand due to the removal of the proximal cysteine. On the other hand, activities of both F103A and F103A/F186A were determined to increase about 5-fold compared to that of the wtCPO, which could be attributed to the decreases of steric effects as well as Pi-interactions of phenylalanine and substrates, since the substitution of alanine for phenylalanine enlarges the space around the heme and eliminates the aromatic ring, consequently enabling wider access of substrate to the enzyme's active site and diminishing the stabilization effects derived from Pi-interactions on substrates.

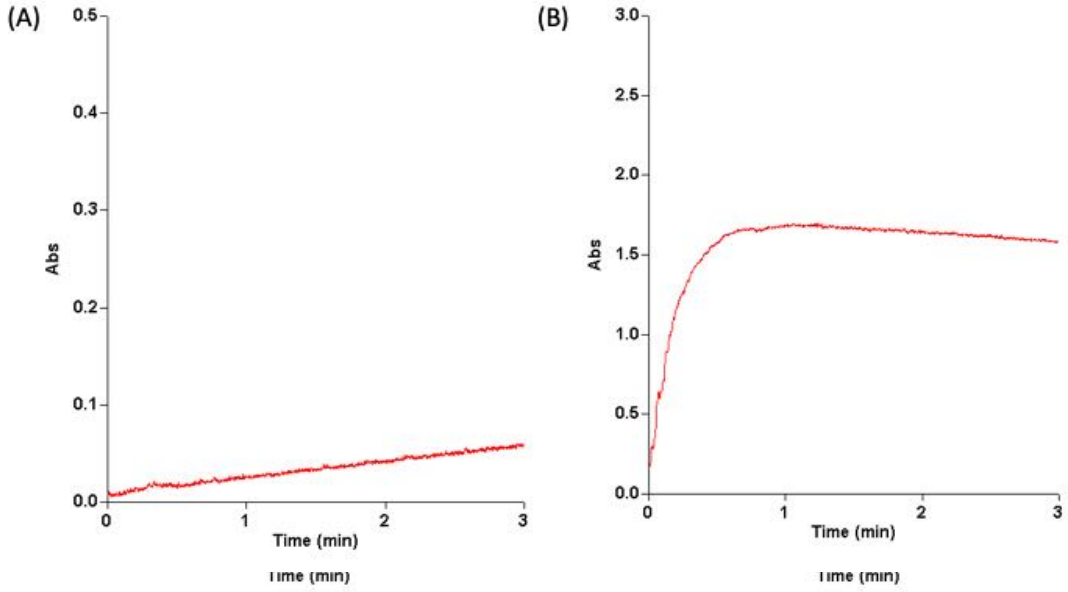

Figure 4.4 Peroxidation reaction of ABTS catalyzed by 0.065 μM of the wild type CPO (A), 0.1 μM of the C29H CPO (B), 0.1 μM of the F186A (C) and 0.1 μM of the F103A/F186A (D) monitored at 405 nm.

4.3.3 Epoxidation Activities of C29H, F186A and F103A/F186A

The chiral separation was applied to analyze the styrene epoxidation reactions catalyzed by C29H, F186A, F103A/F186A. The mutant CPO C29H was observed to present comparable enantioselectivity to that of the wtCPO, which dwarfs the effect of the proximal thiolate ligand on CPO-catalyzed epoxidations, and is consistent with previous study of C29H expressed in *C. fumago* [38]. However, the stereoselectivity of F186A decreased darmatically, with ee% of 9.74%, which could be explained as the lack of interactions between the substrate styrene and Phe186, indicating the contribution of this amino acid to CPO-catalyzed enantioselective epoxidations. Particularly, F103A/F186A was observed to catalyze styrene epoxidation with very low enantioselectivity (ee% of 2.68%), and significantly, the main product is not (R)-styrene epoxide but (S)-styrene epoxide. Both the sharp decrease in stereoselectivity and the conversion of major product confirmed the critical role of Phe103 in CPO-catalyzed epoxidations. To some extent, the adjustment of substrate by Phe103 was also identified. It is also possible that the combination effects of Phe103 and Phe186 contribute to the high enantioselectivity of

CPO-catalyzed epoxidation reactions of olefins.

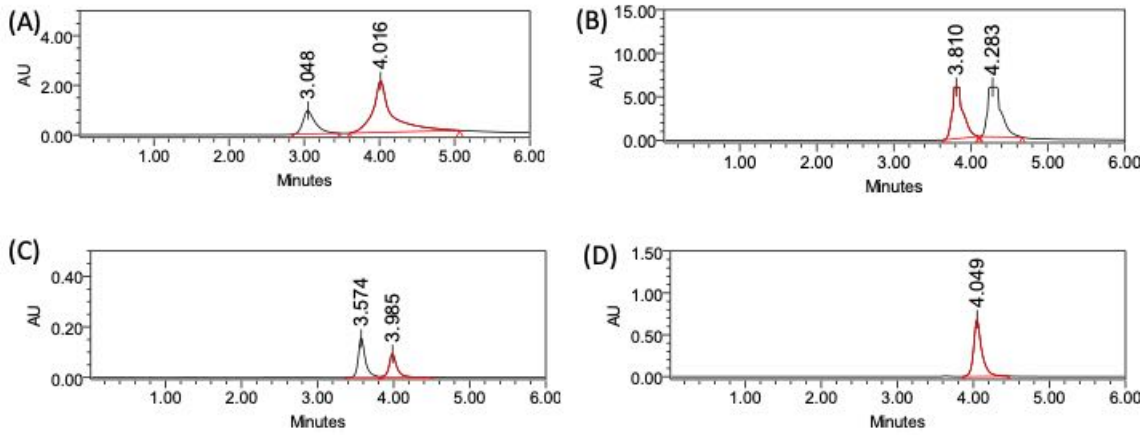

Figure 4.5 Chiral separation of styrene epoxide catalyzed by C29H with ee% of 54.46% (A), F186A with ee% of 9.74% (B) and F103A/186A with ee% of 2.68%. (D) Standard sample of the (R)-styrene epoxide.

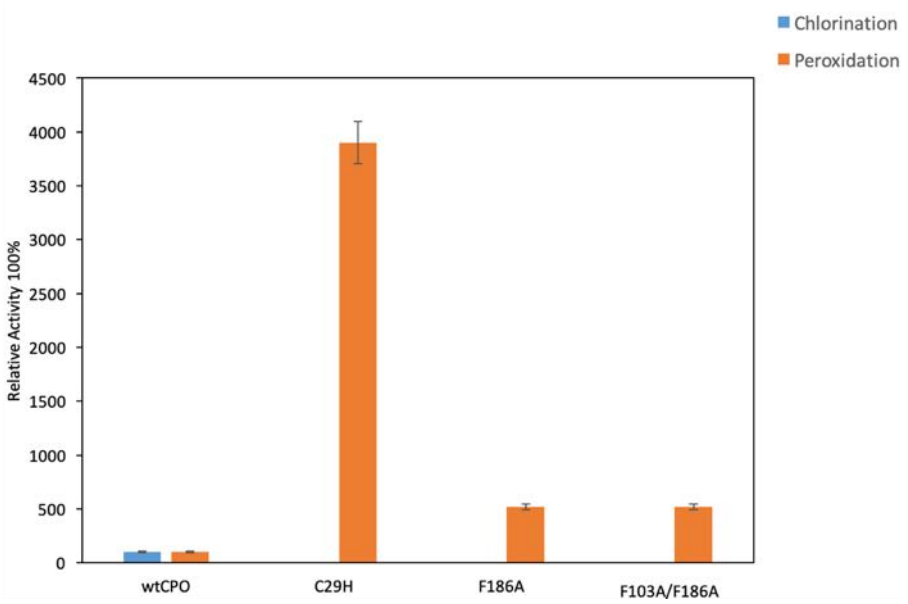

Figure 4.6 Relative activities of the wild type CPO, CPO mutants of C29H, F103A and F103A/F186A-CPO for chlorination of MCD and peroxidation of ABTS. Reactions were performed under the optimum pH respectively.

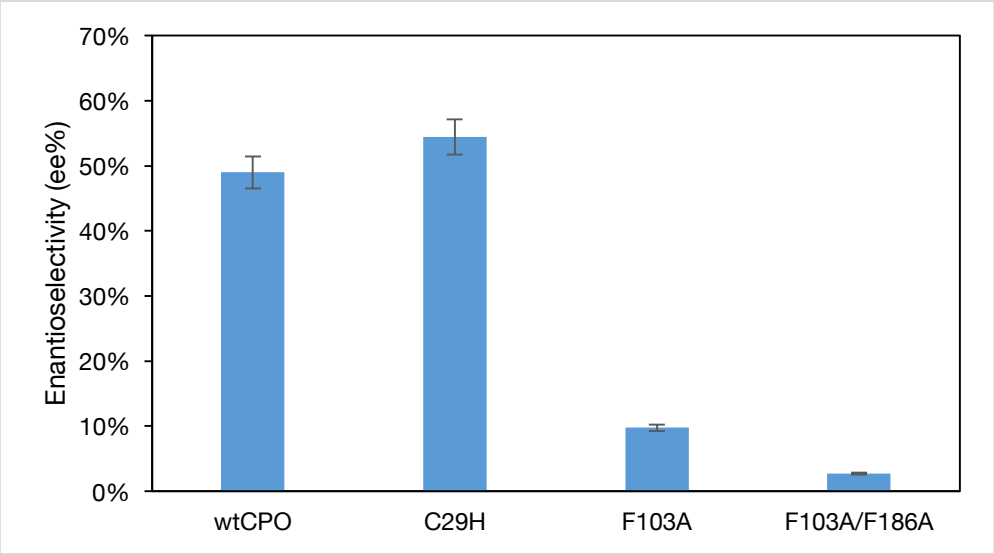

Figure 4.7 Enantioseletivities (indicated by ee%) of styrene epoxidations catalyzed by the wild type CPO, CPO mutants of C29H, F103A and F103A/F186A.

4.4 Conclusion and Discussion

Crystallographic studies of CPO indicated that the substrate binding pocket was bracketed by Phe103 and Phe186, and the Phe103 positioned at the bottom of the pocket could adjust to substrate binding [24]. The unique proximal thiolate ligand in CPO has been reported to be important to enantioselective epoxidations, since it determines the preferred electron transfer mechanism [59]. Thus, here we introduced three mutants of C29H, F186A and F103A/F186A to explore the roles of these residues in CPO catalysis. As previously mentioned, the *A. niger* system is available for CPO expression, so three mutants were expressed in this system heterogeneously and fortunately all of them were obtained. Besides, catalytic activities of mutant CPO were determined via chlorination of MCD, peroxidation of ABTS and epoxidation of styrene. Results indicated that CPO mutants present poor activities in chlorination, even if reactions were performed at the optimum pH.

However, the peroxidation activities of mutant CPO were observed to be enhanced significantly. For C29H, the redox potential of heme iron was decreased by the substitution of histidine for Cys29, which consequently increased the basicity of the ferryl oxygen and removed NH—S hydrogen bonds within the proximal pocket, leading to the increase in peroxidase reactivity. As for F186A and F103A/F186A, increased peroxidation activities could be attributed to the improved access of substrate to the heme center, since mutations provided larger space in the active site. Particularly, C29H was observed to catalyze the epoxidation of styrene with almost equivalent enantioselectivity compared with that of wtCPO. This result confirmed that the thiolate ligand has negligible effects of on CPO catalyzed enantioselective epoxidations, and also indicated CPO catalyzes epoxidations via a different mechanism. Contrary to C29H, both F186A and F103A/F186A present poor stereoselectivity in styrene epoxidations, which is in good agreement with previously reported adjustment of Phe103 to substrate binding, providing supports on interactions between these two residues and the substrate [24], [31].

The crystal structure determination of a protein requires suitable crystals for X-ray diffraction. Despite large amounts of efforts has been put, obtaining suitable crystals for diffraction remains to be a challenge. The crystal formation is mainly dependent on the concentration and nature of the protein, and also related to the methods for setting up crystallization trials (e.g., sitting drop vapor diffusion, hanging drop vapor diffusion, free interface diffusion). Moreover, crystallization conditions including temperature, pH, buffer types and salt solutions are essential for protein crystallization, too. Even though the same condition was applied for mutant proteins, there was no crystal formed in the drop. If the mutation lies within a dominant crystal interface of the wild-type structure, it may directly

interfere with crystallization in the same grid as the wild type. The mutation might lower the stability or increase the flexibility of the protein, which consequently favors aggregations or precipitations in the crystallization. We used wtCPO as seeds for the mutant, but unfortunately this approach failed to solve the problem. Actually, the purity of the protein sample is critical to crystallization since impure proteins might not able to form crystals, or form small crystals which are not suitable for X-ray diffraction experiments. Sometimes impure protein samples form crystals which fail to scatter X-rays well, because impure crystals lead to lattice strain and decrease the crystalline order, resulting in low quality of the diffraction pattern [60], [61], [62], [63], [64], [65]. Thus, high purity (95%-99%) is an essential prerequisite for protein crystallization, which requires an efficient approach for mutant CPO purification.

CHAPTER V. SYSTEM FOR THE EXPRESSION OF MUTANT CHLOROPEROXIDASE IN *ESCHERICHIA COLI*

5.1 Background and Theory

Spectroscopic and crystallographic investigations indicated that chloroperoxidase shared structural properties with both Cytochromes P450 and heme peroxidases. CPO contains a thiolate-ligand in the P450-like proximal pocket, and a peroxidase-like polar distal pocket, which enables it to catalyze various reactions. The formation of an oxo-ferryl radical intermediate, Compound I, is the prerequisite for all CPO-catalyzed reactions. Among them, enantioselective epoxidations of alkenes and their derivatives are highly intriguing because enantiopure products are extremely important to fine chemical industry, particularly to drug and nature product synthesis. Also, CPO-catalyzed epoxidations dwarf traditional chemical routes due to relatively high stereoselectivities, low expenses and moderate reaction conditions.

Considering the biotechnological and pharmaceutical potentials [57], large number of investigations on CPO-catalyzed epoxidations were carried out, and several factors related to enantioselectivities were reported. For reaction conditions, oxidant species has little effect, even though TBHP could accelerate the epoxidation in the case of 3-chloropropene. On the other hand, enantioselectivities are highly dependent on the pH of reaction systems, because CPO are extremely unstable in alkaline or strong acidic conditions [66, 67]. Typically, aqueous media is employed for epoxidations catalyzed by CPO, however, several non-aqueous media indicate that the presence of organic phase could either inhibit reactions or improve catalytic efficiency, depending on the nature of

substrates. Specifically, ironic liquids is able to increase substrate solubility and improve the affinity as well as selectivity of CPO to substrate, thus enhance enantioselectivities [68]. Steric effects of substrates are also critical factors. cis-disubstituted alkenes bearing alkyl substituents and 2-methyl-1-alkenes are excellent substrates with high enantioselectivities. In addition to the position of substitute group, the increase of carbon chain length of alkenes improves stereoselectivities until an optimum is reached, and then ee % starts to decrease. As a hybrid of heme peroxidase and Cytochrome P450, both distal pocket and proximal pocket contribute to epoxidations. The reaction barrier for epoxidation of CBMS is decreased by the self-adjustment on size of distal pocket, to fit the binding stage and the transition state. Particularly, the rearrangement of Glu183 through interactions within the distal pocket enables CPO to mimic both peroxidase-like and P450-like distal pockets to tune its catalytic efficiency [21]. On the other hand, the proximal pocket improves the reaction activity of olefin epoxidations via combined effects of the NH−S hydrogen bonds and the dipole moment of the proximal helix [20]. More importantly, the proximal pocket determines the preference of electron transfer mechanism of epoxidations, which indeed affect enantioselective [59].

Since the first reported of chloroperoxidase in 1966 [69], researchers have put numerous effort to investigate the catalytic mechanism of asymmetric epoxidations. Although it has not been fully understood yet, some theoretical and experimental investigations offer important clues. From crystallographic works, we could hypothesize that certain amino acid side chains within the distal pocket might guide or interact with substrates and induce them to specific configurations, leading to enantioselectivities. So far, many investigations on mutant CPO like C29H and E183H have proved effects of these

residues on catalytic activities [38, 39], however, structural information is limited, which restrict approaches to exploring specific catalytic mechanism, because the structure is always recognized as the fundamental base for functions. Thus, obtaining fine diffraction data of mutant CPO or CPO-substrate complexes from crystals with excellent quality might be a way to elucidating the mechanism. However, the difficulty in crystallizing mutant CPO hinders the application of this method. Usually, large amount of highlyconcentrated proteins with high purity are required for crystallization, however, expressing and purifying mutant CPO is actually a long-time and tedious work.

Escherichia coli. has been recognized as the most efficient, productive, and low-cost system to express recombinant proteins, so constructing an available *Escherichia coli.* system for mutant CPO expression would circumvent the drawbacks of *A. niger* system. Among eukaryotic organisms, glycosylation is one of the most common post-translational modification and critical to protein folding and function [70]. Fortunately, many studies indicated that glycosylation is not required for CPO's refolding [55] as deglycosylation has little influence on enzyme activity once CPO is properly folded [56], [71]. However, expression of hemoproteins in *E. coli* is always restricted due to the lack of heme group which is necessary for function [72], [73], [74], [75], [76], [77] due to lack of synchronization between rates of protein and heme biosynthesis. So far, many approaches have been attempted to increase heme binding. One way is to reduce the protein synthesis rate [72], but the subsequent decreased expression rate dwarfs the improvement of heme group binding. Another method is to add large amount of heme precursor, δ-aminolevulinic acid (δ-ALA) to accelerate the biosynthesis of heme [73], [74], [75]. Although this

approach is effective for the expression of hemoproteins, consumption of considerable amount of δ-ALA is quite expensive.

Adding heme to the medium in the process of hemoprotein expression has been considered as the easiest way, but most *E. coli* strains lack the ability to use exogenous heme as an iron source for growth [78], [79], [80], [81]. Significantly, *E. coli* O157:H7 was reported to express a TonB-dependent outer membrane-bound heme receptor gene using heme from extracellular environment as a source of porphyrin as well as iron [79], offering a ray to overcome the limitation of heme incorporation. In addition, a new *E. coli* system based on plasmids containing an outer membrane-bound heme receptor gene (*ChuA*) from *E. coli* O157:H7 was developed to express catalase-peroxidase with a dramatic increase in both heme content and activity. This system might be applicable for other hemoproteins, so *ChuA* gene was employed to develop an *E. coli*. system to express active CPO.

5.2 Experimental Methods

5.2.1 Materials and Reagents

The *E. coli* strain BL-21(DE3) was purchased from New England Biolabs (Ipswich, MA). All buffers and media were freshly prepared by water purified through Milli-Q Biocel (Millipore, Billerica, MA). Plasmids based on pET to express mutant CPO gene and *ChuA* gene were purchased from GeneScript (Piscataway, NJ). All equipment for *E. coli* cultivation were sterilized. All buffers and media were freshly prepared by water purified through Milli-Q Biocel (Millipore, Billerica, MA).

5.2.2 Construction of Plasmids

5.2.2.1 Codon Optimization of the Mutant CPO-C29H Gene and ChuA Gene

A wide variety of factors regulate and influence gene expression levels. Here we take as many of them as possible into considerations to produce the single gene that can reach the highest possible level of expression. In this case, the native gene employs tandem rare codons that can reduce the efficiency of translation or even disengage the translational machinery. For the mutant CPO-C29H gene, the codon usage bias in *E. coli* was increased by upgrading the Codon Adaptation Index (CAI) from 0.51 to 0.96. GC content and unfavorable peaks have been optimized to prolong the half-life of the mRNA. The Stem-Loop structures, which impact ribosomal binding and stability of mRNA, were broken. As for the *ChuA* gene, similar optimizations were undertaken and the codon usage bias in *E. coli* was increased by upgrading the CAI to 0.96.

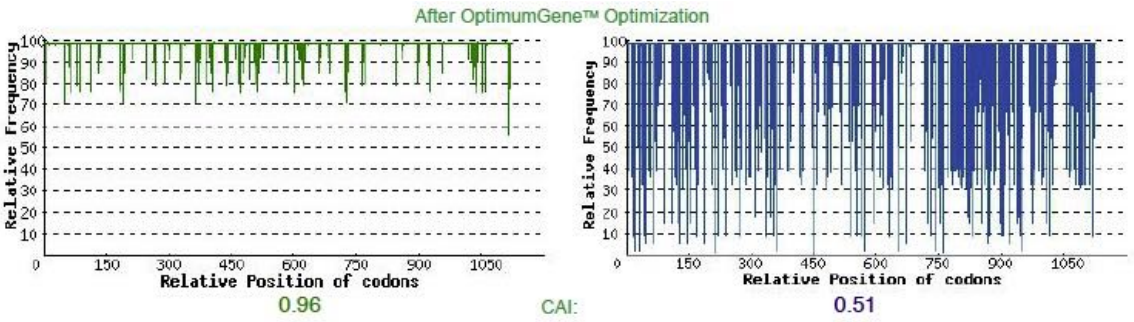

Figure 5.1 The distribution of codon usage frequency of the mutant CPO-C29H gene along the length of the gene sequence. A CAI of 1.0 is considered to be perfect in the desired expression organism, and a CAI of > 0.8 is regarded as good, in terms of high gene expression level.

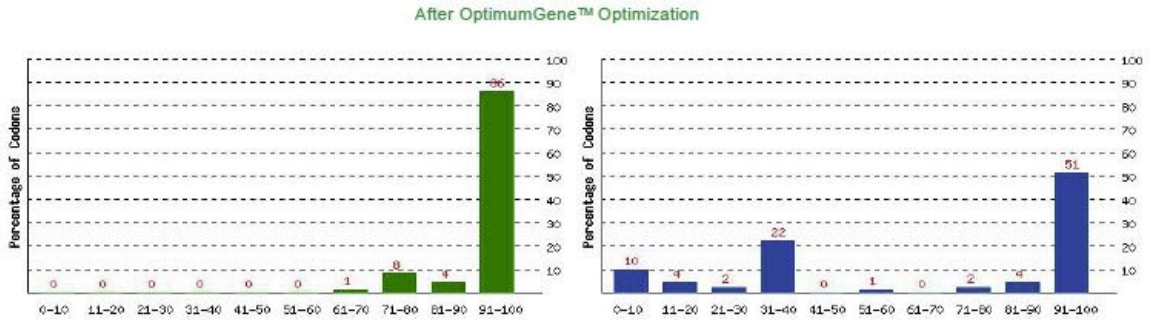

Figure 5.2 The percentage distribution of the mutant CPO-C29H codons in computed codon quality groups. The value of 100 is set for the codon with the highest usage frequency for a given amino acid in the desired expression organism.

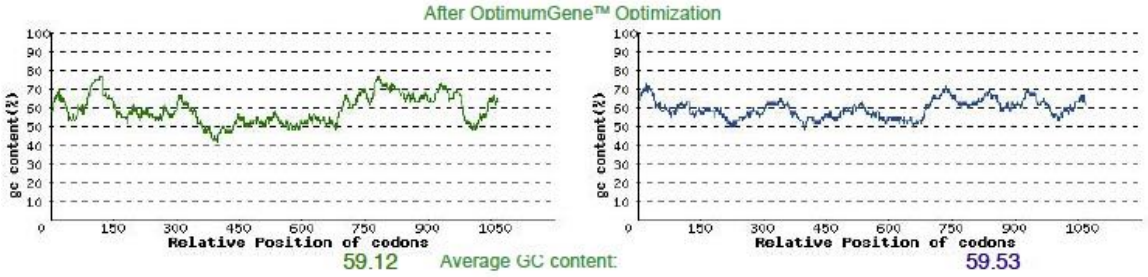

Figure 5.3 GC content adjustment of the mutant CPO-C29H gene. The ideal percentage of GC content is between 30-70%. Peaks of %GC content in a 60 bp window have been removed.

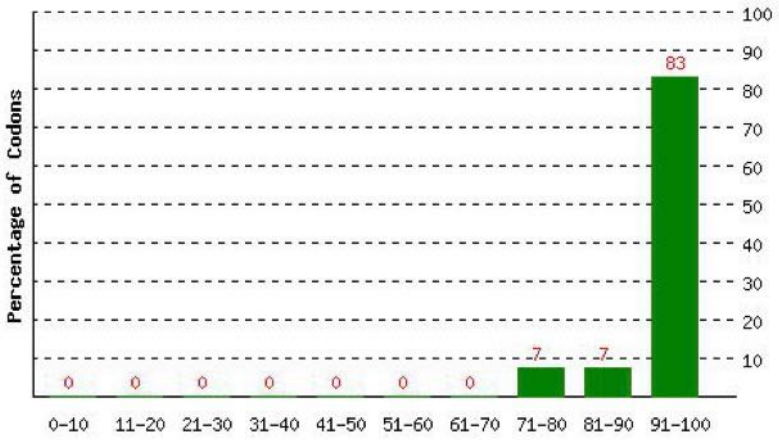

CAI: 0.96

Figure 5.4 The distribution of codon usage frequency of the ChuA gene along the length of the gene sequence. A CAI of 1.0 is considered to be perfect in the desired expression organism, and a CAI of > 0.8 is regarded as good, in terms of high gene expression level.

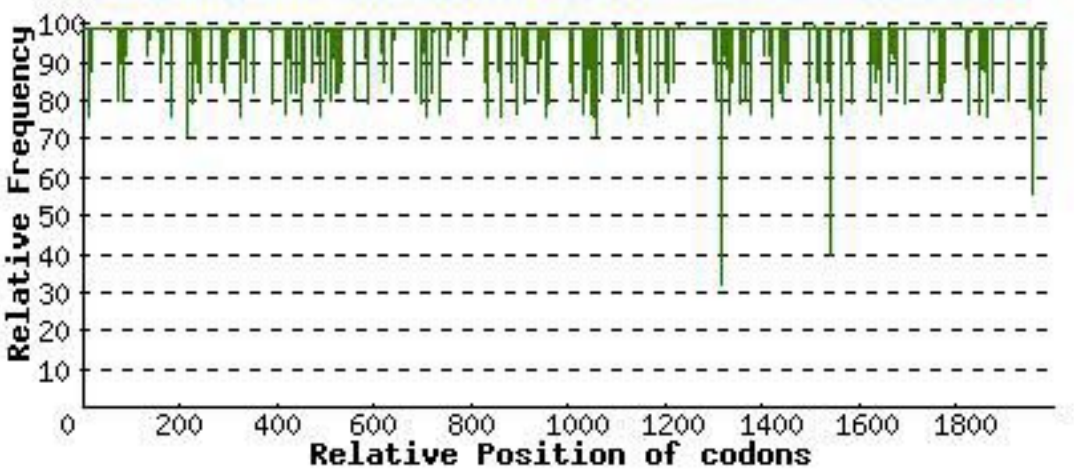

Figure 5.5 The percentage distribution of the ChuA codons in computed codon quality groups. The value of 100 is set for the codon with the highest usage frequency for a given amino acid in the desired expression organism.

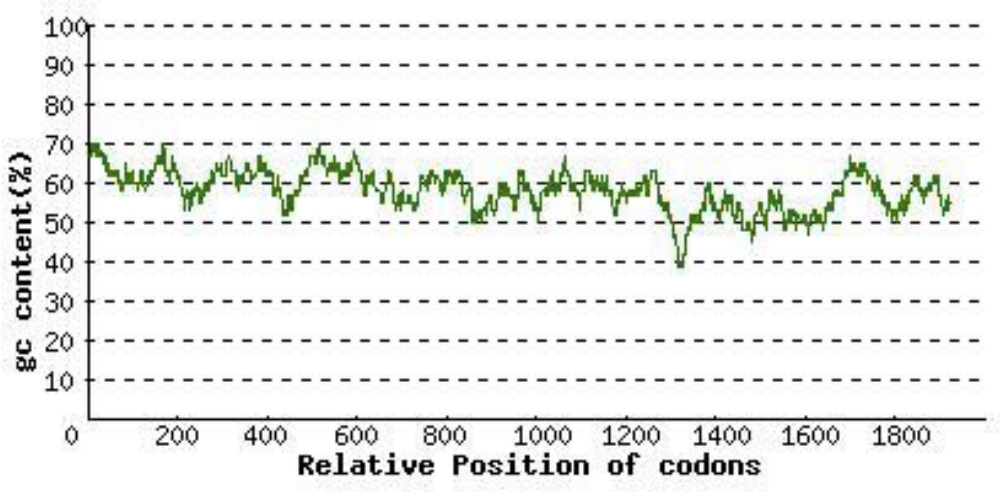

Figure 5.6 The average GC content of the ChuA gene is 58.11%. The ideal percentage of GC content is between 30-70%. Peaks of %GC content in a 60 bp window have been removed.

5.2.3 Heme Iron Utilization by Untransformed and p*ChuA*-Transformed *E. coli*

The plasmid p*ChuA*, a pET-based plasmid for expression of the *ChuA* gene, was transformed into *E. coli* BL-21 (DE3) strain and then inoculated to Luria-Bertani broth (LB) agar plate containing 100 μg/mL kanamycin for antibiotic selection.

Figure 5.7 Successful transformants of pChuA on the LB agar antibiotic selection plate.

To compare the ability of heme iron utilization, both untransformed *E. coli* BL-21 (DE3) and p*ChuA*-transformed strains were cultured in M9 minimal media supplemented with different concentrations of filter sterilized 2,2'-bipyridine. Bacteria were grown at 37 ℃with 200 rpm shaking for 7 days. The OD_{600} values over time were record for growth determination. The best inhibition effect was observed in the media supplemented with 0.20 mM of 2,2'-bipyridine. Then 76.70 μM of hemin was added into M9 minimal media with 0.20 mM 2,2'-bipyridyl for the culture of *E. coli* with and without p*ChuA* plasmid, and the OD_{600} values were record to compare heme iron utilization.

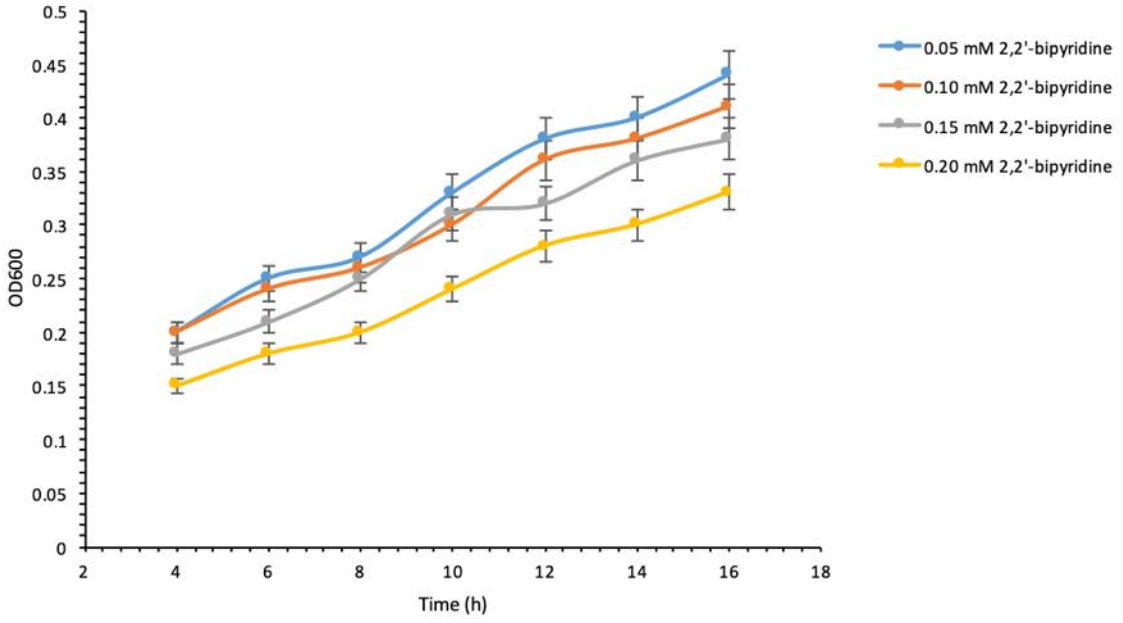

Figure 5.8 Inhibitory effects on pChuA transformed E. coli BL21 (DE3) growing in M9 minimal media with different concentrations of 2,2'-bipyridine.

5.2.4 Expression and Purification of Mutant Chloroperoxidase

The pET-based plasmid for expression of the histidine-tagged mutant CPO-C29H was transformed into *E. coli* BL21 (DE3) and then inoculated to Luria-Bertani broth (LB) agar

plate containing 50 μg/mL carbenicillin for antibiotic selection. The plate was incubated at 37℃ overnight and a single colony was selected to grow in several cell culture tubes containing 6 mL of the liquid LB media and 50 μg/mL carbenicillin, respectively. The bacterial culture was incubated at 37℃ with 250 rpm shaking overnight. The growth was determined by measuring the value of OD_{600}. Once OD_{600} reaches about 2.1, 10 mL of the culture was transferred into a 2L flask containing 1L of the LB media with antibiotic to incubate at 37℃ with 250 rpm shaking. The value of OD_{600} was monitored during this period. Then 0.2 mM of IPTG was added into the culture once OD_{600} reaches 0.5~0.7. The bacterial culture was incubated for 3 more hours under the same condition. The samples were collected every 1h to perform SDS-PAGE to check the expression of the mutant enzyme. The bacterial was harvested by centrifugation at 6500 rpm and 4℃ for 15min. Then the bacterial pellets were resuspended in 25 mL of lysis buffer (14.4 M β-mercaptoethanol, tablets of protease inhibitor, lysozyme) and incubated on ice for 1h with frequent inverting. After that, the lysate was incubated at 37℃ for 5 minutes and stored at -80℃ for further purification.

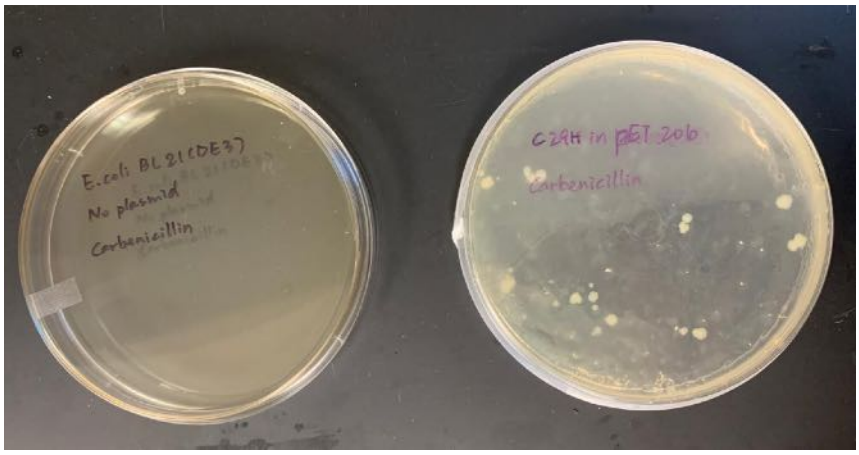

Figure 5.9 Successful transformants on the LB agar antibiotic selective plate.

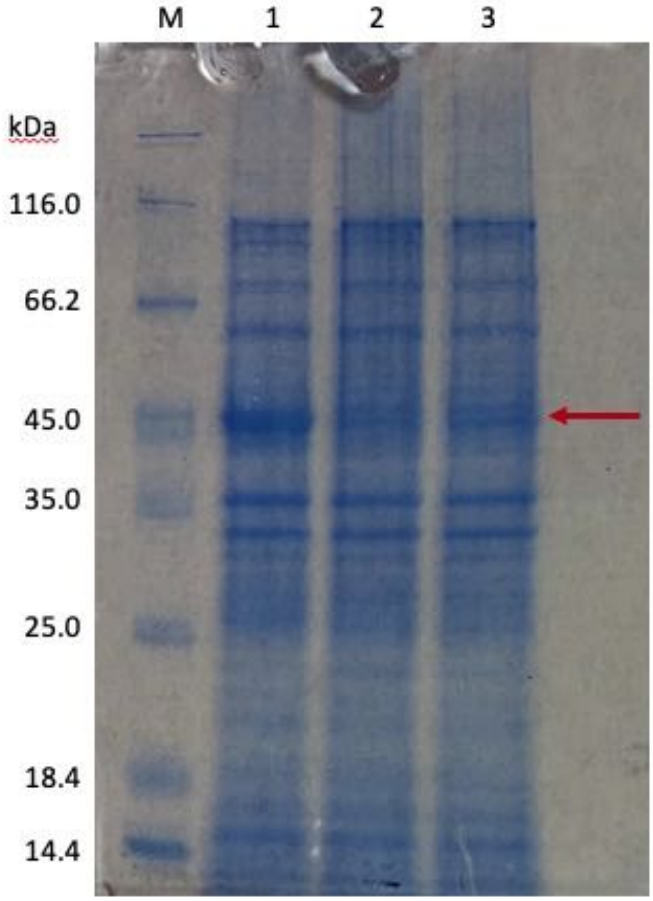

Figure 5.10 Mutant CPO-C29H expression by E. coli BL21 (DE3). Proteins from BL21 (DE3) (Lanes 1, 2 and 3) were separated by SDS-PAGE. Lane 1 was obtained from LB media added with 0.2 mM IPTG.

The frozen bacterial lysate was thawed on ice for several minutes and sonicated to reduce its viscosity. Then the lysate was centrifuged at 15,500 rpm and 4℃ for 30 minutes and the supernatant was collected for chromatography. The His-tag Ni-NTA resin column (volume 10 mL) was washed with DI water first and then washed with 50~100 mL of 50 mM Tris-HCl buffer, pH 8.0 containing 0.5 M NaCl, 5 mM imidazole, 1mM PMSF, and 5 mM β-mercaptoethanol. The lysate supernatant was loaded onto the column and washed with 50 mM Tris-HCl buffer, pH 8.0 containing 0.5 M NaCl, 5 mM imidazole, 10% glycerol, 1 mM PMSF and 5 mM β-mercaptoethanol. Protein was eluted with 50 mL of 50

mM Tris-HCl buffer, pH 8.0 containing 0.5 M NaCl, 250 mM imidazole, 10% glycerol, 1 mM PMSF and 5 mM β-mercaptoethanol. The protein concentration was measured by Bradford assay and its molecular weight was determined by SDS-PAGE. The products were further purified through ion-exchange and gel-filtration chromatography as procedures described in 3.2.3 to remove unwanted proteins. Finally, the purified protein was characterized by UV-vis spectrum.

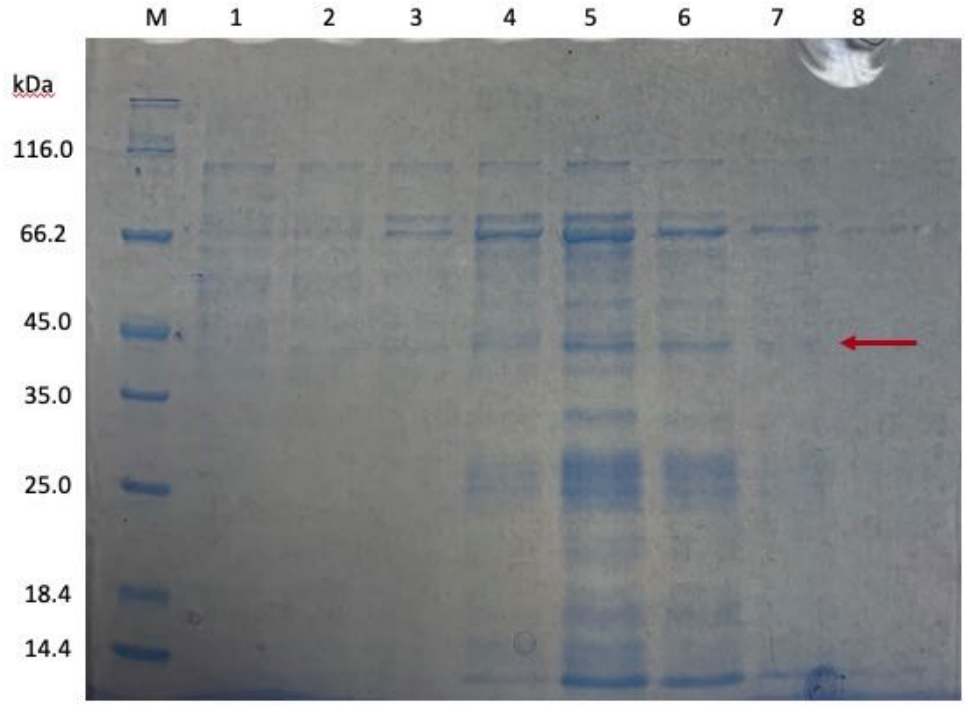

Figure 5. 11 Proteins from E. coli BL21 (DE3) lysate after Ni-NTA column purification.

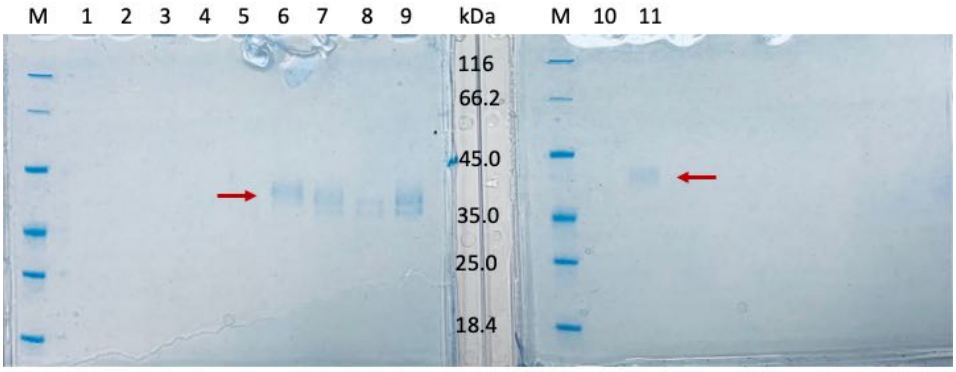

Figure 5.12 Purified recombinant mutant CPO-C29H after ion-exchange and gel-filtration chromatography.

5.2.5 Co-expression of ChuA gene and Mutant CPO-C29H

Expressing hemoproteins in *E. coli system* has been constrained by the difficulty of heme group binding [72], [73], [74], [75], [76], [77]. In order to improve heme binding of the mutant CPO, both plasmid p*ChuA* containing the outer membrane-bound heme receptor gene and plasmid pCPO3.I-AmdS-C29H encoding the mutant were constructed into the gene of mutant CPO-C29H and were co-transformed into *E. coli* strain BL21 (DE3). The transformants were inoculated to Luria-Bertani broth (LB) agar plate containing 50 μg/mL carbenicillin and 100 μg/ml kanamycin for antibiotic selection. The plate was incubated at 37℃overnight and only transformants with both p*ChuA* and pCPO3.I-AmdS-C29H could survive on the plate with two different types of antibiotics. Single colonies were then selected to grow in several cell culture tubes containing 6 mL of the liquid LB media and 50 μg/mL carbenicillin as well as 100 μg/ml kanamycin.

Bacterial culture and protein purification procedures were the same as experimental methods described in 5.2.4.

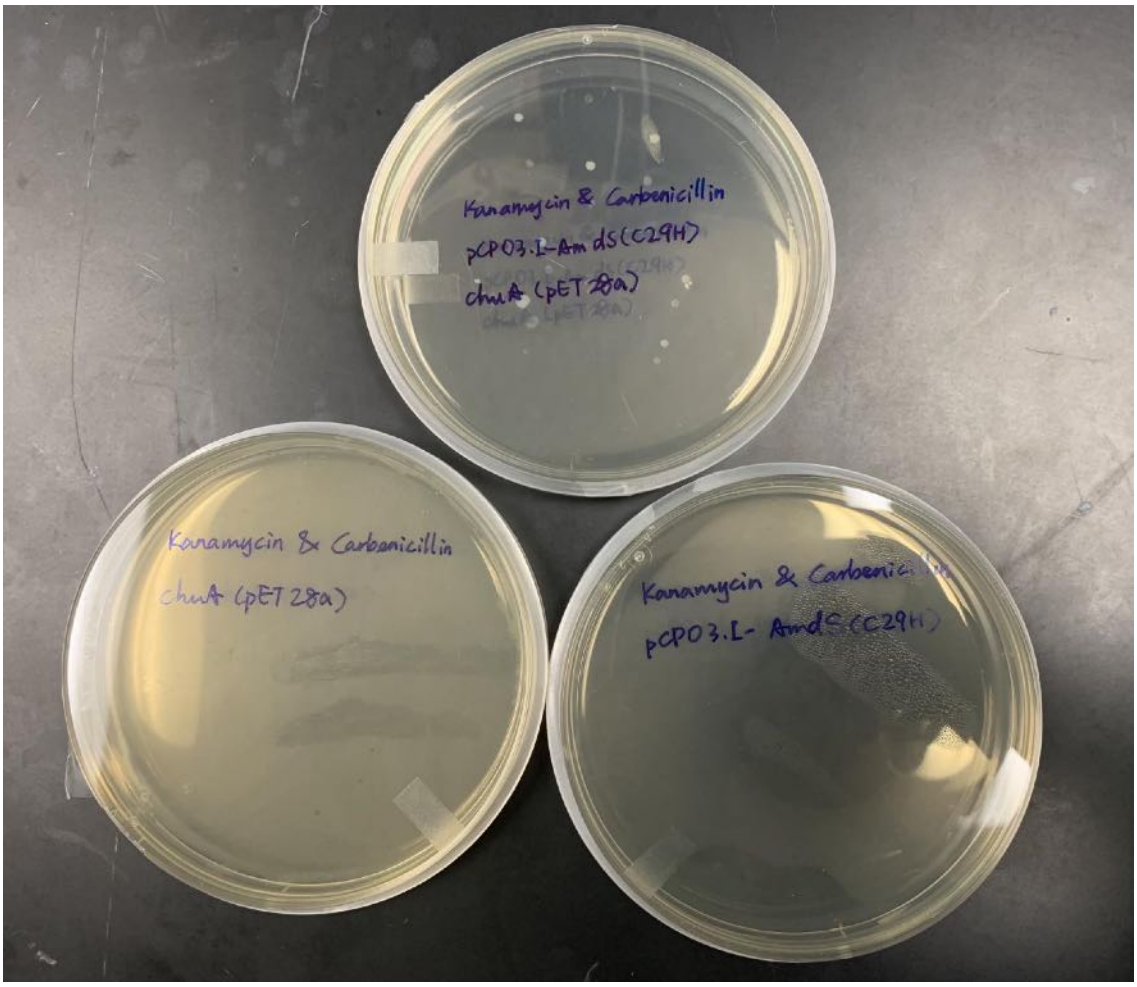

Figure 5.13 Successful co-transformants on the LB agar antibiotic selection plate containing both carbenicillin and kanamycin.

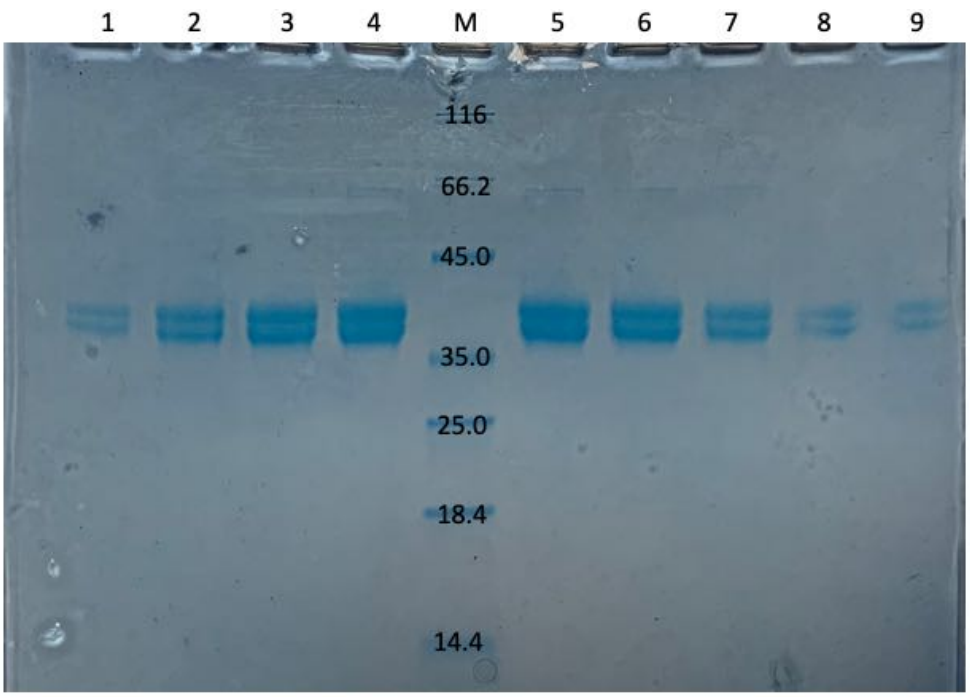

Figure 5.14 Purified mutant CPO-C29H with the assistant gene of ChuA after ion-exchange and gel-filtration chromatography.

5.3 Results

5.3.1 Expression and Function of *ChuA* Gene

The abilities of p*ChuA*-transformed and untransformed *E.coli* strains to grow in iron-deficient media was determined by monitoring OD_{600}. The results indicated that strains without *ChuA* gene was not capable of surviving in M9 minimal media even if they were supplemented with hemin as an iron source. However, once the outer-membrane heme receptor *ChuA* gene was introduced, the growth was observed to increase significantly, indicating the cells' ability to utilize hemin. Interestingly, addition of different concentrations of IPTG were observed to have little effects on *ChuA* gene expression, possibly due to "leaky expression", or in other word, the basal level expression of T7 RNA

polymerase in *E. coli* BL-21 (DE3). It is also possible that the concentration of IPTG added into medium was not high enough to induce the expression of the target gene. Additionally, the time that IPTG was added might not be suitable. Once there was plenty of glucose in the medium, the lac operon would be inhibited, leading to the restriction of target protein expression.

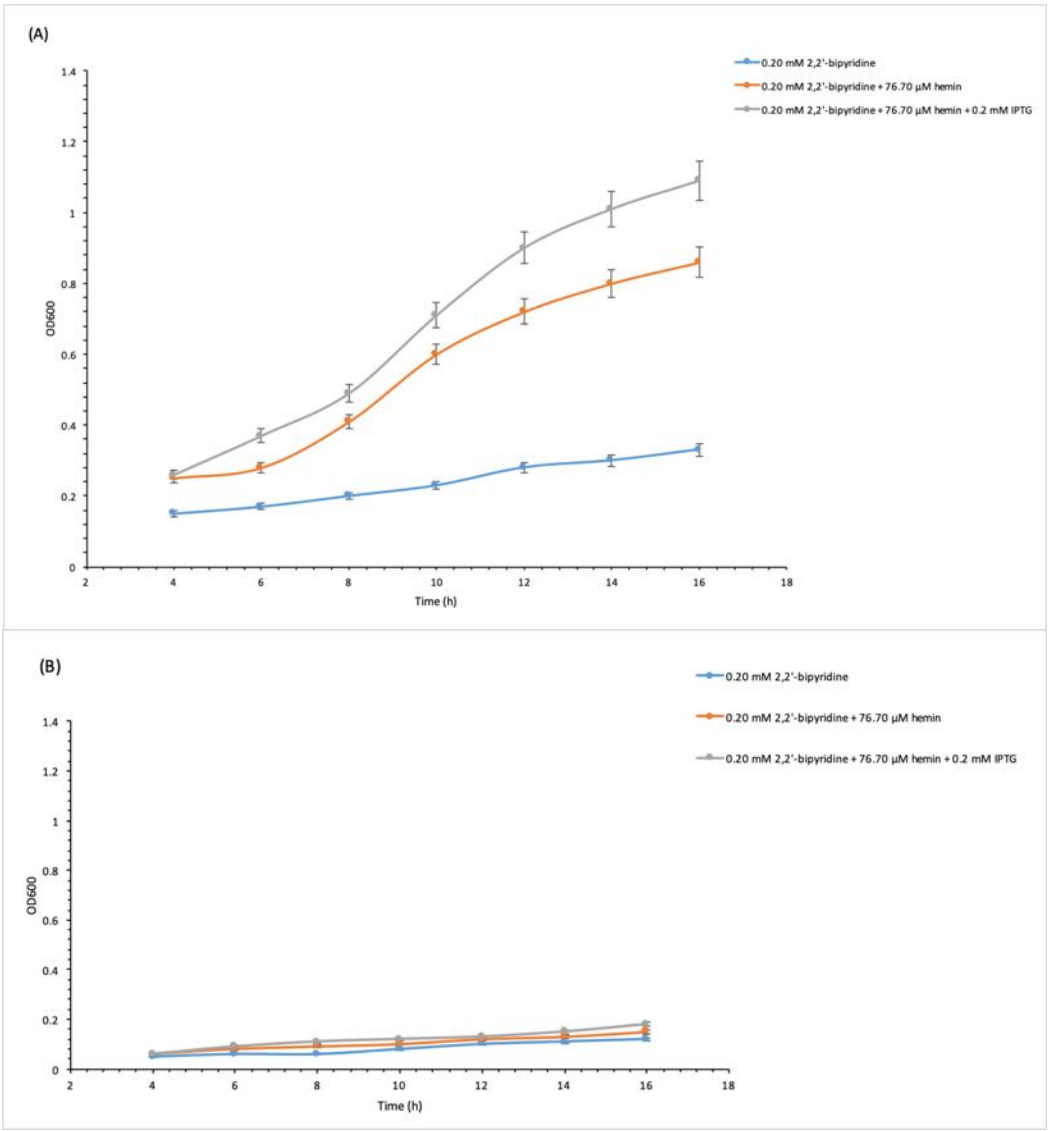

Figure 5.15 Hemin utilization efficiency in E. coli strain BL21 (DE3). Growth of pChuA transformed strains is shown in (A) and growth of untransformed strains is shown in (B).

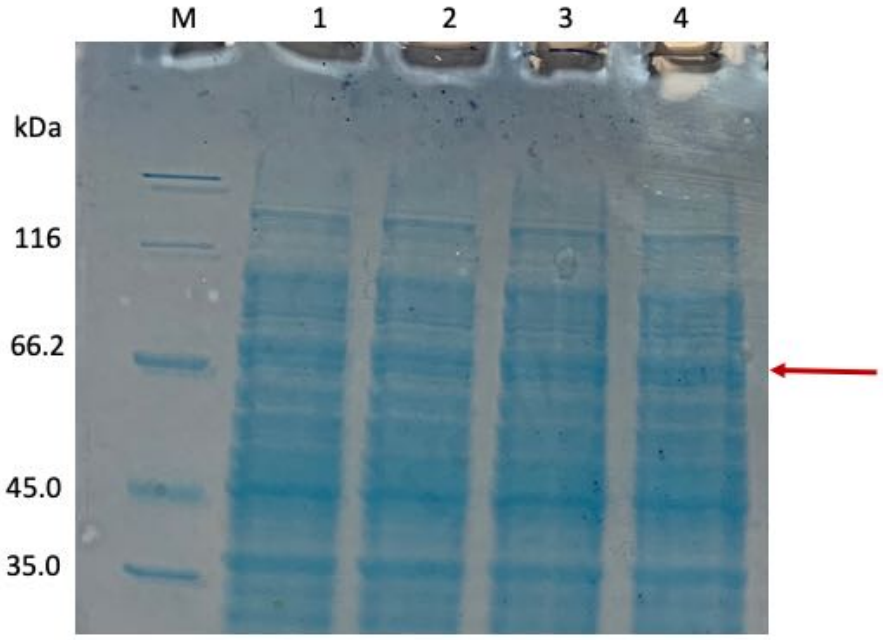

Figure 5.16 Outer membrane-bound heme receptor expression by pChuA transformed E. coli BL-21 (DE3). Proteins from BL-21 (DE3) were analyzed by SDS-PAGE. Proteins in lane 2 - 4 were obtained from LB media added with 0.2 mM, 0.3 mM and 0.5 mM IPTG respectively.

5.3.2 Characterization of the Recombinant Mutant CPO-C29H expressed in BL-21 (DE3) pET-20b

Although SDS-PAGE results confirmed the existence of recombinant C29H, neither chlorination nor peroxidation activity was observed (Figure V.17 and Figure V.18). Also, the purified C29H was colorless, indicating little heme binding. This is further proved by the lack of the Soret peak in UV-vis spectrum around 400 nm.

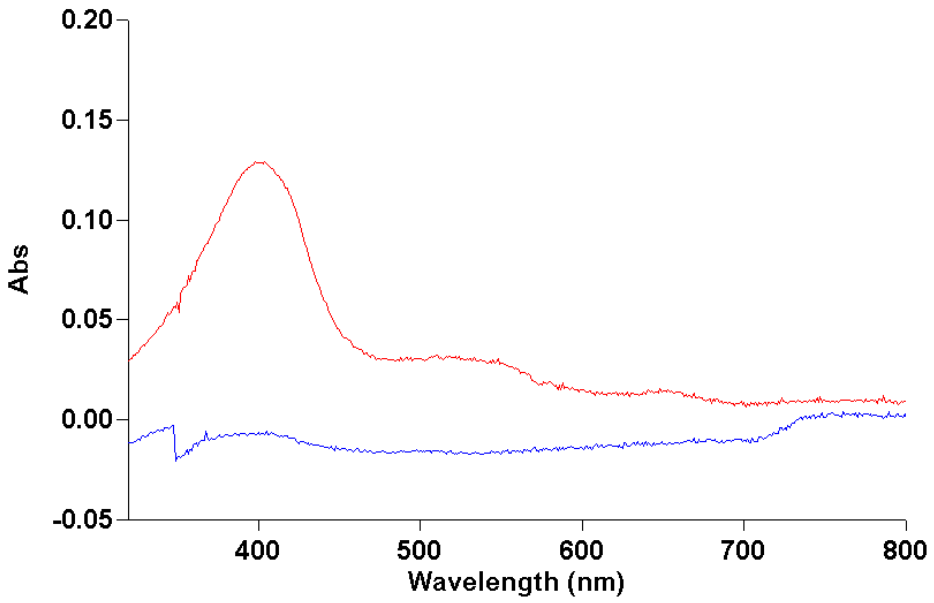

Figure 5.17 UV-vis spectrum of wtCPO and C29H expressed in BL-21 (DE3) pET-20b. The Soret peak of wtCPO was observed at 400 nm while no absorption was identified for C29H.

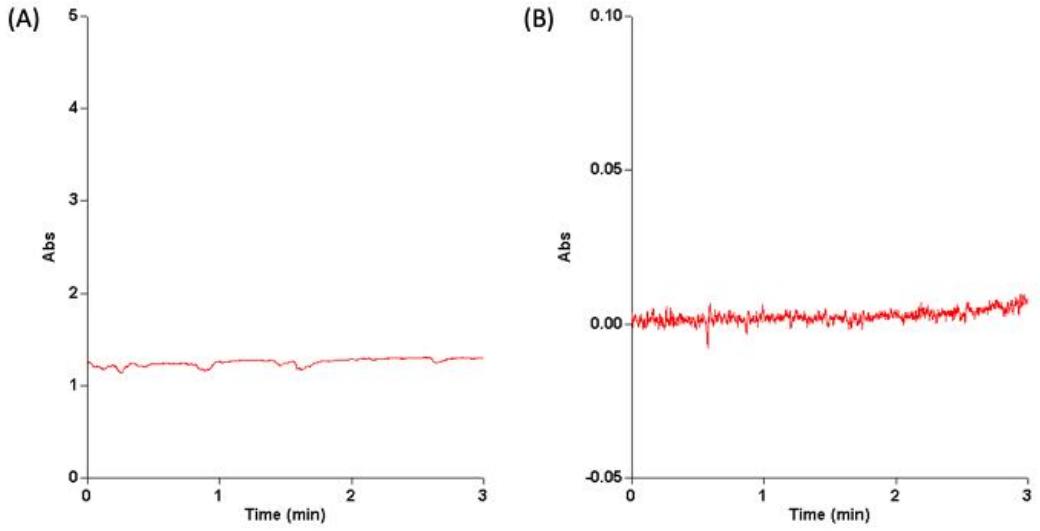

Figure 5.18 (A) Chlorination of MCD catalyzed by the 1 µM C29H expressed in BL-21 (DE3) pET-20b monitored at 278 nm. (B) Peroxidation reaction of ABTS catalyzed by 1 µM C29H expressed in BL-21 (DE3) pET-20b monitored at 405 nm.

5.3.3 Spectroscopic Properties and Catalytic Activities of CPO-C29H expressed in BL-21 (DE3) p*ChuA*-pCPO3.I-AmdS

Interestingly, C29H expressed in BL-21 (DE3) p*ChuA*-pCPO3.I-AmdS not only displayed a light brick red color but also gave a characteristic absorption at 400 nm in UV-vis spectrum (Figure 5.19), confirming the improvement in heme incorporation with the assistance of *ChuA* gene. To our dismay, C29H expressed in this system possessed no chlorination and poor peroxidation activities (Figure 5.20), even if it possesses sufficient heme bindings.

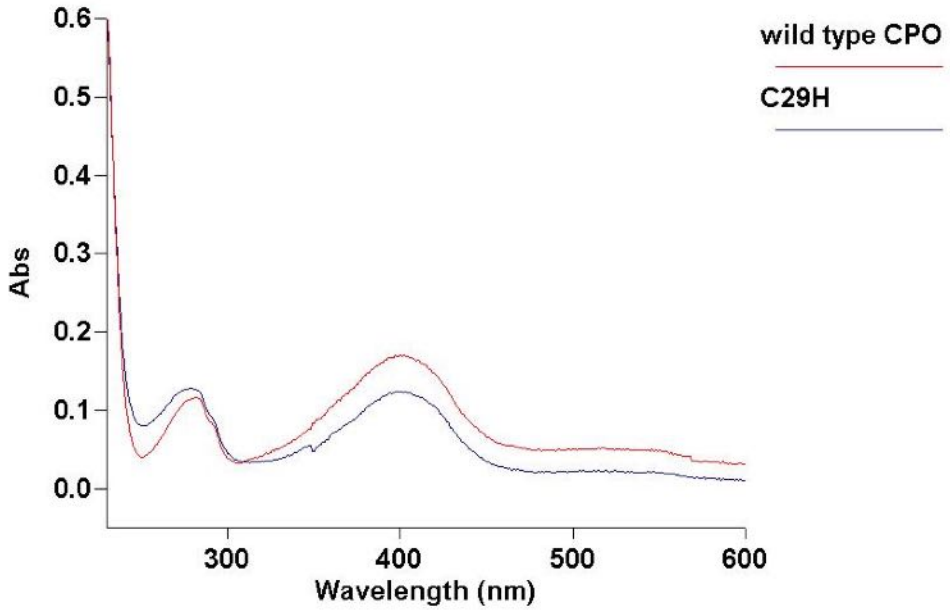

Figure 5.19 The Soret peaks of wtCPO and C29H expressed in BL-21 (DE3) pChuA-pCPO3.I-AmdS were both observed at 400 nm.

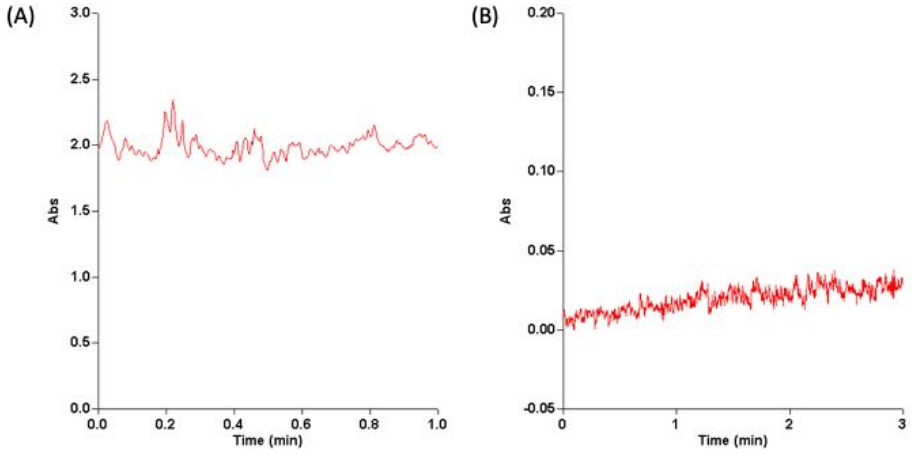

Figure 5. 20 (A) Chlorination of MCD catalyzed by 1 μM C29H expressed in BL-21 (DE3) pChuA-pCPO3.I-AmdS monitored at 278 nm. (B) Peroxidation reaction of ABTS catalyzed by 1 μM C29H expressed in BL-21 (DE3) pChuA-pCPO3.I-AmdS monitored at 405 nm.

5.4 Conclusions and Discussion

Chloroperoxidase catalyzes various reactions and the enantioselective transformations are highly intriguing due to potential applications in both biochemical and pharmaceutical industries. Our lab has focused on the relationship between the structure and function of CPO for decades, in order to elucidate the specific mechanism of CPO-catalyzed epoxidations and to further develop cost-effective enzymes for chiral synthesis. The crystallographic approach has always been recognized as one of the most powerful methods for the structure-function relationships of proteins, which is essential to establishing catalytic mechanisms of enzymes. Although crystallography has been widely applied, investigations on structures of mutant CPO have been restricted, since large amounts of relatively pure enzyme with high concentrations are required. Despite several

species of CPO mutants have been expressed in *A. niger* system successfully, low yields or efficiency has not been overcome yet. Here we employed prokaryotic system to express mutant CPO-C29H since it is highly efficient. Our results indicated that C29H expressed in BL-21 (DE3) pET-20b alone presented neither heme binding nor catalytic activities. However, with the assistance of outer membrane-bound heme receptor gene *ChuA*, C29H expressed in BL-21 (DE3) p*ChuA*-pCPO3.I-AmdS was observed to have equivalent absorption at 400 nm essentially identical to that of wtCPO, confirming the successful incorporation of heme to the apo protein. Thus, the employment of *ChuA* gene might be a promising assistant gene for the expression of not only CPO but also other hemoproteins. Unfortunately, no chlorination activity and poor peroxidation ability were identified, which might be attributed to the lack of post-translational modifications. Even though several studies demonstrated that glycosylation is not required for catalytic activity of wtCPO [56], [71], our results indicated that post-translational modifications in eukaryotic systems are necessary for activities of mutant CPO. Glycosylation might play an indispensable role in ensuring proper folding of CPO.

Significantly, the *ChuA* gene was observed to express even in the absence of IPTG, indicating leaky expression of T7 RNA polymerase. This leaky expression might lead to the decrease of bacterial growth or cell death if there is a toxic gene downstream the T7 promotor. Therefore, the use of *E. coli* BL-21(DE3)-pLysS cells could be applied to improve the expression of *ChuA* gene, since this strain is able to produce T7 lysozyme, which reduces basal expression of the target gene. Also, adding higher concentrations of IPTG might be effective in the induction of *ChuA* gene expression

REFERENCES

1. Kasai, N., T. Suzuki, and Y. Furukawa, *Chiral C3 epoxides and halohydrins: their preparation and synthetic application.* Journal of Molecular Catalysis B: Enzymatic, 1998. **4**(5-6): p. 237-252.

2. Besse, P. and H. Veschambre, *Chemical and biological synthesis of chiral epoxides.* Tetrahedron, 1994. **50**(30): p. 8885-8927.

3. Van Deurzen, M.P., F. van Rantwijk, and R.A. Sheldon, *Selective oxidations catalyzed by peroxidases.* Tetrahedron, 1997. **53**(39): p. 13183-13220.

4. Sharpless, K.B., *Searching for new reactivity (Nobel lecture).* Angewandte Chemie International Edition, 2002. **41**(12): p. 2024-2032.

5. Irie, R., et al., *Catalytic asymmetric epoxidation of unfunctionalized olefins using chiral (salen) manganese (III) complexes.* Tetrahedron: Asymmetry, 1991. **2**(7): p. 481-494.

6. Tu, Y., Z.-X. Wang, and Y. Shi, *An efficient asymmetric epoxidation method for trans-olefins mediated by a fructose-derived ketone.* Journal of the American Chemical Society, 1996. **118**(40): p. 9806-9807.

7. Santhanam, L. and J.S. Dordick, *Chloroperoxidase-catalyzed epoxidation of styrene in aqueous and nonaqueous media.* Biocatalysis and Biotransformation, 2002. **20**(4): p. 265-274.

8. Hager, L.P., F.J. Lakner, and A. Basavapathruni, *Chiral synthons via chloroperoxidase catalysis.* Journal of Molecular Catalysis B: Enzymatic, 1998. **5**(1-4): p. 95-101.

9. Lakner, F.J. and L.P. Hager, *Chloroperoxidase as enantioselective epoxidation catalyst: an efficient synthesis of (R)-(−)-mevalonolactone.* The Journal of organic chemistry, 1996. **61**(11): p. 3923-3925.

10. Lakner, F.J. and L.P. Hager, *Chloroperoxidase-mediated asymmetric epoxidation. Synthesis of (R)-dimethyl 2-methylaziridine-1, 2-dicarboxylate—a potential α-methylamino acid synthon.* Tetrahedron: Asymmetry, 1997. **8**(21): p. 3547-3550.

11. Osborne, R.L., et al., *Caldariomyces fumago chloroperoxidase catalyzes the oxidative dehalogenation of chlorophenols by a mechanism involving two one-electron steps.* Journal of the American Chemical Society, 2007. **129**(48): p. 14838-14839.

12. Gruia, F., et al., *Low-frequency dynamics of caldariomyces fumago chloroperoxidase probed by femtosecond coherence spectroscopy.* Biochemistry, 2008. **47**(18): p. 5156-5167.

13. Ayala, M., et al., *Reduced coke formation and aromaticity due to chloroperoxidase-catalyzed transformation of asphaltenes from Maya crude oil.* Fuel, 2012. **92**(1): p. 245-249.

14. Rutter, R. and L. Hager, *The detection of two electron paramagnetic resonance radical signals associated with chloroperoxidase compound I.* Journal of Biological Chemistry, 1982. **257**(14): p. 7958-7961.

15. Kim, S.H., et al., *Rapid freeze-quench ENDOR study of chloroperoxidase compound I: the site of the radical.* Journal of the American Chemical Society, 2006. **128**(17): p. 5598-5599.

16. Zhang, R., et al., *Paramagnetic nuclear magnetic resonance relaxation and molecular mechanics studies of the chloroperoxidase–indole complex: insights into the mechanism of chloroperoxidase-catalyzed regioselective oxidation of indole.* Biochemistry, 2013. **52**(21): p. 3688-3701.

17. Zhang, R., et al., *Spectroscopic and QM/MM investigations of Chloroperoxidase catalyzed degradation of orange G.* Archives of biochemistry and biophysics, 2016. **596**: p. 1-9.

18. Chen, H., et al., *Quantum mechanical/molecular mechanical study on the mechanisms of compound I formation in the catalytic cycle of chloroperoxidase: an overview on heme enzymes.* The Journal of Physical Chemistry B, 2008. **112**(31): p. 9490-9500.

19. Morozov, A.N., et al., *Enantiospecificity of chloroperoxidase-catalyzed epoxidation: biased molecular dynamics study of a Cis-β-methylstyrene/chloroperoxidase-compound I complex.* Biophysical journal, 2011. **100**(4): p. 1066-1075.

20. Morozov, A.N., A.D. Pardillo, and D.C. Chatfield, *Chloroperoxidase-catalyzed epoxidation of cis-β-methylstyrene: NH–S hydrogen bonds and proximal helix dipole change the catalytic mechanism and significantly lower the reaction barrier.* The Journal of Physical Chemistry B, 2015. **119**(45): p. 14350-14363.

21. Morozov, A.N. and D.C. Chatfield, *Chloroperoxidase-catalyzed epoxidation of cis-β-methylstyrene: Distal pocket flexibility tunes catalytic reactivity.* The Journal of Physical Chemistry B, 2012. **116**(43): p. 12905-12914.

22. D'Cunha, C., A.N. Morozov, and D.C. Chatfield, *Theoretical study of HOCl-catalyzed keto–enol tautomerization of β-cyclopentanedione in an explicit water environment.* The Journal of Physical Chemistry A, 2013. **117**(35): p. 8437-8448.

23. Chatfield, D.C. and A.N. Morozov, *Proximal Pocket Controls Alkene Oxidation Selectivity of Cytochrome P450 and Chloroperoxidase toward Small, Nonpolar Substrates.* J Phys Chem B, 2018. **122**(32): p. 7828-7838.

24. Sundaramoorthy, M., J. Terner, and T.L. Poulos, *The crystal structure of chloroperoxidase: a heme peroxidase–cytochrome P450 functional hybrid.* Structure, 1995. **3**(12): p. 1367-1378.

25. Beckwith, J.R. and L.P. Hager, *Biological Chlorination: VIII. LATE INTERMEDIATES IN THE BIOSYNTHESIS OF CALDARIOMYCIN.* Journal of Biological Chemistry, 1963. **238**(9): p. 3091-3094.

26. Kuhnel, K., et al., *Crystal structures of chloroperoxidase with its bound substrates and complexed with formate, acetate, and nitrate.* J Biol Chem, 2006. **281**(33): p. 23990-8.

27. Dexter, A.F., et al., *Highly enantioselective epoxidation of 1, 1-disubstituted alkenes catalyzed by chloroperoxidase.* Journal of the American Chemical Society, 1995. **117**(23): p. 6412-6413.

28. Axley, M.J., P. Kenigsberg, and L.P. Hager, *Fructose induces and glucose represses chloroperoxidase mRNA levels.* Journal of Biological Chemistry, 1986. **261**(32): p. 15058-15061.

29. Hager, L.P., et al., *Chloroperoxidase II. Utilization of halogen anions.* Journal of Biological Chemistry, 1966. **241**(8): p. 1769-1777.

30. Allain, E.J., et al., *Highly enantioselective epoxidation of disubstituted alkenes with hydrogen peroxide catalyzed by chloroperoxidase.* Journal of the American Chemical Society, 1993. **115**(10): p. 4415-4416.

31. Kühnel, K., et al., *Crystal structures of chloroperoxidase with its bound substrates and complexed with formate, acetate, and nitrate.* Journal of Biological Chemistry, 2006. **281**(33): p. 23990-23998.

32. de Wijn, R., et al., *Crystallization and Structural Determination of an Enzyme: Substrate Complex by Serial Crystallography in a Versatile Microfluidic Chip.* Journal of visualized experiments: JoVE, 2021(169).

33. Wang, X. and H.M. Goff, *A nuclear paramagnetic relaxation study of the interaction of the cyclopentanedione substrate with chloroperoxidase.* Biochimica et Biophysica Acta (BBA)-Protein Structure and Molecular Enzymology, 1997. **1339**(1): p. 88-96.

34. Casella, L., et al., *The chloroperoxidase-catalyzed oxidation of phenols. Mechanism, selectivity, and characterization of enzyme-substrate complexes.* Biochemistry, 1994. **33**(21): p. 6377-6386.

35. Domanski, T. and J. Halpert, *Analysis of mammalian cytochrome P450 structure and function by site-directed mutagenesis.* Current drug metabolism, 2001. **2**(2): p. 117-137.

36. Kao, Y.C., et al., *Evaluation of the mechanism of aromatase cytochrome P450: A site‐directed mutagenesis study.* European Journal of Biochemistry, 2001. **268**(2): p. 243-251.

37. Doyle, W.A., et al., *Two substrate interaction sites in lignin peroxidase revealed by site-directed mutagenesis.* Biochemistry, 1998. **37**(43): p. 15097-15105.

38. Yi, X., et al., *Replacement of the proximal heme thiolate ligand in chloroperoxidase with a histidine residue.* Proceedings of the National Academy of Sciences, 1999. **96**(22): p. 12412-12417.

39. Yi, X., et al., *Examining the role of glutamic acid 183 in chloroperoxidase catalysis.* Journal of Biological Chemistry, 2003. **278**(16): p. 13855-13859.

40. Li, J.S., et al., *Novel glycosidic linkage in aedes Aegypti chorion peroxidase N-mannosyl tryptophan.* Journal of Biological Chemistry, 2005. **280**(46): p. 38513-38521.

41. Sundaramoorthy, M., *Chloroperoxidase.* Encyclopedia of Inorganic and Bioinorganic Chemistry, 2011.

42. Black, A.K. and C. Reddy, *Cloning and characterization of a lignin peroxidase gene from the white-rot fungus Trametes versicolor.* Biochemical and biophysical research communications, 1991. **179**(1): p. 428-435.

43. Godfrey, B.J., et al., *Characterization of a gene encoding a manganese peroxidase from Phanerochaete chrysosporium.* Gene, 1990. **93**(1): p. 119-124.

44. Mayfield, M.B., B.J. Godfrey, and M.H. Gold, *Characterization of the mnp2 gene encoding manganese peroxidase isozyme 2 from the basidiomycete Phanerochaete chrysosporium.* Gene, 1994. **142**(2): p. 231-235.

45. Sawai-Hatanaka, H., et al., *Cloning, sequencing, and heterologous expression of a gene coding for Arthromyces ramosus peroxidase.* Bioscience, biotechnology, and biochemistry, 1995. **59**(7): p. 1221-1228.

46. Zhang, Y., C. Reddy, and A. Rasooly, *Cloning of several lignin peroxidase (LIP)-encoding genes: sequence analysis of the LIP6 gene from the white-rot basidiomycete, Phanerochaete chrysosporium.* Gene, 1991. **97**(2): p. 191-198.

47. Conesa, A., et al., *Expression of the Caldariomyces fumagoChloroperoxidase in Aspergillus niger and Characterization of the Recombinant Enzyme.* Journal of Biological Chemistry, 2001. **276**(21): p. 17635-17640.

48. Brown, D., et al., *Twenty-five coregulated transcripts define a sterigmatocystin gene cluster in Aspergillus nidulans.* Proceedings of the National Academy of Sciences, 1996. **93**(4): p. 1418-1422.

49. Williams, P.A., et al., *Crystal structure of human cytochrome P450 2C9 with bound warfarin.* Nature, 2003. **424**(6947): p. 464-468.

50. Liu, X., et al., *Crystal structure and biochemical features of dye-decolorizing peroxidase YfeX from Escherichia coli O157 Asp143 and Arg232 play divergent roles toward different substrates.* Biochemical and biophysical research communications, 2017. **484**(1): p. 40-44.

51. Nicolussi, A., et al., *Secreted heme peroxidase from Dictyostelium discoideum: Insights into catalysis, structure, and biological role.* Journal of Biological Chemistry, 2018. **293**(4): p. 1330-1345.

52. Van Hartingsveldt, W., et al., *Development of a homologous transformation system for Aspergillus niger based on the pyrG gene.* Molecular and General Genetics MGG, 1987. **206**(1): p. 71-75.

53. Hutner, S.H., et al., *Some approaches to the study of the role of metals in the metabolism of microorganisms.* Proceedings of the American Philosophical Society, 1950. **94**(2): p. 152-170.

54. Lis, H. and N. Sharon, *Protein glycosylation: structural and functional aspects.* European Journal of Biochemistry, 1993. **218**(1): p. 1-27.

55. Zong, Q., P.A. Osmulski, and L.P. Hager, *High-pressure-assisted reconstitution of recombinant chloroperoxidase.* Biochemistry, 1995. **34**(38): p. 12420-12425.

56. Hüttmann, S., M. Buchhaupt, and J. Schrader, *Identification of a Caldariomyces fumago mutant secreting an inactive form of chloroperoxidase lacking the heme group and N-glycans.* PloS one, 2013. **8**(7): p. e67857.

57. Hofrichter, M. and R. Ullrich, *Heme-thiolate haloperoxidases: versatile biocatalysts with biotechnological and environmental significance.* Applied microbiology and biotechnology, 2006. **71**(3): p. 276.

58. Pardillo, A.D., A.N. Morozov, and D.C. Chatfield, *Proximal pocket hydrogen bonds significantly influence the mechanism of chloroperoxidase Compound I formation.* The Journal of Physical Chemistry B, 2015. **119**(39): p. 12590-12602.

59. Morozov, A.N. and D.C. Chatfield, *How the proximal pocket may influence the enantiospecificities of chloroperoxidase-catalyzed epoxidations of olefins.* International journal of molecular sciences, 2016. **17**(8): p. 1297.

60. Benvenuti, M. and S. Mangani, *Crystallization of soluble proteins in vapor diffusion for x-ray crystallography.* Nature protocols, 2007. **2**(7): p. 1633-1651.

61. Giegé, R., et al., *The role of purification in the crystallization of proteins and nucleic acids.* Journal of Crystal Growth, 1986. **76**(3): p. 554-561.

62. Zulauf, M. and A. D'Arcy, *Light scattering of proteins as a criterion for crystallization.* Journal of Crystal Growth, 1992. **122**(1-4): p. 102-106.

63. Thomas, B., D. Carter, and F. Rosenberger, *Effect of microheterogeneity on horse spleen apoferritin crystallization.* Journal of crystal growth, 1998. **187**(3-4): p. 499-510.

64. Rosenberger, F., *Protein crystallization.* Journal of crystal growth, 1996. **166**(1-4): p. 40-54.

65. Pusey, M.L., et al., *Life in the fast lane for protein crystallization and X-ray crystallography.* Progress in biophysics and molecular biology, 2005. **88**(3): p. 359-386.

66. Lambeir, A.-M. and H.B. Dunford, *A kinetic and spectral study of the alkaline transitions of chloroperoxidase.* Archives of biochemistry and biophysics, 1983. **220**(2): p. 549-556.

67. Wu, J., et al., *Synthesis of chiral epichlorohydrin by chloroperoxidase-catalyzed epoxidation of 3-chloropropene in the presence of an ionic liquid as co-solvent.* Catalysis Communications, 2010. **11**(8): p. 727-731.

68. Liu, Y., et al., *Biocatalytic synthesis of C 3 chiral building blocks by chloroperoxidase‐catalyzed enantioselective halo‐hydroxylation and epoxidation in the presence of ionic liquids.* Biotechnology progress, 2015. **31**(3): p. 724-729.

69. Morris, D.R. and L.P. Hager, *Chloroperoxidase I. Isolation and properties of the crystalline glycoprotein.* Journal of Biological Chemistry, 1966. **241**(8): p. 1763-1768.

70. Valderrama-Rincon, J.D., et al., *An engineered eukaryotic protein glycosylation pathway in Escherichia coli.* Nature chemical biology, 2012. **8**(5): p. 434-436.

71. Haines, W.R., *Deglycosylation and molecular weight analysis of chloroperoxidase from the fungus Caldariomyces fumago.* 1994.

72. Jung, Y., J. Kwak, and Y. Lee, *High-level production of heme-containing holoproteins in Escherichia coli.* Applied microbiology and biotechnology, 2001. **55**(2): p. 187-191.

73. Nishimoto, M., J.E. Clark, and B.S.S. Masters, *Cytochrome P450 4A4: expression in Escherichia coli, purification, and characterization of catalytic properties.* Biochemistry, 1993. **32**(34): p. 8863-8870.

74. Sinha, N. and S.J. Ferguson, *An Escherichia coli ccm (cytochrome c maturation) deletion strain substantially expresses Hydrogenobacter thermophilus cytochrome c 552 in the cytoplasm: availability of haem influences cytochrome c 552 maturation.* FEMS microbiology letters, 1998. **161**(1): p. 1-6.

75. Chouchane, S., I. Lippai, and R.S. Magliozzo, *Catalase-peroxidase (Mycobacterium tuberculosis KatG) catalysis and isoniazid activation.* Biochemistry, 2000. **39**(32): p. 9975-9983.

76. Nie, G., N.S. Reading, and S.D. Aust, *Expression of the lignin peroxidase h2 gene fromphanerochaete chrysosporiuminescherichia coli.* Biochemical and biophysical research communications, 1998. **249**(1): p. 146-150.

77. Smith, M., et al., *Expression of a biologically active plant cytochrome b5 in Escherichia coli.* Biochemical Journal, 1994. **303**(1): p. 73-79.

78. Varnado, C.L. and D.C. Goodwin, *System for the expression of recombinant hemoproteins in Escherichia coli.* Protein Expr Purif, 2004. **35**(1): p. 76-83.

79. Mills, M. and S.M. Payne, *Genetics and regulation of heme iron transport in Shigella dysenteriae and detection of an analogous system in Escherichia coli O157: H7.* Journal of Bacteriology, 1995. **177**(11): p. 3004-3009.

80. Wandersman, C. and I. Stojiljkovic, *Bacterial heme sources: the role of heme, hemoprotein receptors and hemophores.* Current opinion in microbiology, 2000. **3**(2): p. 215-220.

81. Bracken, C.S., et al., *Use of heme-protein complexes by the Yersinia enterocolitica HemR receptor: histidine residues are essential for receptor function.* Journal of Bacteriology, 1999. **181**(19): p. 6063-6072.

APPENDICES

Figure A1. DNA sequence of the wild-type CPO.

ATGTTCTCCAAGGTCCTTCCCTTCGTGGGAGCGGTTGCCGCCCTCCCTCACTC
CGTCCGTCAGGAGCCTGGCTCCGGCATTGGCTACCCATACGACAACAACACC
CTGCCATATGTCGCCCCAGGTCCTACCGACTCTCGTGCTCCTTGCCCAGCTCT
GAACGCTCTTGCCAACCACGGTTACATTCCTCACGATGGCCGTGCCATCAGC
AGGGAGACCCTCCAGAACGCTTTCCTCAACCACATGGGTATTGCCAACTCCG
TCATTGAGCTTGCTCTGACCAACGCCTTCGTCGTCTGCGAGTACGTTACTGGC
TCCGACTGTGGTGACAGCCTTGTCAACCTGACTCTGCTCGCCGAGCCCCACGC
TTTCGAGCACGACCACTCCTTCTCCCGCAAGGATTACAAGCAGGGTGTCGCC
AACTCCAACGACTTCATCGACAACAGGAACTTCGATGCCGAGACCTTCCAGA
CCTCTCTGGATGTCGTTGCAGGCAAGACCCACTTCGACTATGCCGACATGAA
CGAGATCCGCCTTCAGCGCGAGTCCCTCTCCAACGAGCTTGACTTCCCCGGTT
GGTTCACCGAGTCCAAGCCAATCCAGAACGTCGAGTCTGGCTTCATCTTCGCC
CTTGTCTCTGACTTCAACCTGCCCGACAACGATGAGAACCCTCTGGTTCGCAT
TGACTGGTGGAAGTACTGGTTCACCAACGAGTCCTTCCCATACCACCTCGGCT
GGCACCCCCCGTCTCCAGCCAGGGAGATCGAGTTCGTCACCTCCGCCTCCTCC
GCTGTCCTGGCTGCCTCTGTCACCTCTACTCCATCTTCCCTTCCATCCGGTGCC
ATCGGCCCAGGTGCCGAGGCTGTCCCTCTCTCCTTCGCCTCCACCATGACCCC
ATTCCTCCTCGCCACCAATGCTCCTTACTACGCCCAGGACCCAACTCTCGGCC
CCAACGACAAGCGTGAGGCTGCCCCAGCTGCCACCACCTCCATGGCCGTCTT
CAAGAACCCATACCTCGAGGCCATTGGCACCCAGGACATCAAGAACCAGCA
GGCTTACGTCAGCTCCAAGGCTGCTGCCATGGCCTCTGCCATGGCCGCCAAC
AAGGCCCGCAACCTTTAA

Figure A2. Protein sequence of the wild-type CPO gene.

1 MFSKVLPFVGAVAALPHSVRQEPGSGIGYPYDNNTLPYVAPGPTDSRAPC

51 PALNALANHGYIPHDGRAISRETLQNAFLNHMGIANSVIELALTNAFVVC

101 EYVTGSDCGDSLVNLTLLAPHAFEHDHSFSRKDYKQGVANSNDFIDNRN

151 FDAETFQTSLDVVAGKTHFDYADMNEIRLQ RESLSNELDFPGWFTESKPI

201 QNVESGFIFALVSDFNLPDNDENPVRIDWWKYWFTNESFPYHLGWHPPS

251 PAREIEFVTSASSAVLAASVTSTPSSLPSGAIGPGAEAVPLSFASTMTPF

301 LLATNAPYYAQDPTLGPNDKREAAPAATTSMAVFKNPYLEAIGTQDIKNQ

351 QAYVSSKAAA MASAMAANKA RNL

Figure A3. Optimized DNA sequence of the mutant CPO-C29H (Length: 1122 bp, GC%: 59.12).

ATGTTTAGCAAAGTTCTGCCGTTCGTTGGTGCGGTGGCGGCGCTGCCGCATAG
CGTTCGTCAAGAGCCGGGTAGCGGTATTGGTTATCCGTACGACAACAACACC
CTGCCGTATGTGGCGCCGGGTCCGACCGATAGCCGTGCGCCGCACCCGGCGC
TGAACGCGCTGGCGAACCACGGTTATATTCCGCATGATGGTCGTGCGATCAG
CCGTGAAACCCTGCAGAACGCGTTCCTGAACCACATGGGCATCGCGAACAGC
GTTATTGAGCTGGCGCTGACCAACGCGTTTGTGGTTTGCGAATACGTGACCGG
TAGCGACTGCGGCGATAGCCTGGTTAACCTGACCCTGCTGGCGGAGCCGCAT
GCGTTTGAACACGACCACAGCTTTAGCCGTAAGGATTATAAACAGGGTGTGG
CGAACAGCAACGACTTCATTGATAACCGTAACTTCGACGCGGAAACCTTTCA
AACCAGCCTGGATGTGGTTGCGGGCAAGACCCACTTTGACTATGCGGATATG
AACGAAATCCGTCTGCAGCGTGAGAGCCTGAGCAACGAACTGGATTTCCCGG
GTTGGTTTACCGAGAGCAAACCGATCCAAAACGTGGAAAGCGGCTTCATTTT
TGCGCTGGTTAGCGACTTCAACCTGCCGGACAACGATGAGAACCCGCTGGTT
CGTATCGATTGGTGGAAGTACTGGTTCACCAACGAGAGCTTCCCGTATCATCT
GGGTTGGCACCCGCCGAGCCCGGCGCGTGAGATTGAATTTGTGACCAGCGCG
AGCAGCGCGGTGCTGGCGGCGAGCGTTACCAGCACCCCGAGCAGCCTGCCGA
GCGGTGCGATTGGTCCGGGTGCGGAAGCGGTTCCGCTGAGCTTCGCGAGCAC
CATGACCCCGTTTCTGCTGGCGACCAACGCGCCGTACTATGCGCAGGACCCG
ACCCTGGGTCCGAACGATAAACGTGAGGCGGCGCCGGCGGCGACCACCAGC
ATGGCGGTGTTCAAGAACCCGTACCTGGAAGCGATCGGCACCCAAGACATTA
AAAACCAGCAAGCGTATGTTAGCAGCAAGGCGGCGGCGATGGCGAGCGCGA
TGGCGGCGAACAAAGCGCGTAATCTGTAA

Figure A4. DNA Alignment (Optimized Region of the mutant CPO-C29H).

Optimized 1 ATGTTTAGCAAAGTTCTGCCGTTCGTTGGTGCGGTGGCGGCGCTGCCGCATAGCGTTCGT

Original 1 ATGTTCTCCAAGGTCCTTCCCTTCGTGGGAGCGGTTGCCGCCCTCCCTCACTCCGTCCGT

Optimized 61 CAAGAGCCGGGTAGCGGTATTGGTTATCCGTACGACAACAACACCCTGCCGTATGTGGCG

Original 61 CAGGAGCCTGGCTCCGGCATTGGCTACCCATACGACAACAACACCCTGCCATATGTCGCC

Optimized 121 CCGGGTCCGACCGATAGCCGTGCGCCGCACCCGGCGCTGAACGCGCTGGCGAACCACGGT

Original 121 CCAGGTCCTACCGACTCTCGTGCTCCTCACCCAGCTCTGAACGCTCTTGCCAACCACGGT

Optimized 181 TATATTCCGCATGATGGTCGTGCGATCAGCCGTGAAACCCTGCAGAACGCGTTCCTGAAC

Original 181 TACATTCCTCACGATGGCCGTGCCATCAGCAGGGAGACCCTCCAGAACGCTTTCCTCAAC

Optimized 241 CACATGGGCATCGCGAACAGCGTTATTGAGCTGGCGCTGACCAACGCGTTTGTGGTTTGC

Original 241 CACATGGGTATTGCCAACTCCGTCATTGAGCTTGCTCTGACCAACGCCTTCGTCGTCTGC

Optimized 301 GAATACGTGACCGGTAGCGACTGCGGCGATAGCCTGGTTAACCTGACCCTGCTGGCGGAG

Original 301 GAGTACGTTACTGGCTCCGACTGTGGTGACAGCCTTGTCAACCTGACTCTGCTCGCCGAG

Optimized 361 CCGCATGCGTTTGAACACGACCACAGCTTTAGCCGTAAGGATTATAAACAGGGTGTGGCG

Original 361 CCCCACGCTTTCGAGCACGACCACTCCTTCTCCCGCAAGGATTACAAGCAGGGTGTCGCC

Optimized 421 AACAGCAACGACTTCATTGATAACCGTAACTTCGACGCGGAAACCTTTCAAACCAGCCTG

Original 421 AACTCCAACGACTTCATCGACAACAGGAACTTCGATGCCGAGACCTTCCAGACCTCTCTG

Optimized 481 GATGTGGTTGCGGGCAAGACCCACTTTGACTATGCGGATATGAACGAAATCCGTCTGCAG

Original 481 GATGTCGTTGCAGGCAAGACCCACTTCGACTATGCCGACATGAACGAGATCCGCCTTCAG

Optimized 541 CGTGAGAGCCTGAGCAACGAACTGGATTTCCCGGGTTGGTTTACCGAGAGCAAACCGATC

Original 541 CGCGAGTCCCTCTCCAACGAGCTTGACTTCCCCGGTTGGTTCACCGAGTCCAAGCCAATC

Optimized 601 CAAAACGTGGAAAGCGGCTTCATTTTTGCGCTGGTTAGCGACTTCAACCTGCCGGACAAC

Original 601 CAGAACGTCGAGTCTGGCTTCATCTTCGCCCTTGTCTCTGACTTCAACCTGCCCGACAAC

Optimized 661 GATGAGAACCCGCTGGTTCGTATCGATTGGTGGAAGTACTGGTTCACCAACGAGAGCTTC

Original 661 GATGAGAACCCTCTGGTTCGCATTGACTGGTGGAAGTACTGGTTCACCAACGAGTCCTTC

Optimized 721 CCGTATCATCTGGGTTGGCACCCGCCGAGCCCGGCGCGTGAGATTGAATTTGTGACCAGC

Original 721 CCATACCACCTCGGCTGGCACCCCCCGTCTCCAGCCAGGGAGATCGAGTTCGTCACCTCC

Optimized 781 GCGAGCAGCGCGGTGCTGGCGGCGAGCGTTACCAGCACCCCGAGCAGCCTGCCGAGCGGT

Original 781 GCCTCCTCCGCTGTCCTGGCTGCCTCTGTCACCTCTACTCCATCTTCCCTTCCATCCGGT

Optimized 841 GCGATTGGTCCGGGTGCGGAAGCGGTTCCGCTGAGCTTCGCGAGCACCATGACCCCGTTT

Original 841 GCCATCGGCCCAGGTGCCGAGGCTGTCCCTCTCTCCTTCGCCTCCACCATGACCCCATTC

Optimized 901 CTGCTGGCGACCAACGCGCCGTACTATGCGCAGGACCCGACCCTGGGTCCGAACGATAAA

Original 901 CTCCTCGCCACCAATGCTCCTTACTACGCCCAGGACCCAACTCTCGGCCCCAACGACAAG

Optimized 961 CGTGAGGCGGCGCCGGCGGCGACCACCAGCATGGCGGTGTTCAAGAACCCGTACCTGGAA

Original 961 CGTGAGGCTGCCCCAGCTGCCACCACCTCCATGGCCGTCTTCAAGAACCCATACCTCGAG

Optimized 1021
GCGATCGGCACCCAAGACATTAAAAACCAGCAAGCGTATGTTAGCAGCAAGGCGGCGGCG

Original 1021 GCCATTGGCACCCAGGACATCAAGAACCAGCAGGCTTACGTCAGCTCCAAGGCTGCTGCC

Optimized 1081 ATGGCGAGCGCGATGGCGGCGAACAAAGCGCGTAATCTGTAA

Original 1081 ATGGCCTCTGCCATGGCCGCCAACAAGGCCCGCAACCTTTAA

Figure A5. Protein Alignment of the mutant CPO-C29H (Optimized region).

Optimized 1 MFSKVLPFVGAVAALPHSVRQEPGSGIGYPYDNNTLPYVAPGPTDSRAPHPALNALANHG

Original 1 MFSKVLPFVGAVAALPHSVRQEPGSGIGYPYDNNTLPYVAPGPTDSRAPHPALNALANHG

Optimized 61 YIPHDGRAISRETLQNAFLNHMGIANSVIELALTNAFVVCEYVTGSDCGDSLVNLTLLAE

Original 61 YIPHDGRAISRETLQNAFLNHMGIANSVIELALTNAFVVCEYVTGSDCGDSLVNLTLLAE

Optimized 121 PHAFEHDHSFSRKDYKQGVANSNDFIDNRNFDAETFQTSLDVVAGKTHFDYADMNEIRLQ

Original 121 PHAFEHDHSFSRKDYKQGVANSNDFIDNRNFDAETFQTSLDVVAGKTHFDYADMNEIRLQ

Optimized 181 RESLSNELDFPGWFTESKPIQNVESGFIFALVSDFNLPDNDENPLVRIDWWKYWFTNESF

Original 181 RESLSNELDFPGWFTESKPIQNVESGFIFALVSDFNLPDNDENPLVRIDWWKYWFTNESF

Optimized 241 PYHLGWHPPSPAREIEFVTSASSAVLAASVTSTPSSLPSGAIGPGAEAVPLSFASTMTPF

Original 241 PYHLGWHPPSPAREIEFVTSASSAVLAASVTSTPSSLPSGAIGPGAEAVPLSFASTMTPF

Optimized 301 LLATNAPYYAQDPTLGPNDKREAAPAATTSMAVFKNPYLEAIGTQDIKNQQAYVSSKAAA

Original 301 LLATNAPYYAQDPTLGPNDKREAAPAATTSMAVFKNPYLEAIGTQDIKNQQAYVSSKAAA

Optimized 361 MASAMAANKARNL*

Original 361 MASAMAANKARNL*

Figure A6. Optimized DNA sequence of the *ChuA* gene (Length: 1980 bp, GC%: 58.11).

ATGAGCCGTCCGCAATTCACCAGCCTGCGTCTGAGCCTGCTGGCGCTGGCGG
TTAGCGCGACCCTGCCGACCTTTGCGTTTGCGACCGAAACCATGACCGTTACC
GCGACCGGTAACGCGCGTAGCAGCTTCGAAGCGCCGATGATGGTGAGCGTTA
TCGATACCAGCGCGCCGGAGAACCAAACCGCGACCAGCGCGACCGACCTGCT
GCGTCATGTTCCGGGTATTACCCTGGATGGCACCGGTCGTACCAACGGTCAG
GATGTGAACATGCGTGGTTACGATCACCGTGGCGTGCTGGTTCTGGTGGACG
GTGTGCGTCAAGGCACCGATACCGGTCACCTGAACGGCACCTTCCTGGACCC
GGCGCTGATCAAGCGTGTTGAGATTGTGCGTGGTCCGAGCGCGCTGCTGTAT
GGTAGCGGCGCGCTGGGTGGCGTTATCAGCTATGATACCGTGGACGCGAAAG
ATCTGCTGCAGGAAGGTCAAAGCAGCGGCTTCCGTGTTTTTGGCACCGGTGG
CACCGGCGATCACAGCCTGGGTCTGGGTGCGAGCGCGTTTGGTCGTACCGAG
AACCTGGACGGCATTGTGGCGTGGAGCAGCCGTGACCGTGGTGATCTGCGTC
AGAGCAACGGCGAAACCGCGCCGAACGACGAGAGCATCAACAACATGCTGG
CGAAGGGCACCTGGCAGATTGATAGCGCGCAAAGCCTGAGCGGCCTGGTTCG
TTACTATAACAACGACGCGCGTGAACCGAAAAACCCGCAGACCGTTGAGGCG
AGCGAAAGCAGCAACCCGATGGTGGACCGTAGCACCATCCAGCGTGATGCG
CAACTGAGCTACAAGCTGGCGCCGCAAGGCAACGACTGGCTGAACGCGGAT
GCGAAAATCTATTGGAGCGAAGTGCGTATTAACGCGCAGAACACCGGTAGCA
GCGGCGAGTACCGTGAACAAATTACCAAGGGTGCGCGTCTGGAGAACCGTAG
CACCCTGTTCGCGGATAGCTTTGCGAGCCACCTGCTGACCTATGGTGGCGAAT
ACTATCGTCAAGAGCAACATCCGGGTGGCGCGACCACCGGTTTCCCGCAGGC
GAAAATCGACTTTAGCAGCGGCTGGCTGCAAGACGAGATCACCCTGCGTGAT
CTGCCGATTACCCTGCTGGGTGGCACCCGTTACGACAGCTATCGTGGTAGCA
GCGATGGCTACAAGGACGTTGATGCGGACAAATGGAGCAGCCGTGCGGGTAT
GACCATCAACCCGACCAACTGGCTGATGCTGTTCGGTAGCTACGCGCAGGCG
TTTCGTGCGCCGACGATGGGTGAAATGTATAACGATAGCAAGCACTTCAGCA
TTGGTCGTTTTTACACCAACTATTGGGTTCCGAACCCGAACCTGCGTCCGGAA
ACCAACGAAACCCAAGAGTACGGTTTCGGCCTGCGTTTTGACGATCTGATGC
TGAGCAACGACGCGCTGGAGTTCAAAGCGAGCTACTTTGACACCAAGGCGAA
AGATTATATCAGCACCACCGTGGATTTCGCTGCGGCGACCACCATGAGCTAT
AACGTTCCGAACGCGAAGATTTGGGGTTGGGACGTGATGACCAAATACACCA
CCGACCTGTTTAGCCTGGATGTTGCGTATAACCGTACCCGTGGTAAAGATACC

GACACCGGCGAATACATCAGCAGCATTAACCCGGACACCGTGACCAGCACCC
TGAACATCCCGAACGCGCACAGCGGCTTCAGCGTTGGTTGGGTGGGCACCTT
TGCGGATCGTAGCACCCACATCAGCAGCAGCTACAGCAAACAGCCGGGTTAT
GGCGTTAACGACTTCTACGTGAGCTATCAGGGTCAGCAAGCGCTGAAGGGCA
TGACCACCACCCTGGTGCTGGGTAACGCGTTTGACAAAGAGTACTGGAGCCC
GCAGGGTATCCCGCAGGACGGTCGTAATGGTAAAATCTTCGTGAGCTATCAG
TGG

Figure A7. Protein sequence of the *ChuA* gene.

1 MSRPQFTSLRLSLLALAVSATLPTFAFATETMTVTATGNARSSFEAPMMV

51 SVIDTSAPENQTATSATDLLRHVPGITLDGTGRTNGQDVNMRGYDHRGVL

101 VLVDGVRQGT DTGHLNGTFLDPALIKRVEIVRGPSALLYGSGALGGVISY

151 DTVDAKDLLQ EGQSSGFRVF GTGGTGDHSLGLGASAFGRTENLDGIVAWS

201 SRDRGDLRQSNGETAPNDESINNMLAKGTW QIDSAQSLSG LVRYYNNDAR

251 EPKNPQTVEA SESSNPMVDR STIQRDAQLS YKLAPQGNDW LNADAKIYWS

301 EVRINAQNTG SSGEYREQIT KGARLENRST LFADSFASHL LTYGGEYYRQ

351 EQHPGGATTG FPQAKIDFSS GWLQDEITLR DLPITLLGGT RYDSYRGSSD

401 GYKDVDADKWSSRAGMTINPTNWLMLFGSAQAFRAPTMGEMYNDSKHFS

451 IGRFYTNYWVPNPNLRPETNETQEYGFGLRFDDLMLSNDALEFKASYFDT

501 KAKDYISTTVDFAAATTMSYNVPNAKIWGWDVMTKYTTDLFSLDVAYNRT

551 RGKDTDTGEY ISSINPDTVT STLNIPNAHS GFSVGWVGTF ADRSTHISSS

601 YSKQPGYGVNDFYVSYQGQQALKGMTTTLVLGNAFDKEYWSPQGIPQDGR

651 NGKIFVSYQW

VITA

XIAOQING TANG

EDUCATION

08/2016-Present	Florida International University, Biochemistry Ph.D. Program
09/2011-06/2015	China Pharmaceutical University B.S. Pharmacy
08/2017-Present	Research Assistant, Department of Chemistry and Biochemistry, Florida International University, Miami, FL Advisor: Dr. Xiaotang Wang
05/2018-08/2018	Collaborative Project with Prof Guo's Group State Key Laboratory of Natural Medicines, Jiangsu Key Laboratory of Carcinogenesis and Intervention, China Pharmaceutical University, Nanjing, China Supervisor: Qinglong Guo
03/2016-06/2016	Internship, Department of Pharmacy, Zhongda Hospital Southeast University, Nanjing, China Supervisor: Hua Shao
04/2015	Outstanding Student Third Scholarship
05/2014	The First Place in "Intellectual Challenges" (over 700 participants)
05/2013	The Third Prize of "Shenlong Cup Knowledge Competition"

PUBLICATIONS AND PRESENTATIONS

[1] Guo, Y., Zhao, Y., Zhou, Y., Tang, X., Li, Z., & Wang, X. (2019). LZ-101, a novel derivative of danofloxacin, induces mitochondrial apoptosis by stabilizing FOXO3a via blocking autophagy flux in NSCLC cells. Cell death & disease, 10(7), 484.

[2] Guo, Y., Wei, L., Zhou, Y., Lu, N., Tang, X., Li, Z., & Wang, X. (2020). Flavonoid GL-V9 induces apoptosis and inhibits glycolysis of breast cancer via disrupting GSK-3β-modulated mitochondrial binding of HKII. Free Radical Biology and Medicine, 146, 119-129.

[3] Deng, P., Meng, C., Wu, Y., Xu, J., Tang, X., Zhang, X., Xiao, Y., Wang, X., Fang, Z. and Fang, W., (2020). An unusual GH1 β-glucosidase from marine sediment with β-galactosidase and transglycosidation activities for superior galacto-oligosaccharide synthesis. Applied microbiology and biotechnology, 104(11), pp.4927-4943.

[4] Wang, J., Chang, F., Tang, X., Li, W., Yin, Q., Yang, Y., & Hu, Y. (2020). Bacterial laccase of Anoxybacillus ayderensis SK3-4 from hot springs showing potential for industrial dye decolorization. Annals of Microbiology, 70(1), 1-9.

[5] Tang, X., Nadar, V. S., Zhou, J., B. Rosen, and Wang, X. “Crystal Structure of Recombinant Chloroperoxidase and Molecular Docking Studies of Chloroperoxidase-Substrate Complex: Insights into the Mechanism of Chloroperoxidase-Catalyzed Enantioselective Epoxidation of Olefin”, Journal of Crystal Growth In preparation

[6] Xiaoqing Tang. “Crystal Structure of Recombinant Chloroperoxidase and Molecular Docking Studies of Chloroperoxidase-Substrate Complex: Insights into the Mechanism of Chloroperoxidase-Catalyzed Enantioselective Epoxidation of Olefin”, ACS Fall 2021, August 22-26, 2021(2021), BIOL (oral presentation).